

MICROWAVE ANTENNAS

**CORRUGATED FLANGE TECHNIQUE FOR BEAM SHAPING  
OF SECTORAL ELECTROMAGNETIC HORN ANTENNAS**

**A THESIS SUBMITTED BY  
E. J. ZACHARIAH  
IN PARTIAL FULFILMENT OF  
THE REQUIREMENTS  
FOR THE DEGREE OF  
DOCTOR OF PHILOSOPHY  
TO  
THE UNIVERSITY OF COCHIN**

**MICROWAVE LABORATORY, DEPARTMENT OF PHYSICS  
UNIVERSITY OF COCHIN, COCHIN 682 022  
INDIA**

**1981**

## DECLARATION

This is to certify that this thesis is a report of the original work carried out by Mr. E.J. Zachariah, under my supervision and guidance in the Microwave Laboratory, Department of Physics, University of Cochin, Cochin-682022, and that no part thereof has been presented for any other degree.

Cochin-682022,  
18th August 1981.

Dr.K.G. Nair  
(Supervising Teacher)  
Professor and Head of the  
Department of Electronics and  
Communication Systems  
University of Cochin.

## ACKNOWLEDGEMENTS

The work presented in this thesis has been carried out under the guidance and supervision of Dr.K.G.Nair, Professor and Head of the Department of Electronics and Communication Systems, University of Cochin. The help and inspiration he gave were indispensable for the progress and completion of this research programme.

The author is grateful to Dr.K.Sathianandan, Professor and Head of the Department of Physics, University of Cochin, for providing all the facilities needed and for the keen interest he has shown in this work. The author acknowledges with deep gratitude the help and encouragement he has obtained from the members of the faculty of the Department of Physics. The author would like to record here his sincere thanks for the help and support he received from the technical and administrative staff of the Physics Department, and Central Workshop and Instrumentation Services Laboratory of the University of Cochin.

Department of Atomic Energy, Government of India, has awarded a liberal Junior Research Fellowship with necessary contingent grant. The author acknowledges with thanks this financial support provided by DAE. In the earlier part of this work, the author was enjoying a Cochin University Junior Research Fellowship. The author would like to express his thanks to the University authorities for the same.

He has received immense help and encouragement from his friend and colleague Mr.K.Vasudevan. All the research scholars in the Physics Department, especially Mr.P. Mohanan, Mr.P.A.Praveen Kumar, Mr.G.Sreenivasan, Mr.V.B.Gopinathan and Mr.P.O. Paul in the Microwave Group extended hearty cooperation throughout the entire programme. He is deeply indebted to all of them. He acknowledges the help extended by Dr.K.T. Mathew, Department of Physics, St. Teresa's College, Ernakulam.

The author is thankful to Professor C.Karunakaran, Director, Centre for Earth Science Studies, Trivandrum, where he joined during the course of this work, for allowing him to complete this thesis. The encouragement and help extended by Dr.S.Sampath, Head, Atmospheric Sciences Division, Centre for Earth Science Studies, is gratefully acknowledged. He acknowledges the keen interest shown by his colleagues in the Atmospheric Sciences Division.

The author is indebted to the authorities of the University Computer Centre, University of Kerala for extending computer facilities. Thanks are also due to the authorities of the Naval Physical and Oceanographic Laboratories, Cochin, for extending library facilities.

Valuable help and cooperation extended by Mr.K.P.Sasidharan, Mr.C.B.Muraleedharan, Mr.N.Appukuttan Nair and Mr.V.M.Peter in bringing out this thesis in this form, are also acknowledged.

## CONTENTS

	Page
LIST OF SYMBOLS USED	.. 5
LIST OF FIGURES	.. 8
LIST OF TABLES	.. 12
CHAPTER I INTRODUCTION	.. 14
CHAPTER II REVIEW OF THE PAST WORK	.. 30
CHAPTER III EQUIPMENT USED AND METHODS OF MEASUREMENT	.. 48
CHAPTER IV EXPERIMENTAL RESULTS	.. 74
CHAPTER V THEORY OF THE CORRUGATED FLANGE MOUNTED SECTORAL HORN	.. 115
CHAPTER VI CONCLUSIONS	.. 132
APPENDIX I DESIGN AND DEVELOPMENT OF A MICROWAVE ANECHOIC CHAMBER FOR ANTENNA MEASUREMENTS	.. 136
APPENDIX II DEVELOPMENT OF A MICROWAVE ABSORBING MATERIAL	.. 157
REFERENCES	.. 166
LIST OF PUBLICATIONS	.. 179
INDEX	.. 180

## LIST OF SYMBOLS USED

- A - Absorption coefficient (Appendix II).
- a - Corrugation period.
- B - Flange width
- $B_p$  - Distance between the  $p^{\text{th}}$  element and horn aperture.
- c - Velocity of light.
- D - Larger dimension of the aperture.
- d - Corrugation width.
- $E_{\mathcal{C}}$  - The resultant electric field at M due to the corrugation tips.
- $E'_{\mathcal{C}}$  - The resultant electric field at M due to primary and images I and I'.
- f - Frequency.
- G - Antenna gain.
- $G_E$  - E-plane gain.
- $G_H$  - H-plane gain.
- h - Corrugation depth.
- $h_1, h_2$  - Corrugation depth at flange edges 1 and 2.
- I, I' - Images of the horn aperture cast by flange elements 1 and 2.
- $I_{\mathcal{C}}$  - Field intensity at the point M.
- K, K' - Amplitude of the resultant due to secondary radiators on flange elements 1 and 2.

- $k$  - Amplitude of excitation of the secondary radiators.
- $M$  - A distant point whose bearing angle at the horn aperture is  $\theta$  .
- $N$  - Number of corrugations on the flange surface.
- $n$  - Corrugation period.
- $\hat{n}_1$  - Unit vector along the direction of the incident wave.
- $\hat{n}_2$  - Unit vector along the direction of the scattered wave.
- $O$  - Horn aperture.
- $P_{\max}$  - Power at the antinode in a standing wave pattern.
- $P_{\min}$  - Power at the node in a standing wave pattern.
- $P_o$  - On-axis power density.  
 - Reference power (Appendix I).
- $P_r$  - Power reflected from the absorbing surface (Appendix I).
- $P_\theta$  - Power density at the point  $M$ .
- $R$  - Resultant field vector (Section 5.1).  
 - Absorption coefficient (Appendix II).
- $R(\text{dB})$  - Reflectivity of the absorbing surface.
- $\bar{r}$  - The radius vector from the origin to the  $(i,k)^{\text{th}}$  scatterer.
- $S$  - Voltage Standing Wave Ratio (VSWR).
- $s$  - The finger pitch of the scattering surface.
- $S_1, S_2$  - Secondary sources (Section 5.1).
- $S_p$  - The  $p^{\text{th}}$  element on the flange surface.

- $Z$  - Distance from the horn aperture.  
 $\alpha_p$  - Relative phase of the  $p^{\text{th}}$  element (Chapter V).  
 $\beta$  - Half the flange angle.  
- Wave number (Appendix I).  
 $\delta, \delta'$  - The relative phase of  $I$  and  $I'$ .  
 $\epsilon, \epsilon'$  - The relative phase of  $E$  and  $E'$  (Section 5.2).  
 $\epsilon_1, \epsilon_2$  - The relative phase of  $S_1$  and  $S_2$  (Section 5.1).  
 $\eta_p$  - The phase difference between the  $p^{\text{th}}$  element on flange element 1 and the horn aperture.  
 $\eta'_p$  - The phase difference between the  $p^{\text{th}}$  element on flange element 2 and the horn aperture.  
 $\theta$  - The bearing angle of point  $M$  at the aperture.  
 $\lambda$  - The operating wavelength.  
 $\varphi$  - The phase of the resultant vector (Chapter V).  
 $\varphi(i,k)$  - The phase of the scattered wave from the  $(i,k)^{\text{th}}$  scatterer.

## LIST OF FIGURES

Figure Number	Page
..	..
1.1(a)	... 16
1.1(b)	.. 16
1.2(a)	.. 18
1.3(a)	.. 22
1.4(a)	.. 25
1.4(b)	.. 25
3.1(iii)(a)	.. 52
3.1(iv)(a)	.. 52
3.1(iv)(b)	.. 55
3.2(a)	.. 55
3.2(b)	.. 62
3.2(c)	.. 63
3.2(d)	.. 63
3.2(e)	.. 59
3.3(a)	.. 66
3.3(b)	.. 70
3.5(a)	.. 70
4.1(i)(a)	.. 76
4.1(i)(b)	.. 76
4.1(i)(c)	.. 77
4.1(i)(d)	.. 77

Figure Number	Page
..	..
4.1(ii)(a)	.. 79
4.1(ii)(b)	.. 80
4.1(ii)(c)	.. 81
4.1(ii)(d)	.. 82
4.1(iii)(a)	.. 84
4.1(iii)(b)	.. 85
4.1(iv)(a)	.. 87
4.1(iv)(b)	.. 88
4.2(i)(a)	.. 90
4.2(i)(b)	.. 90
4.2(i)(c)	.. 91
4.2(i)(d)	.. 91
4.2(i)(e)	.. 93
4.2(i)(f)	.. 93
4.2(i)(g)	.. 94
4.2(i)(h)	.. 94
4.2(i)(i)	.. 95
4.2(i)(j)	.. 95
4.2(i)(k)	.. 97
4.3(i)(a)	.. 98
4.3(i)(b)	.. 99
4.4(i)(a)	.. 103
4.4(i)(b)	.. 103
4.4(i)(c)	.. 105

Figure Number	Page
..	..
4.4(i)(d)	.. 105
4.4(ii)(a)	.. 107
4.4(iii)(a)	.. 107
4.5(i)(a)	.. 110
4.6(i)(a)	.. 112
4.6(i)(b)	.. 113
5.1(a)	.. 116
5.1(b)	.. 116
5.2(a)	.. 119
5.2(b)	.. 120
5.2(c)	.. 120
5.3(i)(a)	.. 127
5.3(i)(b)	.. 128
5.3(ii)(a)	.. 129
5.3(ii)(b)	.. 130
A.I.1(a)	.. 140
A.I.2(a)	.. 142
A.I.2(b)	.. 142
A.I.2(c)	.. 147
A.I.2(d)	.. 147
A.I.3(a)	.. 149
A.I.3(b)	.. 149
A.I.5(a)	.. 154

Figure Number	Page
..	..
A.I.5(b)	.. 155
A.I.5(c)	.. 155
A.II.2(a)	.. 161
A.II.2(b)	.. 164

## LIST OF TABLES

Table Number		Page
..		..
3.1(I)	..	53
3.1(II)	..	56
4.4(i)(I)	..	101
4.4(i)(II)	..	101
4.4(i)(III)	..	104
4.4(i)(IV)		104
A.II(I)	..	159
A.II(II)	..	162

CORRUGATED FLANGE TECHNIQUE FOR BEAM SHAPING  
OF SECTORAL ELECTROMAGNETIC  
HORN ANTENNAS

## CHAPTER I

### INTRODUCTION

1.0           The formulation of the Electromagnetic Field Equations by James Clark Maxwell in 1865 marked the beginning of the study of Electromagnetic waves. The successful generation and detection of these waves by Henrich Hertz, in 1887, started the experimental investigations on the properties of this 'newly discovered' form of energy. Even during those early days, the scientists were able to generate oscillatory fields of very high frequency. Hertz himself was able to generate such oscillations upto a frequency of 500 MHz and he studied their properties. These studies mainly included the generation of oscillatory fields, their transmission into free space, and reception at the other end. The coupling device, which passes on to the free space the electromagnetic energy from the transmission line is called an 'Antenna'. The same antenna can be used to gather energy from free space or any dielectric medium, and to deliver it to the transmission lines. It may be noted that the term 'antenna' is borrowed from Zoology, where it means sensors. (Only difference here, is that an electromagnetic antenna senses electromagnetic fields, whereas a biological antenna senses mechanical disturbances or objects).

Technically, an antenna can be defined as a device for matching the free space impedance with the impedance of the transmission line to which it is connected.

### 1.1 Hertz's Experiments

In 1887, Prof. Henrich Hertz devised equipment with which he generated electromagnetic waves. He could set up experiments to reflect, refract, and polarise these new type of waves.

His transmitter was a spark coil, like the one used in automobile ignition systems. The receiver was a single loop of wire, broken at one point by an adjustable spark gap. It was possible to produce small sparks in the receiving loop, whenever there was sparking at the transmitting spark gap. Fig.1.1(a) shows the arrangement used by Hertz.

He was able to reflect these waves by plane metallic sheets, much in the same way as optical beams are reflected by mirrors. Further, he could focus these waves by keeping the transmitter at the focus of a parabolic reflector made of sheet metal. His arrangement is shown in Fig.1.1(b).

In the place of a loop of wire with an adjustable spark gap, Hertz could successfully use two rods so aligned that they are collinear, with a small gap in between, very much like the transmitting spark gap.



Fig.1.1(a) Hertz's experiment.

E is the transmitter, consisting of the induction coil, make and break contacts etc. R is the receiving loop of wire.  $G_1$  is the transmitting spark gap and  $G_2$  is the receiving spark gap - both are adjustable.

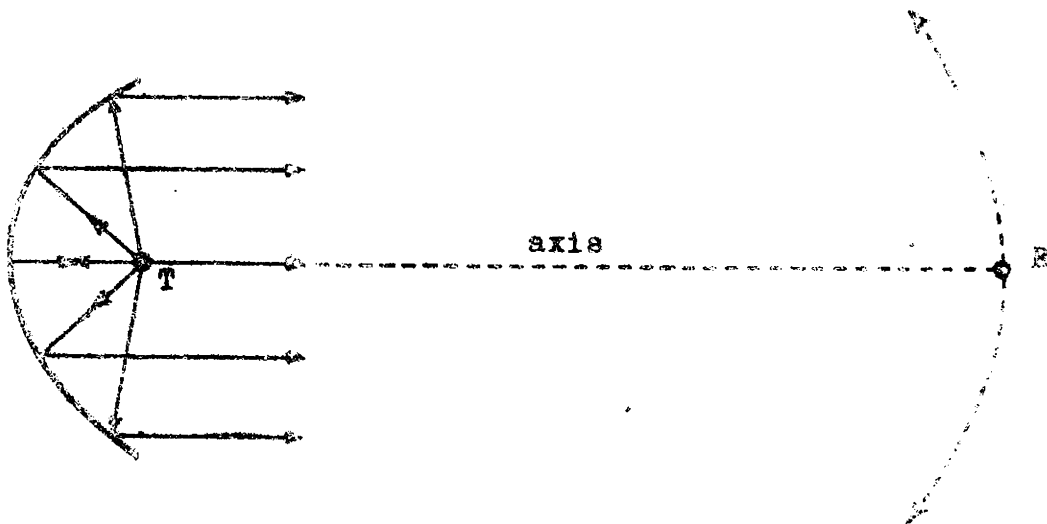


Fig.1.1(b) Focuss'ng of electromagnetic waves by a parabolic reflector.

T is the transmitting gap kept at the focus of the parabola. R is the receiving loop. Intensity of the sparks decreases very rapidly as the receiving loop is moved away from the axis of the parabolic mirror.

The unfortunate demise of Prof. Hertz at a very young age slowed down further developments in this field of activity.

## 1.2 Different Types of Electromagnetic Antennas

Any simple wire, connected to a source of Radio Frequency Energy, acts as a monopole antenna, in that it radiates energy to the surrounding medium. One type of monopole antenna is the vertical whip antenna used for portable communication sets. Such an antenna demands the proximity of a ground plane for its successful operation. The quarter wavelength vertical antenna with one end grounded (the 'Marconi antenna') used by broadcasting stations is another example.

A basic dipole consists of two charges of opposite polarity, or in the case of an actual antenna, it consists of two cylindrical elements which receive signals of opposite polarity. Fig.1.2(a) shows the basic dipole with the voltage and current distribution, which occurs when each of the dipole element is one quarter wavelength long at the frequency at which it is excited.

Electromagnetic horn antennas are characterised by their ability to effect a slow transition from the waveguide to the free space. These antennas exhibit a good

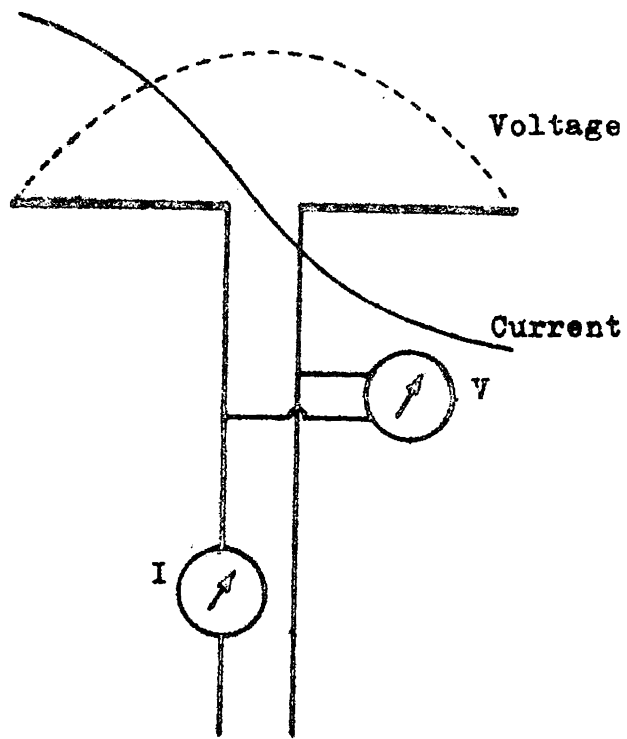


Fig.1.2(a) Current and voltage distribution across the dipole when each of the element is a quarter wavelength long, at the frequency of excitation.

directivity and they can accommodate an exceptionally broad band of frequencies, when compared with other single antennas.

Arrays of single antennas are employed to obtain desired pattern shapes and other qualities which may be lacking in the single antennas which constitute the array.

Similarly, reflector antennas are employed for applications that require very high gain, very narrow beams, good side lobe suppression, etc.

Slots made on the waveguide walls radiate energy. Hence arrays of such slot antennas are also employed.

More recently, microstrip antennas have been developed and they are used in conjunction with microstrip circuits. They find applications in space borne elements, since the printed antenna can be wrapped around the body of a rocket or missile, without causing serious air drag.

### 1.3 Electromagnetic Horn Antennas

Horn antennas constitute a class of antennas by themselves. They have a very broad band of operation, high gain, and good directivity. In one of the earlier papers<sup>(1)</sup>, the horn antennas were described as "having such favourable features and one so ideally adapted to frequencies above about 300 Mc/s, that they deserve serious consideration for applications involving microray communication". Considering

the characteristics of radiating apertures, it may be argued that by choosing a larger waveguide, the required pattern can be obtained from its open end. In such a case, problems arise due to the excitation of higher order modes in the guiding system. Waves of different modes reach the aperture in different phases, depending on the length of the guiding system. This causes pattern shape deterioration. This problem can be overcome by gradually varying the waveguide dimensions to the required aperture dimensions. In this case also, higher order modes may get excited at the waveguide horn junction or throat. But as these waves tend to propagate along the direction of the aperture, they find that the transverse dimensions of the horn in the vicinity of the throat is still small (provided the flare angle is not too large), so that they get attenuated before they reach a region which can support such a mode. Hence none other than the dominant mode reach the aperture. Thus the horn acts as a "mode filter".

If a horn is to operate in a desired manner, there exists definite relations between the flare angle, horn length etc. Barrow and Chu<sup>(2)</sup> and Southworth and King<sup>(3)</sup> give details about rectangular and conical horn design, respectively. These papers are reviewed in more detail in the next chapter.

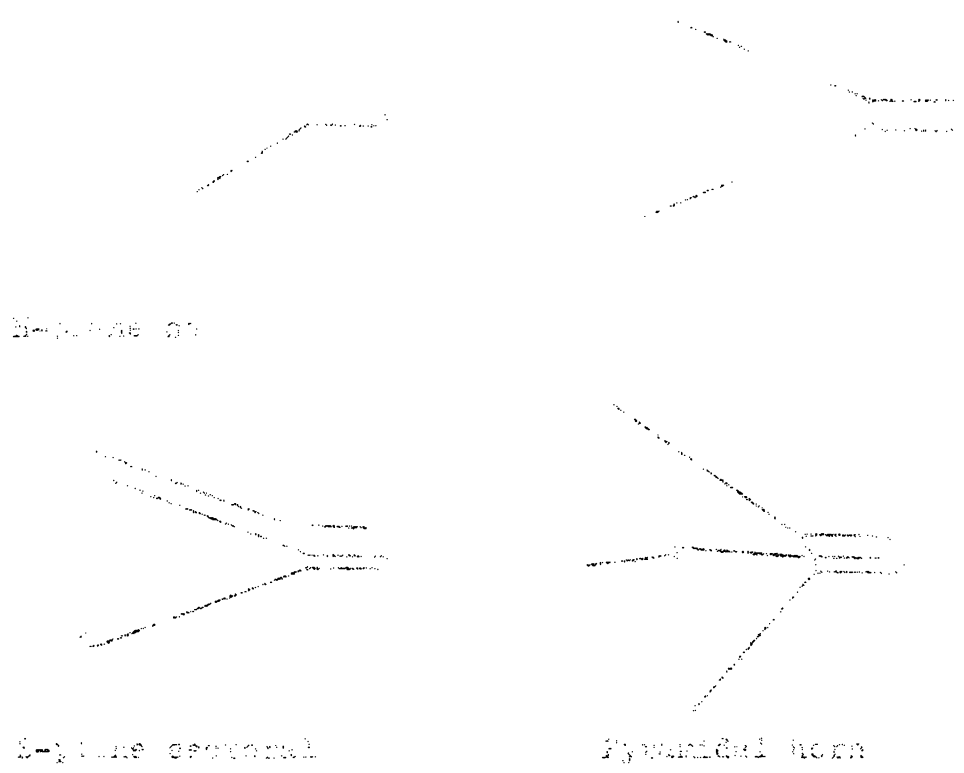
There are various types of horns, depending on the type of waveguide from which it is derived, and also the specific application for which it is used. Fig.1.3(a) shows various horns that are generally used.

Pyramidal horns are used as gain standards and also as feeds. Their radiation pattern and gain can be predicted to a good degree of accuracy. The beam width in both the principal planes can be independently controlled.

Sectoral horns are flared only in one of the principal planes. Thus there are E-plane sectoral horns and H-plane sectoral horns. These produce a fan shaped beam which is very narrow in the plane in which it is flared and very broad in the orthogonal plane. The pattern in the unflared plane is essentially that of an open ended waveguide.

Conical horns are derived from circular waveguides. Because of the axial symmetry, they can handle any polarisation. The gain of the horn can be calculated to a fairly high accuracy.<sup>(15,28,38,66,78)</sup> Hence they are also used as primary gain standards.

Other types of horns are the compound horn, box horn, hog horn etc. These are employed for certain specific applications.



Rectangular

E-plane sectoral

Pyramidal horn

Fig.1.3(a) Sketch of various horn antennas are general used.

#### 1.4 Sectoral Horns

Sectoral horns are flared only in one plane, the other set of walls remain parallel to each other. There are two types of sectoral horns. In one type the flare increases the aperture in the direction of the E-vector. These are called E-plane sectoral horns. In the other type, the flare increases the aperture in the direction of the H-vector, and these are called H-plane sectoral horns.

The radiation pattern in the flared plane is narrow and focussed. But the radiation pattern in the orthogonal plane is very broad and it is the same as that of an open ended waveguide of the same dimensions. Hence the energy radiated by a sectoral horn is distributed in a fan shaped beam. Such a pattern shape may be useful in certain applications like some radars where good resolution is required only in one plane, ie. either in the azimuthal or in the elevation plane, but not both simultaneously. For other applications like point to point communication, illuminating parabolic reflectors etc., an identical pattern shape in both the principal planes is required. Hence the necessity arises to modify the pattern shape in the unflared plane. Many workers have tried to modify the pattern shape of sectoral horn antennas in both the principal planes. The 'grill technique', developed by K.G. Nair and S.Hariharan<sup>(20,23)</sup>, is effective in controlling the E-plane radiation pattern

of E-plane sectoral horns. Here conducting grills are attached to the aperture of the sectoral horn. The dimensions of the grills and their positions are parameters which can be varied to obtain optimum performance. Fig.1.4(a) is a schematic representation of a sectoral horn attached with grills.

The 'flange technique' was first suggested by Owen and Reynolds<sup>(7)</sup>, in 1946. Butson and Thomson<sup>(18)</sup> in 1959 gave an explanation to the effects of flanges on the radiation pattern of sectoral horns. This technique was developed and investigated in detail by later workers.<sup>(36,39-42,44,45,47)</sup> In these studies the effect of plane flanges were investigated. The flange technique is known to have a good control on the E-plane pattern of H-plane sectoral horns and under certain circumstances on the H-plane pattern of E-plane sectoral horns. The important parameters of a flange mounted sectoral horn are:

- (a) flange angle
- (b) flange width
- (c) flange position
- (d) amplitude of excitation of the flange elements.

It has been established that by careful control of these flange parameters, the radiation from this antenna system can be conveniently controlled.<sup>(36,39-42,44,45,47)</sup>

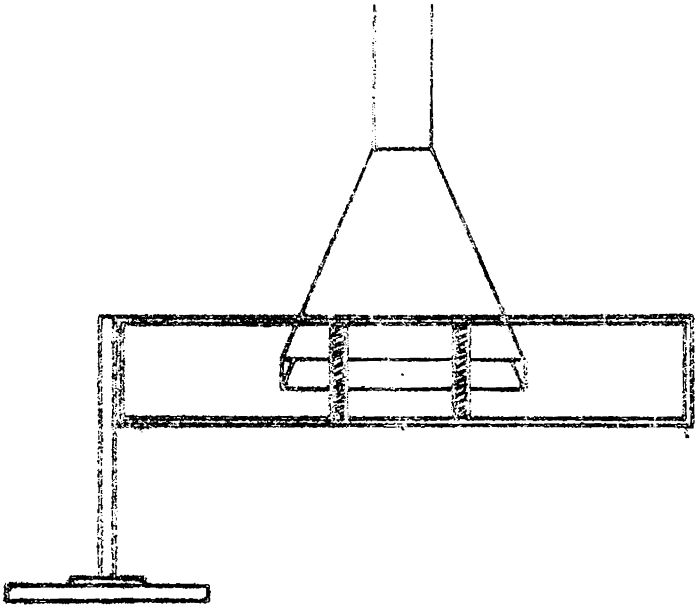


Fig.1.4(a) Schematic representation of a sectoral horn attached with Grills.

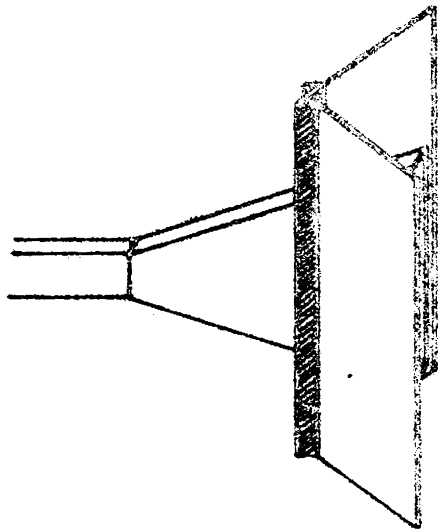


Fig.1.4(b) Schematic representation of a sectoral horn attached with plane flanges.

Advantages of this technique are very efficient control on the radiation pattern and adjustability. The pattern in any one plane can be conveniently modified without seriously affecting the radiation pattern in the other plane. Again, certain types of asymmetries can be introduced into the flange system, to obtain an asymmetric or shaped beam, to suit specific applications. Fig.1.4(b) gives a schematic representation of a sectoral horn attached with plane flanges.

### 1.5 Outline of the Present Work

The need for improved feed systems for large reflector antennas employed in Radio Astronomy and Satellite tracking spurred the interest in horn antenna research in the 1960's. The major requirements were to reduce spill over, cross-polarisation losses, and to enhance the aperture efficiency to the order of about 75-80%. The search for such a feed culminated in the corrugated horn. The corrugated horn triggered widespread interest and enthusiasm, and a large amount of work<sup>(32,34,49,50,52,53,58,65,75,79)</sup> has already been done on this type of antennas. The properties of corrugated surfaces has been investigated in detail.

It was strongly felt that the flange technique and the use of corrugated surfaces could be merged together to obtain the advantages of both. This is the idea behind the present work. Corrugations are made on the surface of flange

elements. The effect of various corrugation parameters are studied. By varying the flange parameters, a good amount of data is collected and analysed to ascertain the effects of corrugated flanges. The measurements are repeated at various frequencies, in the X- and S-bands. The following parameters of the system were studied:

- (a) beam shaping
- (b) gain
- (c) variation of V.S.W.R.
- (d) possibility of obtaining circularly polarised radiation from the flanged horn.

A theoretical explanation to the effects of corrugated flanges is attempted on the basis of the line-source theory. Even though this theory utilises a simplified model for the calculation of radiation patterns, fairly good agreement between the computed pattern and experimental results are observed.

The scheme of the present work is as follows:

Chapter 2 gives a comprehensive review of the research work done in this field. This review starts with papers on horn design, both theoretical and experimental. The attempts made to modify the radiation patterns are reviewed. The efforts made to modify the radiation pattern of sectoral

horns, in their principal planes are studied. This chapter is intended to provide an understanding about the various theoretical and experimental techniques employed in electromagnetic horn antenna research.

Chapter 3 describes the experimental techniques and methods of measurement employed. The major equipment that are used in this study are described. Fabrication of various antenna components used in this study are also described.

Chapter 4 describes the experimental results relating to pattern modification, gain measurement, and variation of V.S.W.R.

Theoretical analysis of the corrugated flange mounted sectoral horn is described in chapter 5. Theoretical and measured patterns are given and a comparison between the two is made. The study is made on the simplified assumption that the aperture of the primary sectoral horn is almost equivalent to a linear source, and the tips of the corrugations are secondary sources excited by the primary.

Chapter 6 contains the conclusions derived from this study on corrugated flange mounted sectoral horns. Suggestions for further work to improve this antenna system is also included in this chapter.

The earlier part of the work described in this thesis was performed with usual facilities in a laboratory. Precise measurement of antenna pattern were conducted in an

anechoic chamber, with automatic pattern recording facility. The design and construction of this anechoic chamber is discussed in Appendix I.

Attempts were made to develop a microwave absorber suited for the interior lining of microwave anechoic chambers. A natural rubber based material was successfully developed. A report of this is given in Appendix II.

## CHAPTER II

### REVIEW OF THE PAST WORK

2.0 This chapter presents a review of the work that has been done in the field of electromagnetic horn antennas in general, and beam shaping of sectoral horns in particular. This chapter has been divided into three sections. The first section reviews some of the important works of general interest that deal with horn antennas in general. The second section reviews the research work done so far on corrugated surfaces and corrugated horns and the third section deals with beam shaping of sectoral horns by various techniques.

#### 2.1 Earlier Important Works of General Interest

Among the early workers on electromagnetic horn antennas, Barrow and Chu<sup>(2)</sup> were the first to give a rigorous analysis of the problem. They studied the propagation of electromagnetic waves through a 'tapered hollow pipe-line', and the radiation from it. They considered an infinitely long, perfectly conducting, hollow tapered section and derived the magnetic and electric field vectors in it. Assuming that the field vectors in a given plane would be the same even if the infinite hollow pipeline is terminated

at that plane, they calculated the radiation field at a large distance from the horn mouth using the Huygen's principle.

Almost at the same time, Southworth and King<sup>(3)</sup> published results of a detailed experimental investigation on conical horns. They described conical horn antennas with gain as high as 20 dB and suggested that these horns could be used in arrays to further improve the gain. They fabricated various components for the study, these include a crystal detector which they fabricated from silicone crystals. They give experimental data on both horns and pipes at  $\lambda = 15.3$  cms.

In the same year, Chu and Barrow<sup>(4)</sup> published another paper which contained quantitative curves using which sectoral and pyramidal horns could be designed. They compared rectangular and pyramidal horns and recommended rectangular horns because of the polarisation purity and possible independent control of beams in both the principal planes. They even went to the extent of predicting that several modes may be employed simultaneously to obtain a desired pattern. They also computed the radiation patterns and studied the effects of various horn parameters.

Later, Chu<sup>(5)</sup> attributed the failure of Kirchhoff's formula to give exact results to the misrepresentation of fields at the boundary surface. He employed a modified Vector-Kirchhoff formula derived by means of the vector equivalent of Green's theorem.

Rust<sup>(6)</sup> proposed a method by which he reduced the phase slip that occurs between the centre and edges of the aperture in an electrically short horn. He stacked parallel metal plates of varying lengths at the aperture; the shortest ones at the centre and longest ones at the edges. This way he could limit the phase error to less than  $90^\circ$ .

Rhodes<sup>(8)</sup> in 1948 made an extensive experimental study on the radiation pattern of horn antennas. He published data on various horns with axial lengths varying from  $1\lambda$  to  $50\lambda$  and flare angle from  $5^\circ$  to  $50^\circ$ . The measurements were made at 24 GHz. He also found that while taking antenna measurements, as the frequency of operation goes higher, the interference from nearby objects become more objectionable.

Horton<sup>(9)</sup> calculated the radiation pattern by the integral method. He found that, for small flare angles, the radiation pattern of waveguides and horns with the same aperture dimensions are the same. He achieved fairly good agreement between experiment and theory.

King<sup>(13)</sup> made a detailed experimental study on the radiation characteristics of conical horns. He defines an

'Optimum horn' as one with maximum gain for a given axial length. He also brings in the concept of 'effective area', and shows that for an optimum horn this is only 52% of the actual aperture area. The effective area of an infinitely long horn would only be 84% of its actual aperture area.

Schorr and Beck<sup>(14)</sup> gave a detailed physical explanation on how the mode filtering occurs in the attenuation region of the small flare angle horn. They calculated the radiation patterns of conical horns and show the results to be in good agreement with measured data.

Jakes<sup>(15)</sup> verified the expression for computing the gain of horn antennas and found that the error due to the edge effects may be ignored. He made experimental studies on the effect of distance between the two horns while taking measurements and found that the separation between their phase centres should be used in the expression instead of the separation between their apertures.

Braun<sup>(16)</sup> discussed the error due to the small separation between the horns while making gain measurements. According to him, the phase error already existing in the aperture of the horn also contributes to the error in measurement. He gives curves from which the measurement error can be estimated and corrections applied.

Braun<sup>(17)</sup> published details on electromagnetic horn design. He included tables giving the antenna gain as a

function of the aperture dimensions. He also describes how to design an optimum horn with equal E- and H-plane patterns.

James J. Epis<sup>(21)</sup> explained that unequal E- and H-plane patterns were due to the fringing electric fields in the E-plane, which increases the effective E-plane width. He put metallic nails radially on the rim of the conical horn, thereby reducing the fringing electric fields in the E-plane whereas nothing happens in the H-plane. Thus a circularly symmetric pattern could be obtained even for a circular polarisation.

Li and Turrin<sup>(26)</sup> predicted the near-field radiation patterns of a conical horn with a view of predicting near-field pattern of Cassegrain antennas fed by conical horns. Using a special phase-amplitude method, they measured the near field pattern inside an anechoic chamber and found it to be in good agreement with theory.

Russo et al.<sup>(27)</sup> calculated the total antenna pattern including the backlobe region using the diffraction theory. They considered cylindrical wave incidence on a thick edge.

Chu and Semplak<sup>(28)</sup> calculated the corrections to be applied to the standard gain formula. They provided tables giving gain corrections for various horn parameters. They conducted precision measurements of antenna gain and the effects due to interaction between the horns were evaluated.

Yu and Ruddock<sup>(31)</sup> analysed the radiation in the E-plane by the edge diffraction theory. They described the radiating mechanism as that of a primary source situated at the aperture and two secondary sources excited by the primary which are the aperture edges. The images of the first order diffraction centres on the aperture edges were also considered. They show that the edge diffraction theory, when the second order effects are also taken into account, is in good agreement with experiment.

Rumsey<sup>(33)</sup> proposed that a synthetic material that responds to both E- and H-fields identically would be needed to make horns with identical E- and H-plane patterns. An alternative to this is to cut grooves perpendicular to the axis in a propagating waveguide. Such a structure responds identically to both E- and H-fields.

Rao and Reddy<sup>(35)</sup> in 1967 studied the radiation from sectoral horn antennas. They modified the radiation patterns using metal plate lenses.

Jull<sup>(38,66,78)</sup> studied the gain of electromagnetic horns. He provided correction factors to be applied to calculated gains. He employed geometrical theory of diffraction to derive on-axis gain of E-plane sectoral horns.

Hamid<sup>(43)</sup> analysed the radiation from a conical horn by extending Brillouin ray tracing techniques to the three dimensional case.

By considering the diffraction from the aperture edges, Yu and Ruddock<sup>(51)</sup> calculated the H-plane radiation pattern of pyramidal horns.

Muelhdorf<sup>(68)</sup> calculated the phase centre of rectangular and conical horn antennas. He showed that the phase centres for H- and E-planes are different. The phase centre for any arbitrary plane can however be determined from the principal plane phase centres. He also showed that E- and H-plane phase centres can be made to coincide by properly choosing the side ratio.

Narasimhan and Rao<sup>(70,72)</sup> presented an analytically simple method to compute the radiation patterns and gain of  $TE_{11}$  mode excited conical horns of narrow and wide flare angles. They made use of the aperture field distribution assuming that the field distribution in the aperture plane would have been the same as would have been, had the sides of the horn extended upto infinity. Good agreement between theory and experiment suggests the validity of their method.

Kerr<sup>(80)</sup> reported about a short ridged broadband horn antenna operating successfully in a 12:1 band. He reported that a linear taper superimposed over the logarithmic curvature of the ridges improved the VSWR performance in the first octave, which was otherwise found objectionably high at the lower end of the band.

## 2.2 Corrugated Surfaces and Corrugated Horns

Simmons and Kay<sup>(32)</sup> in an attempt to reduce spill-over in the E-plane, developed a corrugated horn which they called the 'Scalar feed'. They found that 'a metallic surface corrugated with many closely spaced parallel transverse grooves present a reactive boundary with the same boundary conditions for both TE (Transverse Electric) and TM (Transverse Magnetic) waves at grazing incidence. If the grooves are made deep enough so that the surface reactance is capacitive, surface waves cannot be supported. A wide flare horn lined with such a reactive surface thus has the same boundary conditions for both polarizations'. They compared the radiation pattern of their feed with that of an ordinary horn and established the improvement.

Lawrie and Peters<sup>(34)</sup> devised two methods to reduce the E-plane minor lobes. These were: to use choke slots, and to use a corrugated surface. They found that the choke slots reduced the fringing electric fields outside the horn walls, thereby reducing the minor lobes. By probing the aperture they found that this resulted in an identical E- and H-plane distribution. In the second method, a corrugated, capacitive surface reactance surface, which does not support a surface wave was employed. They found that a horn with such a surface had its E- and H-plane phase centres at the same point. They reported a gain enhancement over the control horn.

Clarricoats<sup>(49)</sup> studied the conical corrugated horn by analysing the spherical hybrid modes. He derived expressions

for the radiation pattern of the corrugated conical horn and compared these with the experimental patterns due to Kay<sup>(32)</sup> and found that there was good agreement within the included angle of the horn. In another paper which closely followed, Clarricoats and Saha<sup>(50)</sup> analysed the same problem using a modal expansion method and Kirchhoff-Huygene method. They showed that both the methods give fairly good agreement with experimental results, even though the modal expansion method gives greater insight into the problem.

Jeuken<sup>(52)</sup> carried out experimental study on small flare angle corrugated conical horn. He found that small flare angle horns with large aperture diameters had a bandwidth of only 1:1.3. In a companion paper Jeuken and Lambrechtse<sup>(53)</sup> analysed radiation from a wide flare angle horn using spherical hybrid modes. This antenna has a large bandwidth. The theoretical values are found to be in agreement with experimental ones. These authors along with Jansen<sup>(75)</sup> conducted detailed theoretical and experimental study of the corrugated conical horn. They derived expressions for the radiation pattern which was validated with experimental data. They also found that for a given geometry of grooves and flare angles, a longer horn provided a better radiation pattern with steeper fall off near the edges.

Narasimhan and Rao<sup>(58)</sup> analysed the corrugated conical horn using the spherical hybrid modes. They provided a simple

solution which does not deviate much from the rigorous solution proposed by Clarricoats.<sup>(49)</sup> Their results are fairly accurate for the small flare angle horns with flare angles in the range of  $20^\circ$  to  $40^\circ$ . When larger flare angles are considered, the phase error across the aperture brings in greater errors. The same authors in another communication which followed<sup>(65)</sup>, analysed the case of wide flare angle horns. In this case the phase error introduced by the larger flare angle is also considered. Their computed patterns were shown to be in good agreement with experimental patterns due to Jeuken.<sup>(53)</sup>

Narasimhan<sup>(79)</sup> studied a corrugated conical horn with arbitrary corrugation depth  $\lambda/4 < h < \lambda/2$  and found that in the limiting case  $h = \lambda/2$ , the hybrid mode solution reduces to the solution for the  $TE_{11}$  mode in a conical horn, which implies that in this case the surface acts as a perfectly conducting surface. The same author in another paper<sup>(82)</sup> considered corrugated conical horn for the illumination of phased arrays. He has given details of optimally flared corrugated conical horns.

Baldwin and McInnes<sup>(60)</sup> derived the radiation pattern of corrugated conical horns. They considered a hybrid mode excited corrugated rectangular waveguide and derived the radiation patterns. Considering that the waveguide aperture has been slowly flared to become a horn,

they modified the expressions. Their predicted patterns were compared with experimental results. The small disagreement at higher frequencies is attributed to the fact that the thick edges of the horn act as flanges, which was not considered in the theory.

Mac A. Thomas<sup>(64)</sup> considered a single hybrid mode ( $HE_{11}$ ) excited and two hybrid mode ( $HE_{11}$  and  $HE_{12}$ ) excited corrugated waveguide radiator. He fabricated two, two hybrid mode feeds, one of which was used in a radio telescope and the other in Appollo 11 lunar programme. Measurements show that the two hybrid mode feeds are 12% more efficient than the one hybrid mode feed.

Clarricoats and Saha<sup>(73,74)</sup> published two papers, the first of which dealt with corrugated waveguide feeds and the second with corrugated horn feeds. They showed that with  $\lambda/4$  deep corrugations, an axially symmetric radiation pattern with good polarisation purity could be obtained. The waveguide feed also has fairly large bandwidth. In the second part, modal expansion method and Kirchhoff-Huygene method were employed and both gave good results.

Mentzer and Peters<sup>(81)</sup> studied in great detail the properties of corrugated surfaces for aiding corrugated horn design. They studied the power loss in the corrugations, the current flowing on the walls of the corrugations, the effect of corrugation period, the effect of corrugation

depth etc. They found that when the depth was  $\lambda/4$ , the energy was being pushed off from the surface. They also studied the ground plane-corrugated surface junction and found that it was the first few corrugations which are the most important.

Mizusawa et al.<sup>(77)</sup> studied the radiation from a conical corrugated horn. They defined two parameters 'X' and 't', upon which the horn performance depends. 'X' depends on the groove dimensions and 't' depends on the aperture diameter, horn length and observation distance. They specified optimum values for these parameters.

Dragone<sup>(90)</sup> fabricated a corrugated conical horn feed which successfully operated in the 17 GHz and 29 GHz band. In this bandwidth the radiation had good polarisation purity. The feed was designed to operate in the fundamental mode.

Baldwin and McInnes<sup>(83)</sup> described a corrugated horn with corrugations only in the E-plane walls. Such a horn can handle linearly polarised radiation as efficiently as a horn with corrugations on all four walls. They considered the waveguide to horn junction and could successfully design a throat with a fairly low VSWR in the band 7.5 GHz to 10 GHz.

Terzouli and Peters<sup>(93)</sup> calculated the VSWR of the E-plane dihedral corrugated horn. They found that the

main contributors to VSWR were the waveguide to horn junction and the region of onset of corrugations. Using a curved horn-waveguide junction, they reduced the first term and a tapered corrugation geometry reduced the second term.

### 2.3 Beam Shaping of Sectoral Horn Antennas

Owen and Reynolds<sup>(7)</sup>, in 1946, attached metal flanges to the aperture of H-plane sectoral horns and studied their E-plane patterns. They found that the flanges are very effective in controlling the E-plane pattern. To explain this phenomenon, they suggested the line source theory, which considers the horn aperture as a primary source and the flanges as secondary sources excited by the primary. The radiation is considered to be the resultant of all these three radiators.

Butson and Thompson<sup>(18)</sup> studied the effects of metal flanges on the radiation patterns of sectoral horns and waveguides. They studied the effects due to different flanges at different frequencies and found that the E-plane pattern of H-plane sectoral horns were modified. According to them there was no change in the H-plane pattern of E-plane sectoral horns.

La Grone and Roberts<sup>(30)</sup> put a choke flange at the aperture of the rectangular horn and found that it suppressed the minor lobes in the E-plane pattern. They suggested an approximate theory by considering the E-plane edges of the

aperture as two identical isotropic radiators or line sources. A  $\lambda/4$  choke was found to give good suppression in the E-plane.

Nair and Srivastava<sup>(36)</sup>, in 1967, were the first to include a third parameter, namely the flange position in the study of flanged sectoral horns. Till then flanges were kept only at the aperture of the horn. They found that if the flanges are pulled back, it could focus or broaden the radiation pattern. They defined certain flange positions as optimum (O-position) and minimum (M-position) positions. They analysed this system using the theory proposed by Owen and Reynolds.<sup>(7)</sup>

Nair et al.<sup>(39)</sup>, in 1968, were the first to find that the H-plane pattern of E-plane sectoral horns could be controlled with metallic flanges. This was contrary to the then existent belief that the radiation pattern of E-plane sectoral horns could not be controlled with flanges. However this phenomenon was observed only for included angles less than  $90^\circ$ . They also found that the optimum flange angle increased as the distance of the flanges from the aperture increased.

Nair et al. in another theoretical analysis<sup>(40)</sup> treated the cases of flange width asymmetry and flange angle asymmetry. When the asymmetry terms in the expression were made zero, their expressions reduced to the form derived by Butson and Thompson.<sup>(18)</sup>

Nair et al.<sup>(41)</sup> in another paper published in 1968 described in great detail the effect of flange position on the radiation pattern of H-plane sectoral horns.

Koshy et al.<sup>(42)</sup> considered the asymmetries in the amplitude of excitation of the flanges and derived expressions for the radiation pattern of an H-plane sectoral horn fitted with an asymmetric flange system.

Nair et al.<sup>(44)</sup> observed that satisfying certain conditions the flanges could completely eliminate the radiation in the H-plane of an H-plane sectoral horn. This phenomenon they called 'Beam Elimination', and proposed a qualitative explanation on the basis of the line source theory.<sup>(7)</sup>

Koshy et al.<sup>(45)</sup> discussed in detail the effect of conducting flanges on the radiation pattern of E-plane sectoral horns in the H-plane.

Singh et al.<sup>(47)</sup> in 1969 conducted experimental studies on the effect of asymmetric flanges on the radiation patterns. They found that an asymmetric flange invariably tilted the radiated beam to either side depending on the asymmetry.

Nair<sup>(59)</sup> derived expressions for the radiation pattern of a flange mounted sectoral horn antenna, considering the primary horn as an aperture antenna and taking into consideration its radiation pattern. In the earlier works the primary horn antenna was considered to be an isotropic linear source.

Koshy et al.<sup>(63)</sup> in 1970 published details of an experimental investigation on the effect of flanges on the radiation pattern of horn antenna. The same authors in 1971 published a report<sup>(71)</sup> on the theoretical analysis of the flanged sectoral horn antenna. Comparison with experimental results show fairly good agreement.

Hariharan and Nair<sup>(20)</sup>, in 1961, reported that the E-plane radiation pattern of E-plane sectoral horns could be modified using a grill system attached to its mouth. Using this method they could obtain very narrow E-plane beams. The same authors in 1962<sup>(23)</sup>, studied the effect of conducting grills on the VSWR of sectoral electromagnetic horn antennas. With a single grill system moved across the aperture of the horn, they determined two optimum positions when the flanges are kept at which, the VSWR is a minimum. At these positions the axial flow of power increased. They devised a double grill system with one grill at each of these positions. They observed that in this configuration the axial flow of power was very high and that the VSWR was a minimum.

Nair et al.<sup>(46)</sup>, in 1969, studied in detail the sectoral horn antennas fitted with grills. They calculated the radiation pattern of this system by considering the re-radiation of energy by the grills excited by the horn. The experimental patterns are found to be in good agreement

with the theoretical ones. The same authors in another paper<sup>(48)</sup> reported results of a detailed experimental investigation.

Srivastava et al.<sup>(84)</sup> reported a slotted flange system which produced a square radiation pattern. They reported an almost ideal 10 dB taper with sharp fall off beyond the 10 dB points. The 10 dB beam width was observed to be very high, which is very suited for feeding deep paraboloids.

Bhan et al.<sup>(98)</sup> found that by inclining the slotted flanges reported earlier<sup>(84)</sup>, good control on the beamwidth of radiation from a waveguide could be obtained.

Nair and Mathews<sup>(89)</sup> observed striking similarities between a flanged sectoral horn and corner reflector antenna. They compared different properties and established that they behave similarly. They suggested that the corner reflector theory could be more suited to explain the behaviour of flanges.

Nair et al.<sup>(85)</sup>, in 1976, found that dielectric flanges are equally effective in controlling radiation from sectoral horn antennas. They could reproduce all the effects observed with metallic flanges with dielectric flanges. They also tried using a hybrid system with one metallic and one dielectric flange element and found that the beam was tilted towards the side of the metallic element.

Cohn<sup>(67)</sup>, in 1970, used flare angle variations in pyramidal horns to control E-plane radiation patterns.

Nair and Mathew<sup>(87)</sup> used a flanged sectoral horn antenna as a feed for parabolic reflector antenna and studied the secondary pattern.

From this review the significance of the studies of horn antennas is evident. The major directions in which efforts are being made are also clear. It gives an insight into the behaviour of the simple horn antenna as well as the more complex systems like corrugated horns and flanged sectoral horns. An important point to be noted here is that the effect of corrugations on the metallic flanges attached to sectoral horns was not a subject of investigation. This work is primarily directed towards this problem.

## CHAPTER III

### EQUIPMENT USED AND METHODS OF MEASUREMENT

3.0 This chapter describes the various equipment used and the methods employed in the measurement of different antenna parameters, which are of interest in the present investigation.

#### 3.1 Description of the Equipment Used

The investigations carried out in this study were conducted at various frequencies in the X- and S-bands. In the X-band, studies were made at four different frequencies, 8.7 GHz, 9.4 GHz, 10.15 GHz and 11.05 GHz. In the S-band, measurements were made at 2.6 GHz. The experiments were conducted mainly in the X-band. The measurements in the S-band were performed with a view to verify the results obtained in the X-band, and hence only a few selected cases were studied. The various equipment used in this study are described below.

##### 3.1(i) Microwave Source

In the X-band, both reflex klystrons and Gunn oscillators were employed as sources at different frequencies.

Klystron oscillator was employed to obtain microwave signal of frequency 9.4 GHz. A Gunn oscillator was employed to obtain other frequencies, viz., 8.7, 10.15, and 11.05 GHz.

The klystron is directly coupled to the waveguide assembly through a klystron mount. In this, the output probe of the klystron enters the waveguide through a hole on the broad side of the waveguide. A klystron power supply meets the power requirements of the klystron oscillator. There is also provision for amplitude modulation of the output from the klystron. By varying the pressure applied to a small diaphragm, the volume of the resonant cavity in the klystron can be altered, and hence the frequency of operation can be altered, through a limited range.

The Gunn diode is mounted inside a waveguide section, one end of which is terminated in a precisely calibrated movable shorting plunger. The waveguide section between the plunger and the diode acts as a resonant cavity, and is used to control the frequency of operation of the oscillator. The reading of the precision short can be converted to the frequency of operation of the Gunn oscillator using a calibration curve supplied by the manufacturer. A 'Gunn power supply' provides the D.C. power required for the oscillator. A PIN diode is used for amplitude modulating the microwave signal. The Gunn power supply also provides the square pulses required for the PIN diode. Good isolation

is provided between the Gunn oscillator and the PIN diode, since the latter reflects back a portion of the microwave power.

In the S-band, a compact U.H.F. source is used. This contains a klystron, a tunable cavity, and a special tracking potentiometer. To tune the oscillator, resonant frequency of the cavity is varied and simultaneously the reflector voltage is also varied to sustain oscillations. The output from the klystron is fed through a co-axial cable to the waveguide assembly.

### 3.1(ii) Waveguide Components

A three port circulator with one port terminated in a matched termination (dummy load) is used as the isolator.

To measure the frequency of the microwaves in the X-band, a cavity wave meter with direct reading facility is used

The microwave power output from the oscillator is monitored with a directional coupler and detector mount to ensure that there are no power fluctuations.

A variable attenuator is employed to control the power level.

### 3.1(iii) Sectoral Horns

Sectoral horns are one of the most important components used in this study. In the present study, H-plane

sectoral horns are employed. These have been fabricated copper sheets. Extreme care was taken to avoid all sorts mechanical imperfections in the fabrication of the horns. The inside walls are highly polished. Precision waveguide flanges supplied by standard manufacturers are fitted to these horns. Fig.3.1(iii)(a) is a photograph showing the sectoral horns used. Table 3.1.I gives the different parameters of the sectoral horns used.

#### 3.1(iv) Flanges

Metallic flanges are the most important components used in this study. These flanges are simply metallic plane or corrugated sheets with specific dimensions and other parameters. They will be attached on the external side of the horn with provision to adjust the included angle and the relative position with respect to the horn aperture. A schematic diagram of a flange-mounted sectoral horn is shown in Fig.1.4(b). In the present study, three types of flanges are used:

- a) Conventional plane flanges
- b) Corrugated flanges with corrugations perpendicular to the E-vector
- c) Corrugated flanges with corrugations inclined at  $45^{\circ}$  to the Electric vector.



Fig.3.1(iii)(a) The sectoral horns used in this study.

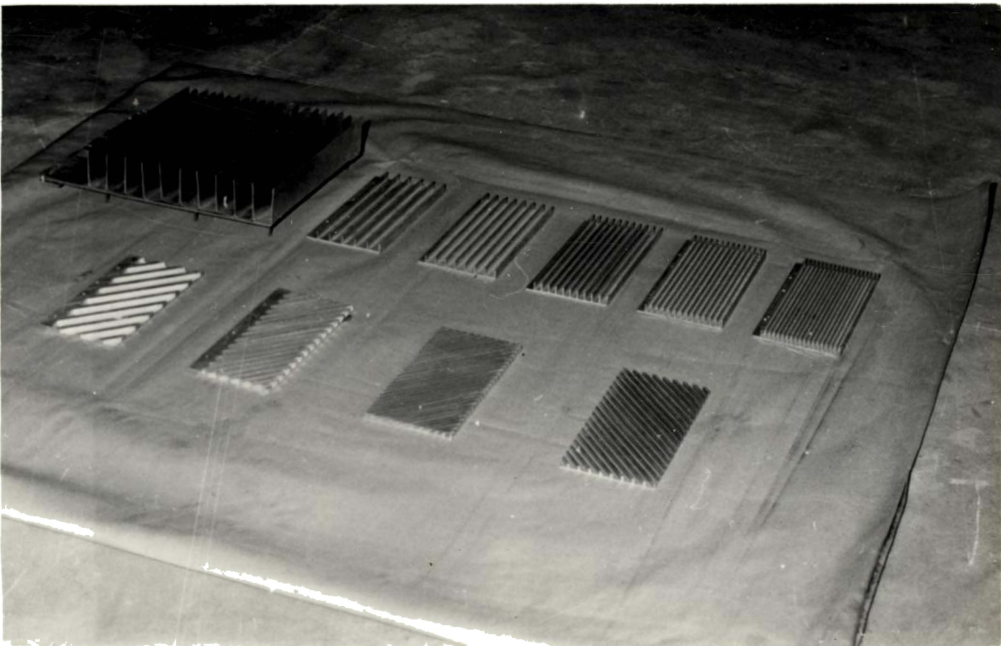


Fig.3.1(iv)(a) The different flanges used in this study.

Table 3.1 (I)

Parameters of the different H-plane sectoral horns used in this study

Horn No.	Band	Horn length (cms)	Aperture in H-plane (cms)	Aperture in E-plane (cms)	Flare angle (deg.)
X 1	X	23.5	10	1	24
X 2	X	14.1	5.5	1	22
X 3	X	16.7	6.5	1	22
S 1	S	42.9	23	3.4	30

Fig.3.1(iv)(a) is a photograph of the different flanges used in this study. The method of fabrication of corrugated flanges is explained in detail in section 3.6. Flange angle and flange position are two important parameters, whose effects in particular are studied in this thesis. For a given set of flange and horn at a given frequency, these are the only variables. Hence arrangements were made to position the flanges precisely on the sectoral horns. This arrangement consists of a frame which moves over the sectoral horn by means of a rack and pinion arrangement. Flange elements are attached to this frame by means of hinges for easily varying the flange-angle. The distance of the flange from the aperture of the horn can be read from a scale attached to the sectoral horns. The flange angle is adjusted using a high precision 'universal bevel protractor'. Fig.3.1(iv)(b) is a photograph showing the flange mounted sectoral horn as the receiver of microwaves, inside the anechoic chamber. Table 3.1.II gives the different parameters of the flanges used.

### 3.1.(v) Other Facilities

Earlier part of this work was conducted inside the laboratory with ordinary facilities. In this set up the antenna under test is mounted on a small wooden turn-table (positioner) capable of rotation about a vertical axis. The

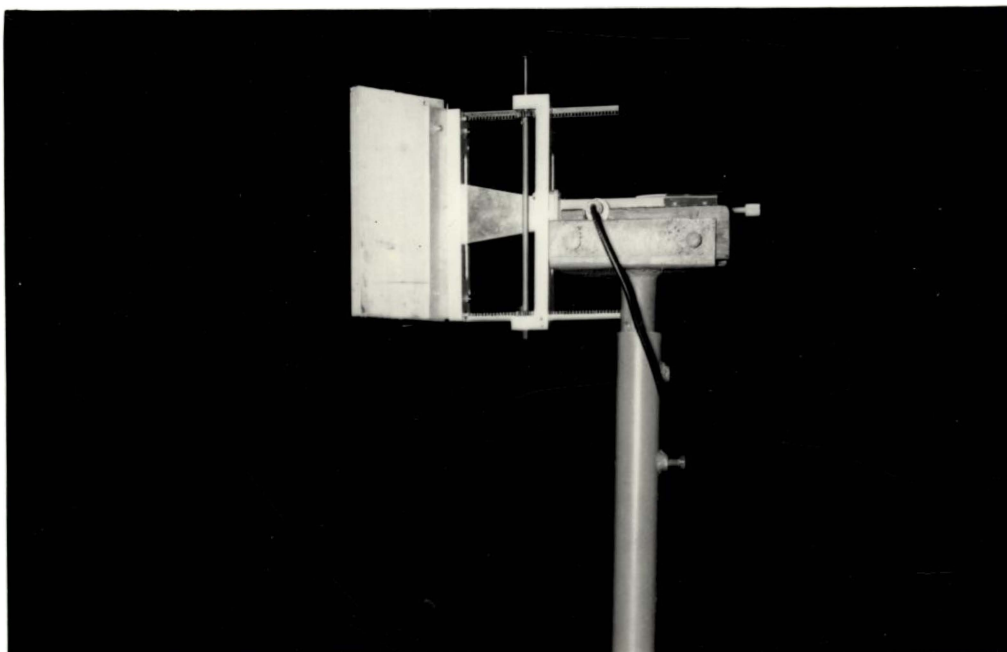


Fig.3.1(iv)(b) The flange mounted sectoral horn used as the receiver.



Fig.3.2(a) The turn-table used for plotting the radiation patterns manually.

Table 3.1(II)

Parameters of the different flanges used  
in this study

Flange No.	Width (mm)	Corrugation depth (mm)		Corrugation period a (mm)	Slot width d (mm)	a/d	Type of flange
		$h_1$	$h_2$				
1	100	10	10	17	--	--	Straight corrugations
2	100	10	10	13	--	--	-do-
3	100	10	10	9	--	--	-do-
4	100	10	10	7	--	--	-do-
5	100	10	10	5	--	--	-do-
6	265	50	10	24	--	--	-do-
7	100	--	--	--	--	--	Plane
8	100	4.5	--	20	14.5	1.38	Inclined corrugations
9	100	4.5	--	6	4.5	1.33	-do-
10	100	4.5	--	10	7	1.43	-do-
11	100	4.5	5.5	8	6	1.33	-do-

turn-table is manually rotated and the received power is measured using a spot galvanometer for each setting of the turn-table.

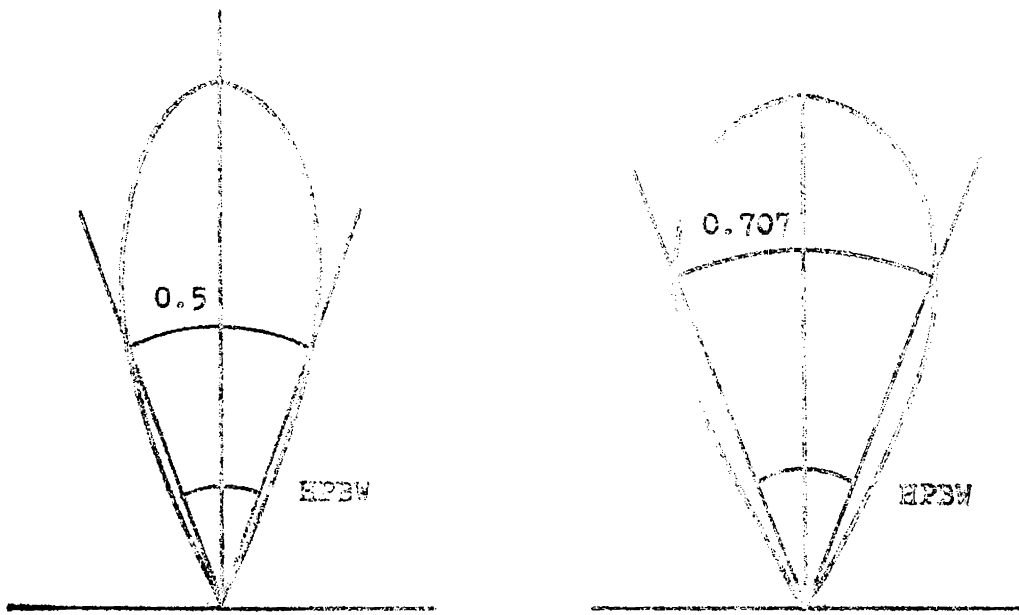
Later, a modern microwave anechoic chamber with facilities for automatic pattern recording was used for the investigation. A considerable amount of time and effort was spent for developing this facility in the microwave laboratory. The automatic pattern recording facility consists of an antenna turn-table, and an X-Y/t recorder. The antenna turn-table is capable of rotation about a vertical axis, and is driven by a reversible electric motor. Using gear arrangements, the speed is reduced to 1 rpm. A linear wirewound potentiometer is arranged so that its shaft also rotates at the same speed as the turn table platform. Hence, when a steady D.C. is applied across the potentiometer, the voltage at the wiper-contact would be directly proportional to the angle through which the platform has rotated. This voltage is fed to the X- input of the X-Y recorder, to synchronise the X- movement with the rotation of the antenna under test. The signal received by the antenna is fed to the Y-axis of the recorder after rectification. The turn-table has brush and ring contacts to take the signal output from the receiving antenna to the recorder. This avoids the possibility of twisting of lead wires. The X- and Y- outputs from the turn-table are fed through shielded cables to the

recorder. Care is taken to reduce noise from external sources by proper shielding. The turn-table is fully automatic and can be controlled manually from the control room of the chamber. The X-Y recorder, turn-table control system, transmitter etc., are situated inside the control room adjacent to the anechoic chamber. Details of design and construction of this anechoic chamber are given in appendix I.

### 3.2 Recording of Radiation Patterns

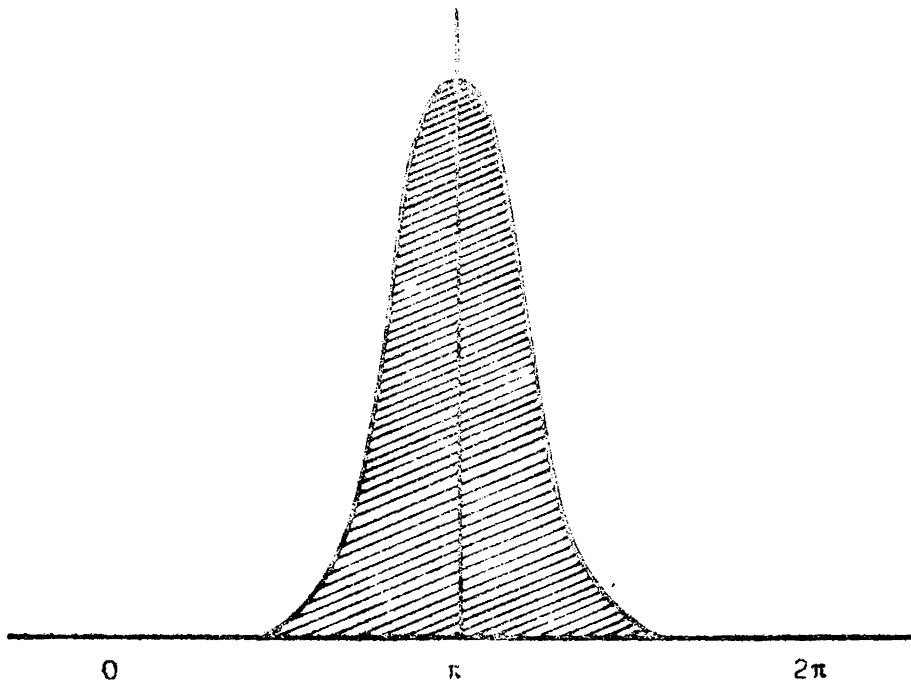
The radiation pattern of an antenna is the plot of the distribution of radiated energy as a function of direction. Radiation characteristics of an antenna can be presented either as power patterns or as intensity patterns. In this work, the radiation patterns presented are power patterns. Intensity patterns are employed only in the calculation of antenna gain by the method of pattern integration. Fig.3.2(e) shows typical patterns.

Different methods can be employed to measure radiation pattern. In one case the test antenna is used as the transmitter of microwave signals. The receiver antenna, which may be either directional or isotropic (it is more advantageous to use directional antennas to reduce noise and interference from nearby r.f. sources, metallic objects etc.), is moved along the circumference of a circle of radius  $R$ , with the transmitter at its center. The signal received is



Power pattern

Intensity pattern



Intensity pattern in rectangular co-ordinates.

Fig.3.2(e) Typical power and intensity patterns.

plotted against the angular position of the receiver antenna with respect to the transmitter. This method is very cumbersome and requires a lot of space.

The same results can be obtained in a much simpler way. Keeping the receiver fixed, the antenna under test is used in the transmit mode and it is rotated about a vertical axis. A plot of the signal from the receiver antenna against the angle through which the test antenna has rotated with respect to a reference direction gives the radiation pattern.

According to the theorem of reciprocity in antennas, radiation pattern of an antenna is the same in both the transmit and receive modes. Hence the test antenna can be used as the receiver, and another standard antenna as the transmitter.

In this study, the last method was used, since it is the most simple and convenient of the three. As mentioned elsewhere, the earlier part of the work was done with a small wooden turn-table which can be rotated manually. A photograph of this arrangement is shown in Fig.3.2(a). The latter part of the work was done inside an anechoic chamber. The test antenna is mounted on an antenna turn table. This system is kept in the quiet zone of the anechoic chamber. The transmitting horn is kept at the apex of the tapered portion. The distance  $R$ , between the transmitting and receiving antennas is greater than  $2D^2/\lambda$ , where  $\lambda$  is the operating

wavelength and  $D$  is the larger dimension of the receiving antenna (This corresponds to the inner limits of the far field region. Ideally the test antenna has to be illuminated by a plane wavefront. Although this requires an infinite separation between the antennas theoretically,  $2D^2/\lambda$  is taken as a practical limit.<sup>(29)</sup> This corresponds to variation of phase which is less than  $\lambda/16$  across the aperture of the antenna. Another consideration is to reduce the mutual interaction between the antennas). Fig.3.2(b) is a schematic representation of the experimental arrangement. The signal received by the receiving antenna is rectified using a microwave diode (Type IN 21C, IN 23C, and IN 415B are used. IN 415B has the advantage that it has a detachable shoe contact, permitting reversal of polarity). The rectified D.C. output from the receiver is fed through shielded cables to the Y- input of the recorder. Information regarding the azimuthal position of the antenna is fed to the X- input of the recorder.

The highly sensitive recorder used has a sensitivity of 2 microvolt ( $\mu\text{V}$ )/millimeter. Hence superheterodyne reception and amplification was not found necessary. Fig.3.2(c) is a photograph of the transmitter set up used in the X-band. The PIN modulator is not used here since CW operation was desired.

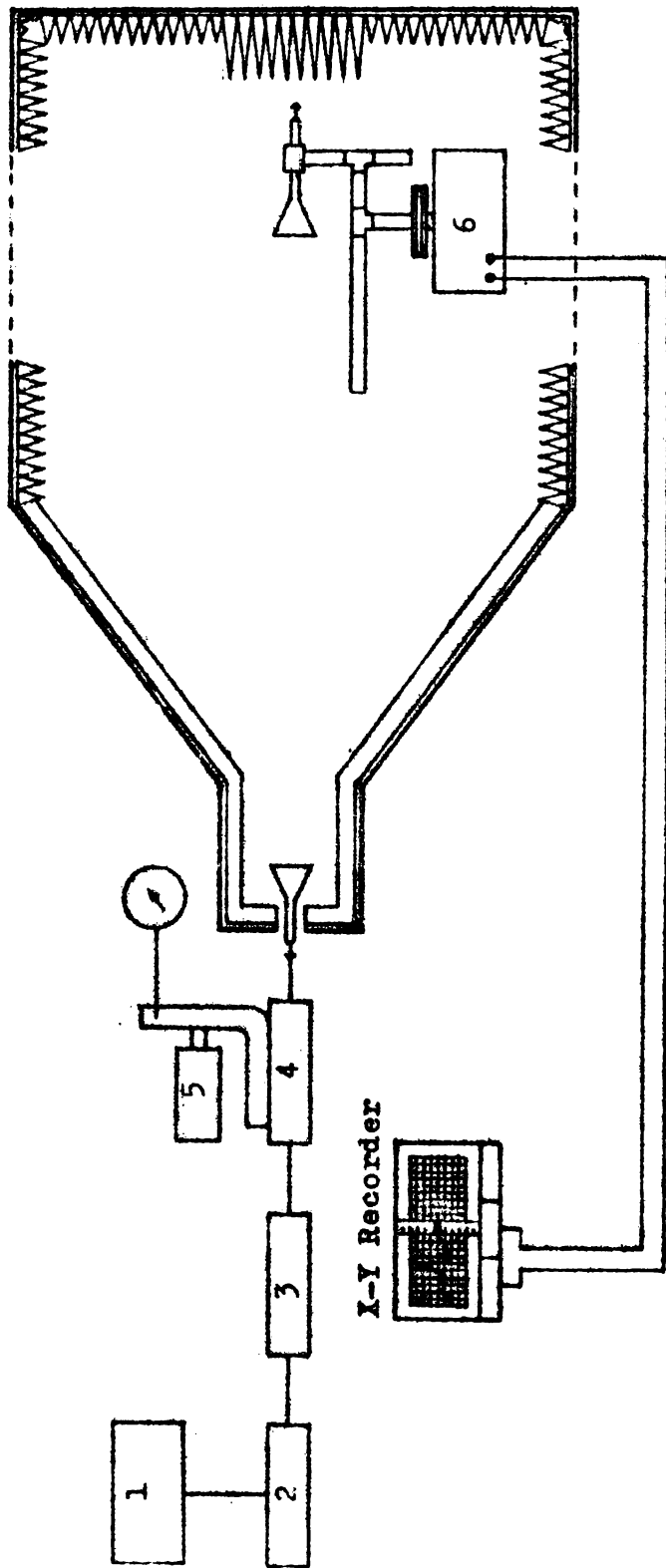


Fig. 3.2(b) Schematic representation of the experimental set up used to plot the radiation patterns. 1. Gunn Power Supply, 2. Gunn Oscillator, 3. Isolator, 4. Directional Coupler, 5. Frequency Meter, 6. Turn-table.

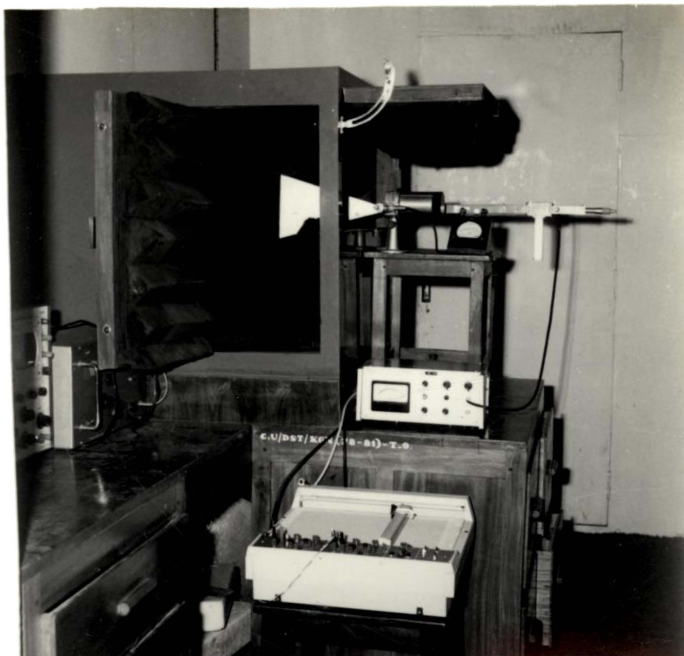


Fig.3.2(c) Transmitter set up for plotting  
radiation patterns at X-band.



Fig.3.2(d) Transmitter set up for plotting  
radiation patterns at S-band.

Fig.3.2(d) is the transmitter set-up used in the S-band. Here the frequency meter, power level monitor, and isolator, are dispensed with, since the compact UHF source employed has these facilities incorporated in it. A variable attenuator included in the waveguide assembly provides some extra isolation. The UHF source has a calibrated dial which gives the frequency of operation. Its calibration was checked using the slotted line technique, and corrections were applied wherever necessary.

### 3.3 Measurement of VSWR and On-axis Power Density

The power radiated along the axis of the antenna is termed the "On-axis power".<sup>(36)</sup> This is an important parameter of the system, since in communication applications it is in the power radiated along the axis of the system that we are most interested.

The VSWR of the antenna is the measure of the impedance mismatch of the antenna. Hence it is also an important parameter from the applications point of view. When the antenna is not perfectly matched, it reflects a portion of the energy back into the source. The advancing wave from the source and this reflected wave interact to set up standing waves in the transmission line. The Voltage Standing Wave Ratio is the ratio of the Electric field intensity at the voltage antinode to that at the node.

It is defined as  $S = \frac{E_{\max}}{E_{\min}}$

It can be seen that in the case of perfect match,

$$E_{\max} = E_{\min}.$$

Hence  $S = 1$ .

In the other extreme case,  $E_{\min} = 0$ .

Hence  $S = \infty$ .

Some authors<sup>(12)</sup> define VSWR as  $S = \frac{E_{\min}}{E_{\max}}$ . In this study the first definition is followed, since it is the more widely accepted one.

Measurement of VSWR and on-axis power were conducted simultaneously using the experimental set up shown schematically in Fig.3.3(a). The set up is kept inside the anechoic chamber to avoid interference from other objects. The termination VSWR<sup>(99)</sup> of the chamber is well within the limits to make accurate VSWR measurements. It was also verified that the interaction between the receiving horn and the test antenna is sufficiently low, not to interfere in the VSWR measurements.

To measure the VSWR, the conventional slotted line technique was employed. The tunable probe attached to the carriage was carefully tuned at each frequency. The probe penetration is reduced to the minimum required, to reduce probe interaction. Further, care was observed to keep the probe at the minimum position while on-axis power readings

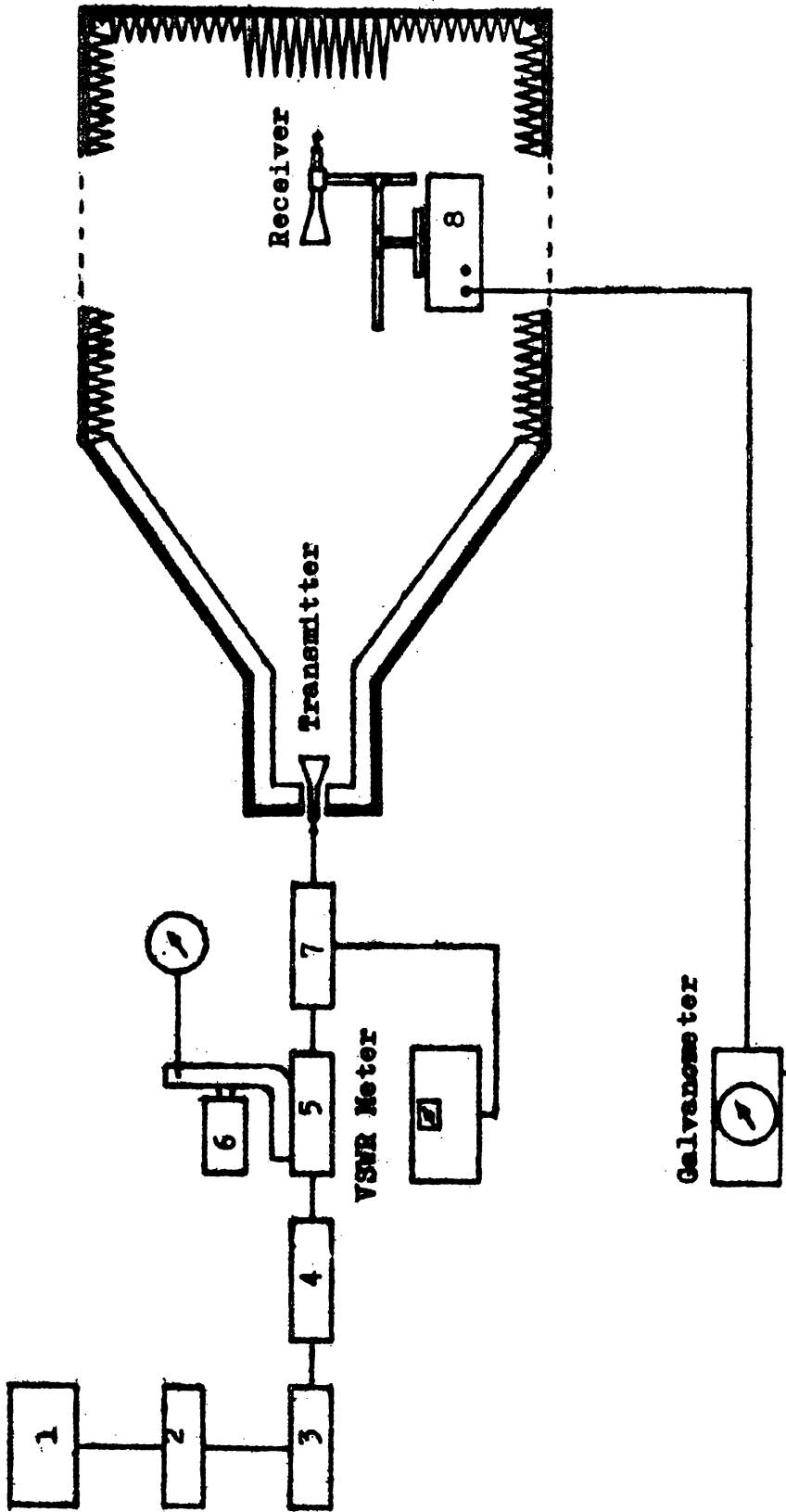


Fig.3.3(a) Schematic diagram of the experimental set up used to measure the VSWR and On-axis power of the corrugated flange mounted sectoral horn.

1. Gunn power supply, 2. Gunn oscillator, 3. Isolator, 4. PIN modulator,
5. Directional coupler, 6. Frequency meter, 7. Slotted section, 8. Turn-table.

were noted to reduce effects of probe interaction. A direct reading VSWR meter was employed to measure the VSWR. This instrument requires that the microwave signal be amplitude modulated at 1000 Hz. A PIN modulator was used for this. To make more accurate measurement of VSWR, the maximum and minimum values of the crystal current was measured with a high sensitivity 'Hewlett Packard' X-Y recorder (The sensitivity of the instrument is better than  $2 \times 10^{-9}$  amps/millimeter). In this set up the recorder is used as a meter only, and the position of the pen is read from the graph paper. Since a crystal is used as the detector, the output current is proportional to the power. Hence VSWR is given by,

$$S = \frac{\sqrt{P_{\max}}}{\sqrt{P_{\min}}} .$$

This value is calculated and tabulated. Fig.3.3(b) is a photograph of the experimental set-up used in the X-band.

To measure the on-axis power, a small pyramidal horn receiver was kept at the axis of the test antenna. The output from the detector mount is fed through shielded cables to the sensitive galvanometer in the control room. The reading is noted manually.

### 3.4 Gain and Half Power Beam Width

Gain of the antenna is defined as the ratio of the maximum radiation intensity in a given direction to the radiation intensity in that direction from an isotropic

antenna with the same power input. In this study, we are interested in the pattern shape and gain of the antenna in the plane orthogonal to the one in which it is flared. Hence the gain in only the E-plane of the H-plane sectoral horns were determined.

The gain in only one plane can be determined by the pattern integration method. In this method, numerical integration of the intensity pattern in rectangular coordinates is employed.

$$\text{Gain } G = \frac{2\pi I_{\max}}{\int_0 I_{\theta} d\theta}$$

where  $I_{\max}$  is the intensity in the direction of maximum radiation and  $I_{\theta}$  is the intensity in any direction, whose bearing angle is  $\theta$ .

$I_{\theta} d\theta$  is given by the area between the intensity curve and the  $\theta$ -axis within the limits  $\theta = 0$  and  $2\pi$ . Gain expressed in decibels is given by

$$G_{\text{dB}} = 20 \text{ Log}_{10} \frac{2\pi I_{\max}}{\int_0 I_{\theta} d\theta}$$

Beam width of the antenna is a measure of the sharpness of its radiation pattern. It is the angle between two directions, on either side of the maximum, along which the power has fallen by a specified amount below the maximum.

The most generally referred values are the half power beam width (3dB), and 10dB beam width. Occasionally other values like 20dB width, and separation between the first nulls on either sides are also specified. In the present study, only the HPBW is measured. It can be measured from either the power pattern or the intensity pattern. Fig.3.2(e) shows a typical power pattern and the corresponding intensity pattern. When it is determined from the power pattern, the angular separation between the points on either side of maximum where the power has fallen to half its value along the maximum is measured. In the case of the intensity pattern, the angular separation between the points where the intensity has fallen to 0.707 of its value along the maximum is measured.

### 3.5 Polarisation Measurements

To measure the axial ratio of an elliptically polarised antenna, the conventional method<sup>(22)</sup> is to use a rotating linearly polarised antenna as the transmitter, while recording the pattern. The transmitter is rotated at a comparatively high speed compared to the scan rate. This method has the advantage that the polarisation ratio in all the parts of the pattern, i.e., main lobe and side lobes, are obtained.

In this investigation, the axial ratio of elliptically polarised antennas were studied using a much simpler experimental set up which does not employ a rotary joint.

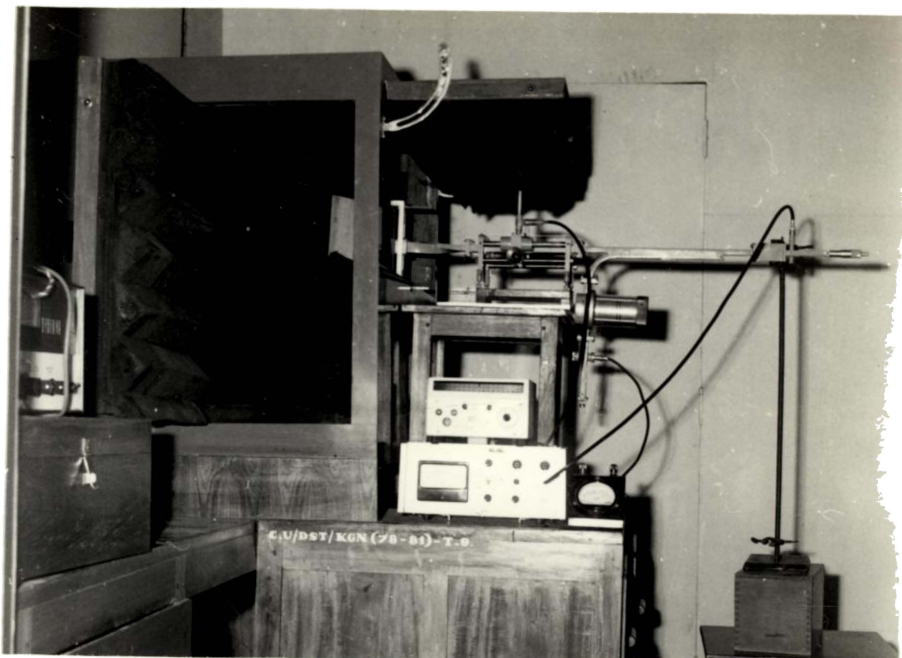


**Fig.3.3(b)** Experimental set up used to measure the  
VSWR of the system in the X-band.



**Fig.3.5(a)** The experimental set up used to  
measure the axial ratio.

The transmitting horn which is linearly polarised and the Gunn oscillator are mounted on a stand, which permit rotation of the horn about a horizontal axis. There is a calibrated dial which shows the angle through which the transmitter has rotated. Fig.3.5(a) is a photograph of the experimental set-up.

To start with, a radiation pattern is plotted keeping the transmitter vertically polarised. The transmitter is rotated through  $45^{\circ}$  and the new pattern plotted over the first one. The patterns are recorded with the transmitter set at  $90^{\circ}$  and  $135^{\circ}$  also. The polarisation ratio along any direction is given by the maximum separation between these curves corresponding to that angle.

### 3.6 Fabrication of Corrugated Flanges

Corrugated flanges for the investigations carried out in this study were made by cutting deep grooves on the surface of solid aluminium blocks. Aluminium was chosen as the material for making flanges for the following reasons:

- 1) Low weight. Aluminium is very much lighter than copper and brass, the ratio being less than  $1/3$ .
- 2) Low cost. Aluminium costs only less than one-fifth of the cost of copper, volume to volume.

- 3) Fairly good conductivity. Even though the conductivity of aluminium is slightly less than that of copper, it is higher than that of other contestants, like brass, steel etc.

Grooves were cut on the surface of solid aluminium blocks by shaving off metal using a shaping machine. In this, the block is firmly held in a vice on the base of the machine. A sharp cutting tool is attached to a movable head, which makes longitudinal sweeps over the block. By lowering the head so that the tool touches the block, a little metal is scooped away as the head makes one sweep. The head is lowered little by little, after each sweep, till the required depth is attained. The tool is now moved to a new position, so that it cuts another groove along side the first one. The depth of the grooves, the wall thickness between adjacent grooves, and the width of the grooves, are carefully controlled.

Another method employed the use of a milling machine. In this the cutting tool rotates around its axis at a very high rate, and can simultaneously travel along a straight line (Usually, the bed on which the work piece is held is moved instead of moving the tool). The aluminium block is firmly held on the machine bed and the rotating tool moves over this. The tool removes the material which comes in its way. Here also, the penetration, slot width, and

separation are carefully controlled. This method is more accurate than the earlier one, and is more convenient, especially when the wall thickness is very small.

Since the flange dimensions depend on the wavelength of excitation, much larger flange elements than those used in the X-band were required in the S-band. Large aluminium blocks of the size required were not available. Again the weight of flanges made from solid blocks would be prohibitively high in the S-band. Hence flanges were made from aluminium sheets. A large sheet was folded into the required shape. Another flat sheet was attached to the back of this to give good mechanical strength. Care was taken to avoid all sorts of mechanical imperfections, and it was contended that the slight imperfections that may still persist can be ignored in view of the larger wavelength. The flanges made in this way are very light, in spite of the larger dimensions, which is a great advantage. This is an advantage over the other solid type flanges.

## CHAPTER IV

### EXPERIMENTAL RESULTS

4.0 This chapter is devoted to the description of the experimental investigations carried out. The results obtained with corrugated flanges and plane flanges are compared. The experimental investigations were carried out in both the X- and S-bands. In the X-band, four different frequencies viz., 8.7, 9.4, 10.15 and 11.05 GHz, were used. In the S-band, 2.6 and 3.2 GHz were used. Different sets of flanges and horns were used in the X- and S-bands. The antenna characteristics which are studied in detail for the purpose of the present investigation are:

- 1) Variation in VSWR
- 2) On-axis power density (Power radiated along the axis)
- 3) Radiation pattern
- 4) Half Power Beam Width (HPBW)
- 5) Gain.

The dependence of these characteristics on flange parameters like flange angle, corrugation period and frequency of operation are investigated and the results presented. Results of

the theoretical analyses based on the model proposed by Butson and Thompson<sup>(18)</sup> are described in a later chapter.

Before concluding the chapter, results of a preliminary investigation on the possibility of developing a circularly polarised flanged horn system is described.

#### 4.1 Voltage Standing Wave Ratio (VSWR)

##### 4.1(i) Dependence of VSWR on Flange Position

Flanges are attached to the flange positioner as shown in the figure 3.1(iv)(b). The position of the flanges relative to the horn aperture is adjustable. The VSWR is measured using the standard slotted line technique.

It is observed that the VSWR of the flange mounted system is very much dependent on the position of the flanges. This is found to be true with all flanges, flange angles and frequencies. The VSWR of the system fluctuates between sharp maxima and minima, as the position of the flanges is varied with respect to the horn aperture.

Figs.4.1(a)-(d) shows the variation of VSWR as the position of the flanges are changed. The variation of the on-axis power density with changes in flange position are also studied. The results of this study is given in sec.4.2(i). A comparison between the results of these two studies would be useful and this is given in sec.4.2(i). From the figures, it can be seen that the shape of the

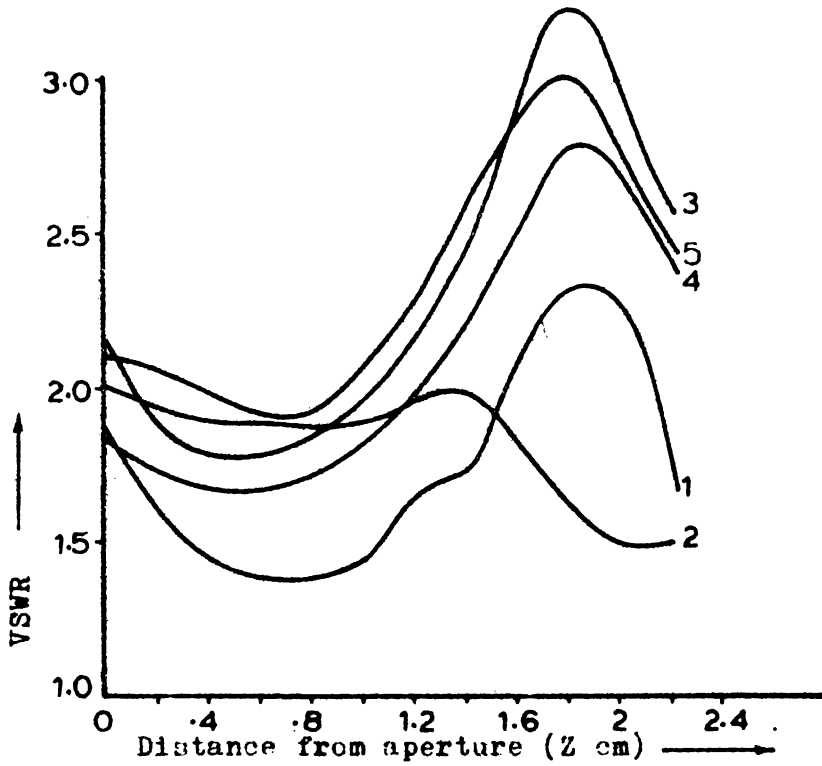


Fig.4.1(i)(a) Variation of VSWR with flange position.  $2\beta = 90^\circ$ ,  
 Frequency = 8.7 GHz, Horn -  $H_3$ . 1 -  $N = 6$ , 2 -  $N = 8$ ,  
 3 -  $N = 11$ , 4 -  $N = 14$ , 5 -  $N = 19$ .

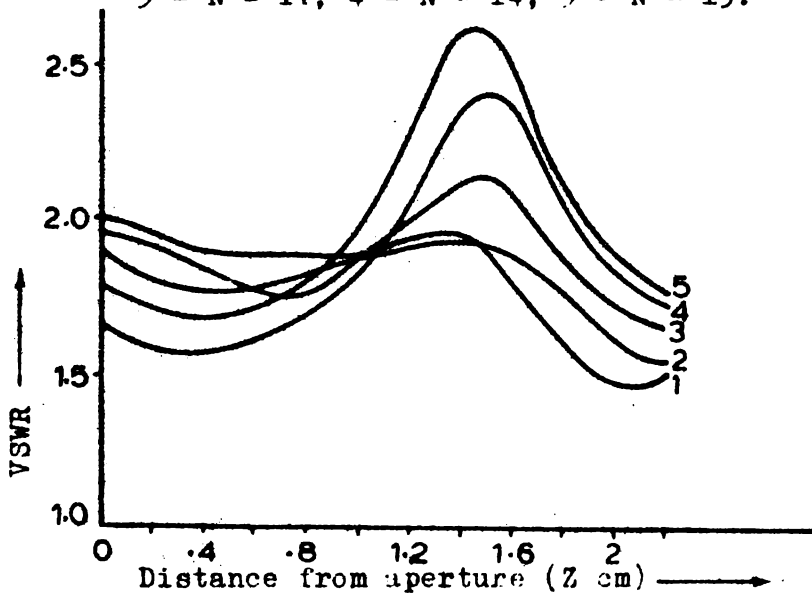


Fig.4.1(i)(b) Variation of VSWR with flange position.  $2\beta = 90^\circ$ ,  
 Frequency = 9.4 GHz, Horn -  $H_5$ . 1 -  $N = 6$ , 2 -  $N = 8$ ,  
 3 -  $N = 11$ , 4 -  $N = 14$ , 5 -  $N = 19$ .

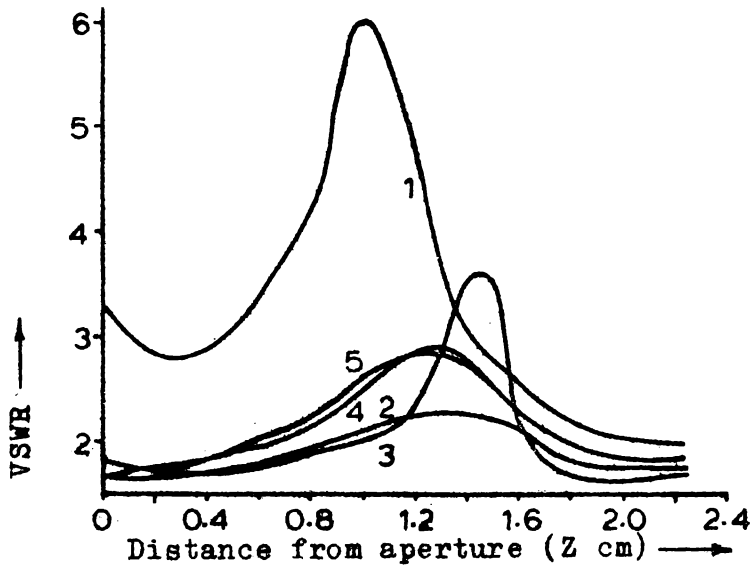


Fig.4.1(i)(c) Variation of VSWR with flange position.  $2\beta = 90^\circ$ ,  
 Frequency = 10.15 GHz, Horn -  $H_3$ . 1 -  $N = 6$ ,  
 2 -  $N = 8$ , 3 -  $N = 11$ , 4 -  $N = 14$ , 5 -  $N = 19$ .

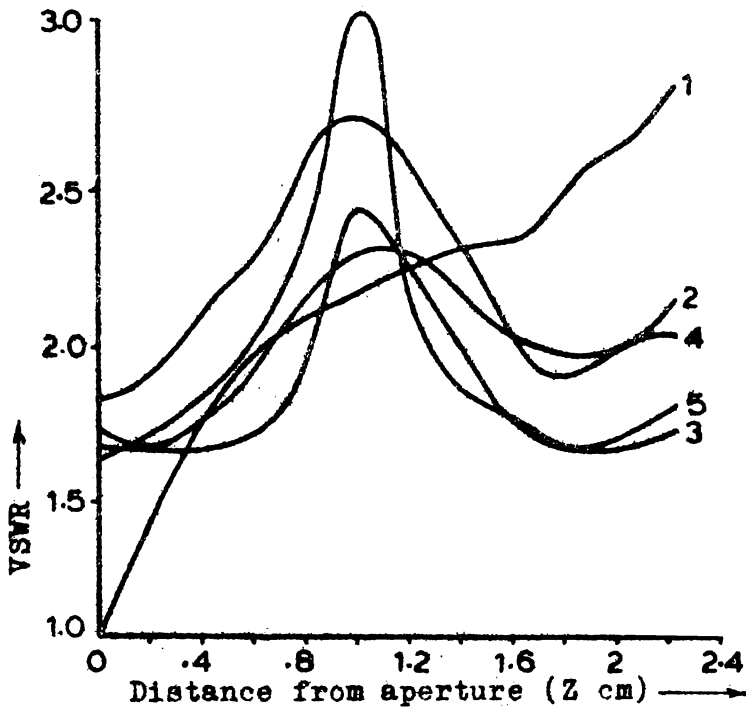


Fig.4.1(i)(d) Variation of VSWR with flange position.  $2\beta = 90^\circ$ ,  
 Frequency = 11.05 GHz, Horn -  $H_3$ . 1 -  $N = 6$ ,  
 2 -  $N = 8$ , 3 -  $N = 11$ , 4 -  $N = 14$ , 5 -  $N = 19$ .

curves corresponding to each flange is more or less the same at any particular frequency. The position of the VSWR maxima and minima are seen to be varying mainly with frequency only.

#### 4.1(ii) Dependence of VSWR on Frequency

It is observed that the VSWR of the system varies with changes in frequency. The VSWR of the system depends on the phase and amplitude of the secondary wavelets from the tips of the corrugations as they reach the horn aperture. They interact with the energy that gets reflected back from the horn-mouth, to add up or reduce the effective reflection, depending on the phase difference between the waves.

It is observed that larger variations in VSWR occur with larger slot-widths when the frequency is varied. This is what we expect, since, as the slot-width becomes very small compared to the wavelength, the surface offers a capacitative surface reactance, which will not support the excitation of the corrugation tips.<sup>(81)</sup> When a plane flange is employed the variation of VSWR is very large when compared with corrugated flanges as is evident from the figure. This is also the case with theory, since the edges of the plane flange would get excited more strongly than the individual elements on a corrugated flange, and since there exists only one such edge per flange element, the variation in phase and amplitude of the wavelets reaching the aperture, with respect to changes in other parameters would be more strong.

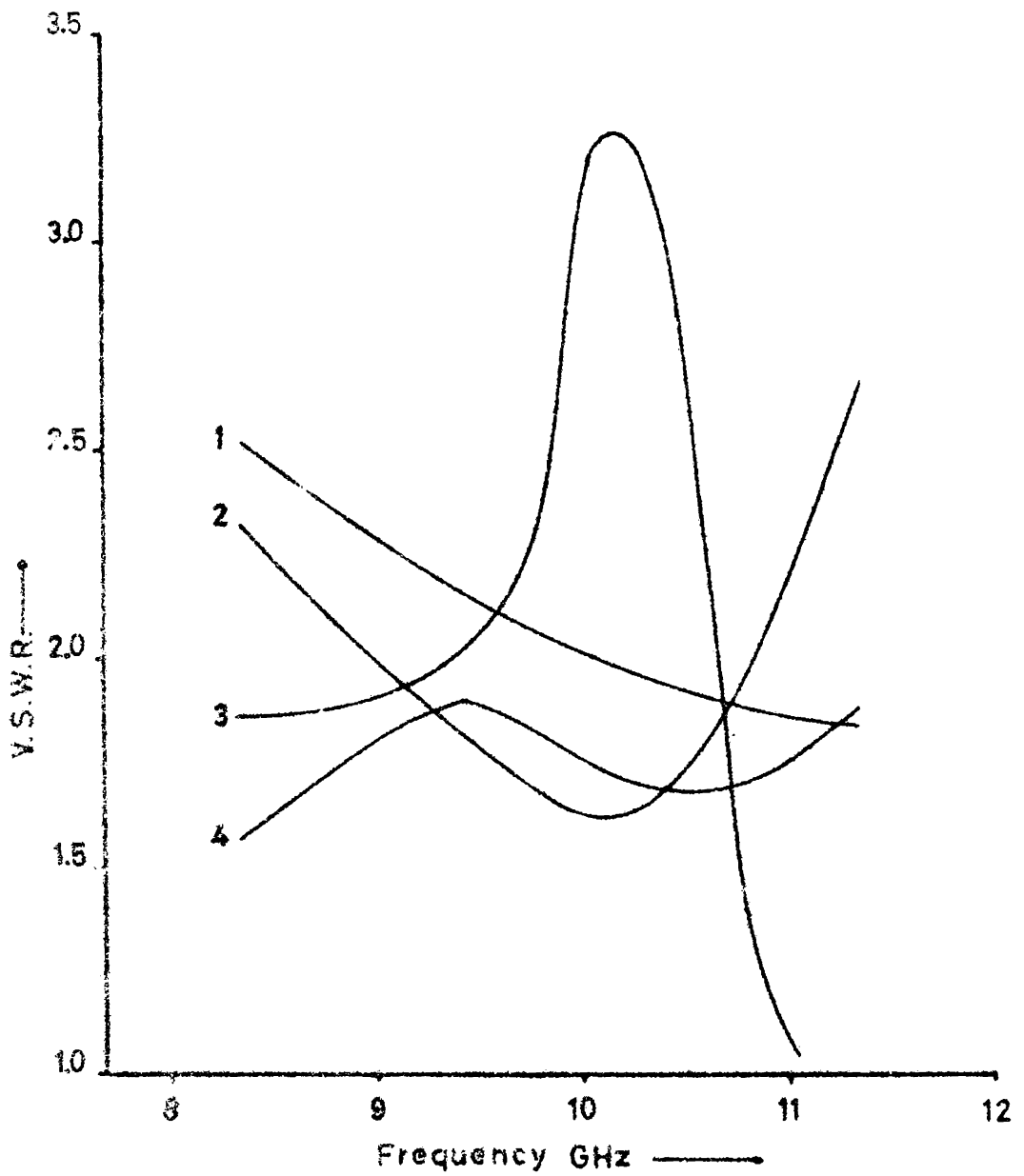


Fig.4.1(ii)(a) Variation of VSWR with frequency.  
 $2\beta = 90^\circ$ , Horn -  $H_2$ . 1 - Horn without flanges.  
 2 - Plane flanges, 3 -  $N = 6$ , 4 -  $N = 8$ .

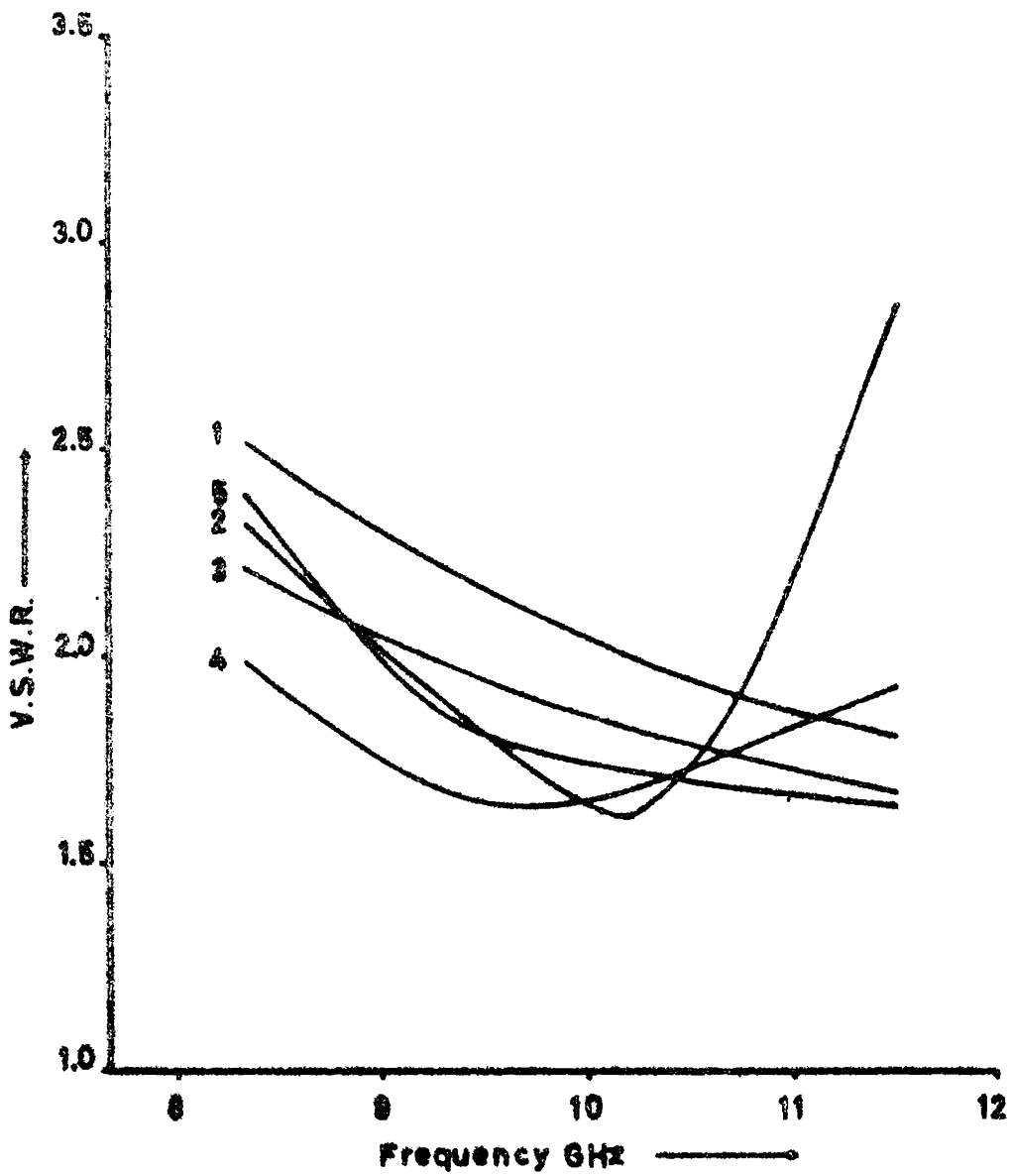


Fig. 4.1(11)(b) Variation of VSWR with frequency.  
 $2\theta = 90^\circ$ , Horn -  $H_3$ . 1 - Horn without flanges,  
 2 - Plane flanges, 3 -  $N = 11$ , 4 -  $N = 14$ ,  
 5 -  $N = 19$ .

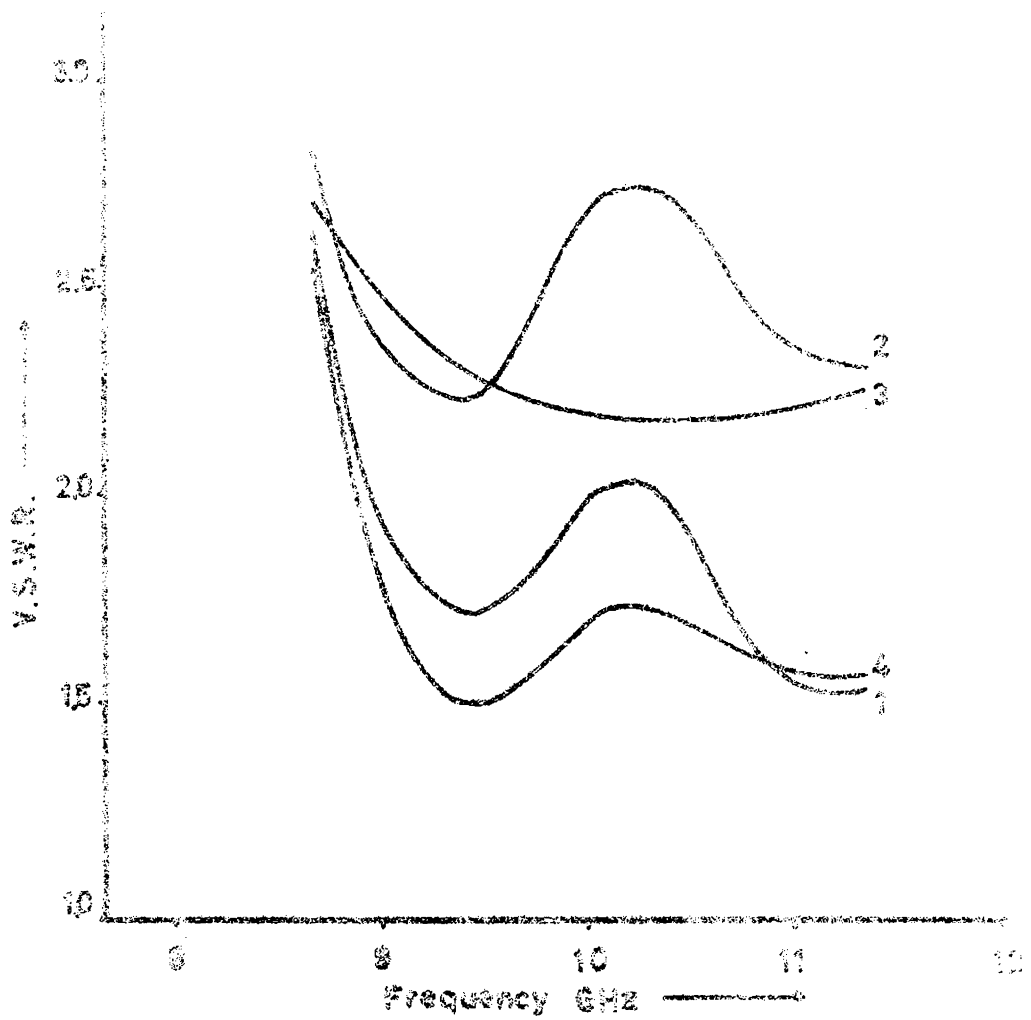


Fig.4.1(11)(c) Variation of VSWR with frequency.  
 $2\theta = 120^\circ$ , Horn -  $H_2$ . 1 - Horn without flanges,  
 2 - Plane flanges, 3 -  $W = 6$ , 4 -  $W = 8$ .

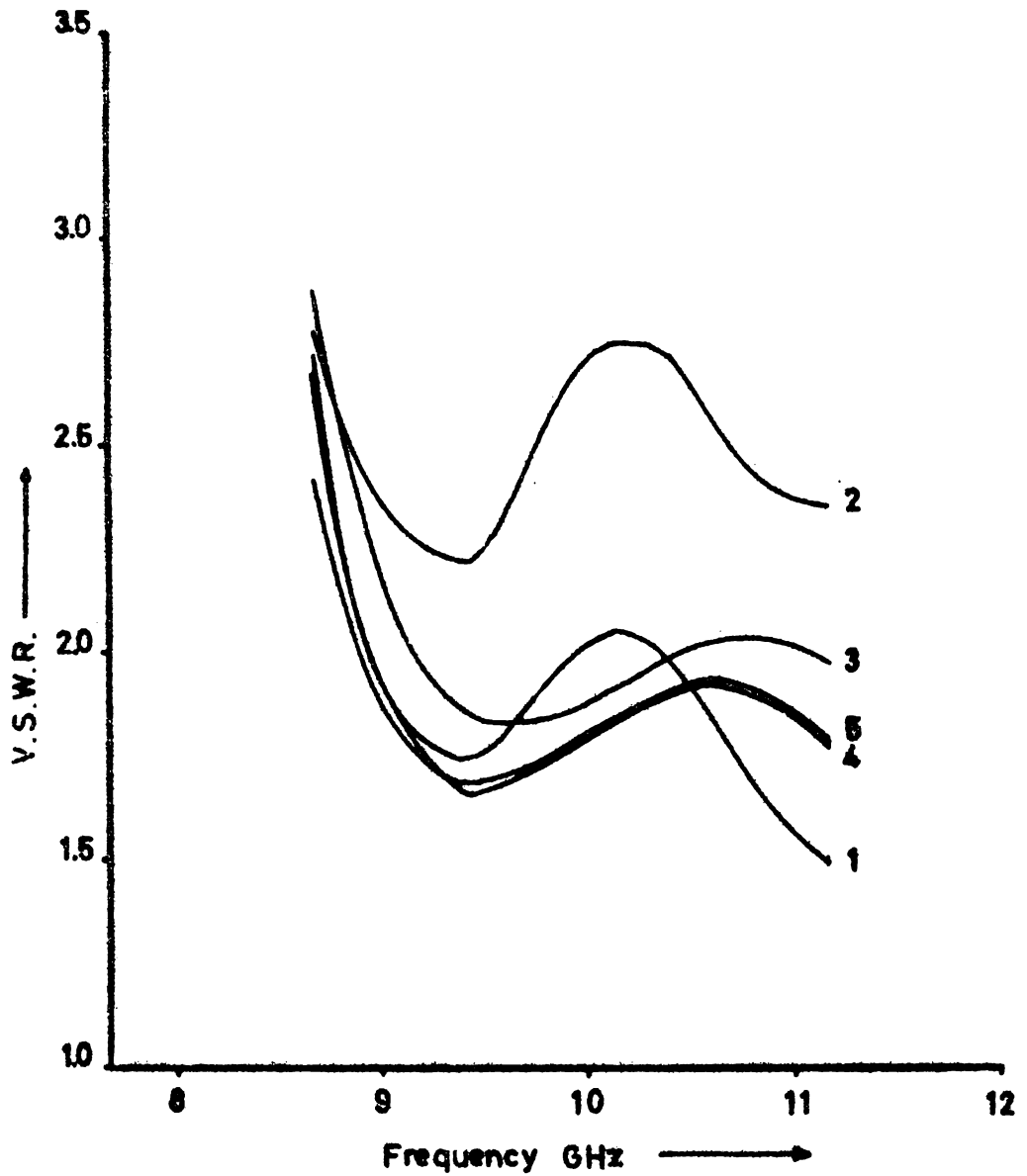


Fig.4.1(ii)(d) Variation of VSWR with frequency.  
 $2\beta = 120^\circ$ , Horn -  $H_2$ . 1 - Horn without flanges,  
 2 - Plane flanges, 3 -  $N = 11$ , 4 -  $N = 14$ ,  
 5 -  $N = 19$ .

Even though a very small value of VSWR is desired, sudden variations like sharp peaks or dips are to be avoided for obvious reasons. Hence, even though the plane flange in Fig.4.1(ii)(b) gives the smallest value of VSWR at 10.15 GHz, other flanges with  $N = 11, 14$ , etc., would be more suited for broad band applications. The flange with  $N = 6$ , is seen to reduce the VSWR to a value less than 1.05, which is considered a fairly good match at 11.05 GHz, this value rises to 3.3 at 10.15 GHz, which indicates a large mismatch. Hence this flange is to be considered inferior to those with  $N = 11, 14$ , etc.

#### 4.1(iii) Dependence of VSWR on Flange Angle

The effect of flange angle on VSWR is also examined in detail. In this study, the flanges were kept at two different positions; the aperture and the optimum (The optimum or O- and minimum or M-positions are described in sec.4.2). At these positions, for different frequencies and different flanges, the effect of the flanges on the VSWR was studied. Figs.4.1(iii)(a) and (b) shows some graphs which show the variation of VSWR with flange angle. Fig.4.1(iii)(a) gives the values when the flanges are kept at the aperture. Fig.4.1(iii)(b) gives the values when the flanges are kept at the optimum.

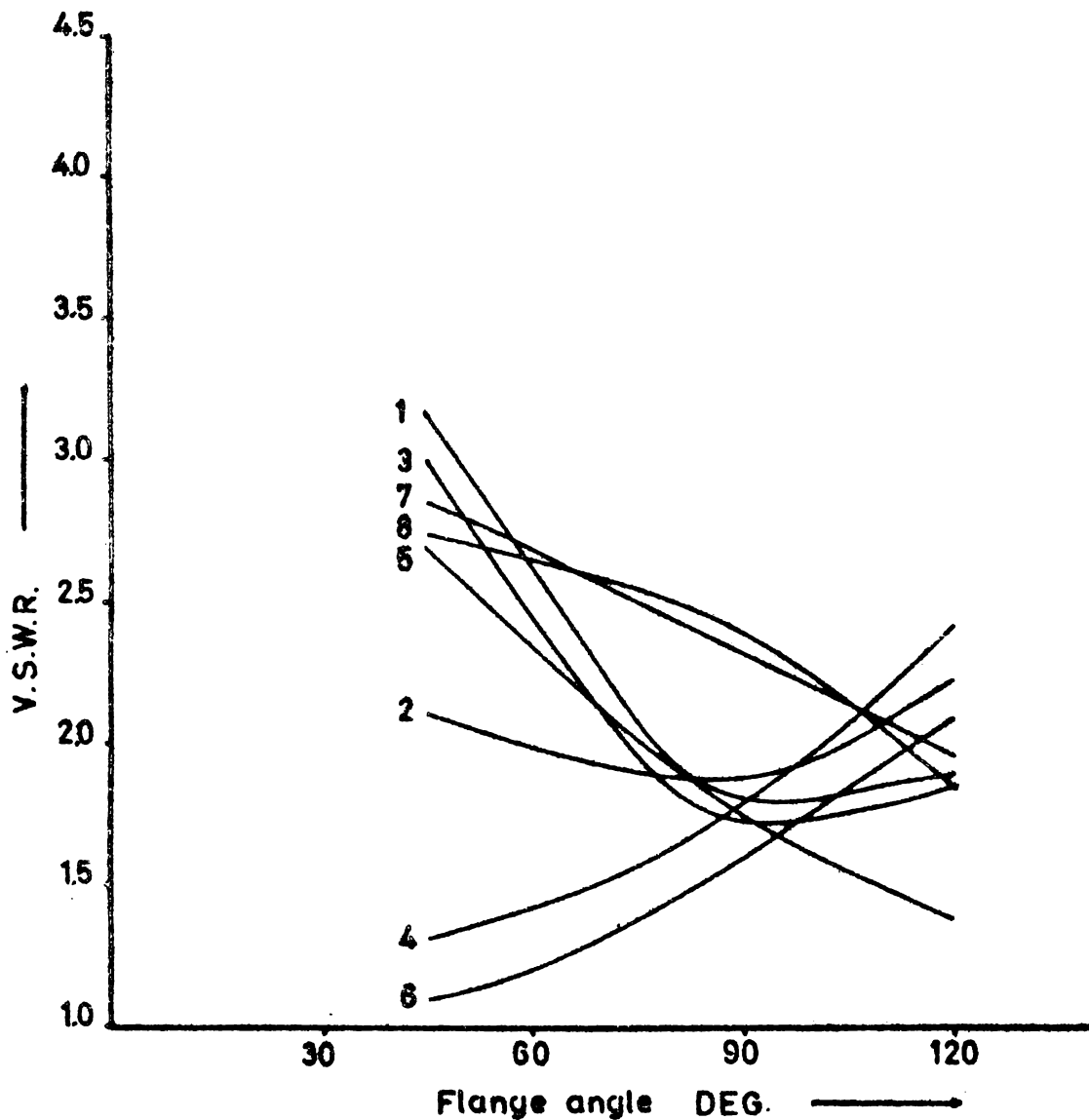


Fig.4.1(iii)(a) Variation of VSWR with flange angle, when the flanges are kept at the aperture.  
 1 -  $N = 6$ , 8.7 GHz; 2 -  $N = 6$ , 11.05 GHz;  
 3 -  $N = 8$ , 8.7 GHz; 4 -  $N = 8$ , 11.05 GHz;  
 5 -  $N = 19$ , 8.7 GHz; 6 -  $N = 19$ , 11.05 GHz;  
 7 - Plane flange, 8.7 GHz; 8 - Plane flange, 11.05 GHz.

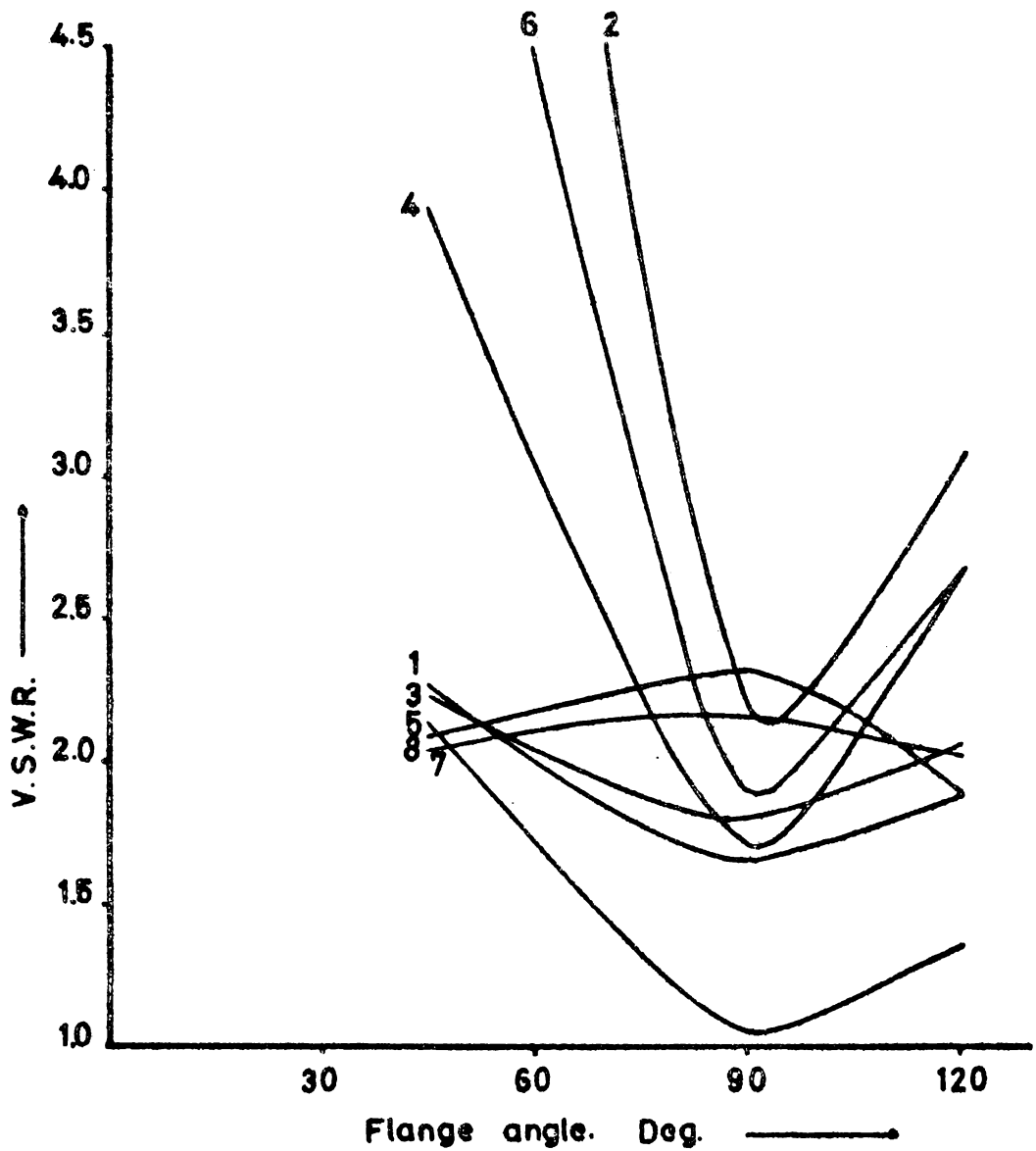


Fig.4.1(iii)(b) Variation of VSWR with flange angle, when the flanges are kept at the 0-position.

1 -  $N = 6$ , 8.7 GHz; 2 -  $N = 6$ , 11.05 GHz;  
 3 -  $N = 8$ , 8.7 GHz; 4 -  $N = 8$ , 11.05 GHz;  
 5 -  $N = 19$ , 8.7 GHz; 6 -  $N = 19$ , 11.05 GHz;  
 7 - Plane flange, 8.7 GHz; 8 - Plane flange, 11.05 GHz.

#### 4.1(iv) Dependence of VSWR on Corrugation Parameters

In this study, the slot depth 'h' was kept constant, it was maintained  $> \lambda/4$ . The corrugation period, or the slot width, (The fin thickness is considered vanishingly small, even though it has a finite value) 'a' is varied and its effects on the VSWR was studied. The results are presented in this section.

Figs.4.1(iv)(a) - (b), show the variation of VSWR for changes in 'a'. It is observed that the VSWR varies in a haphazard way, even though the variation of VSWR for changes in other parameters was more or less systematic. But, since 'a' is a constant for any given set of flanges, this random variation of VSWR for changes in 'a' does not directly affect the performance of any given flange mounted horn.

Another important observation that can be made from Figs.4.1(iv)(a) - (b) is about the band width of operation of the flange mounted sectoral horn. At any point along the X-axis, corresponding to a particular value of 'a', the largest separation in terms of Y- between the different curves corresponding to different frequencies is a measure of the VSWR variations, within the specified band. Hence for a corrugation period, 'a' = 17 (N=6). VSWR varies from 1.06 and 3.25, whereas at 'a' = 13 (N = 8), the fluctuation is between 1.62 and 1.90, within the specified range.

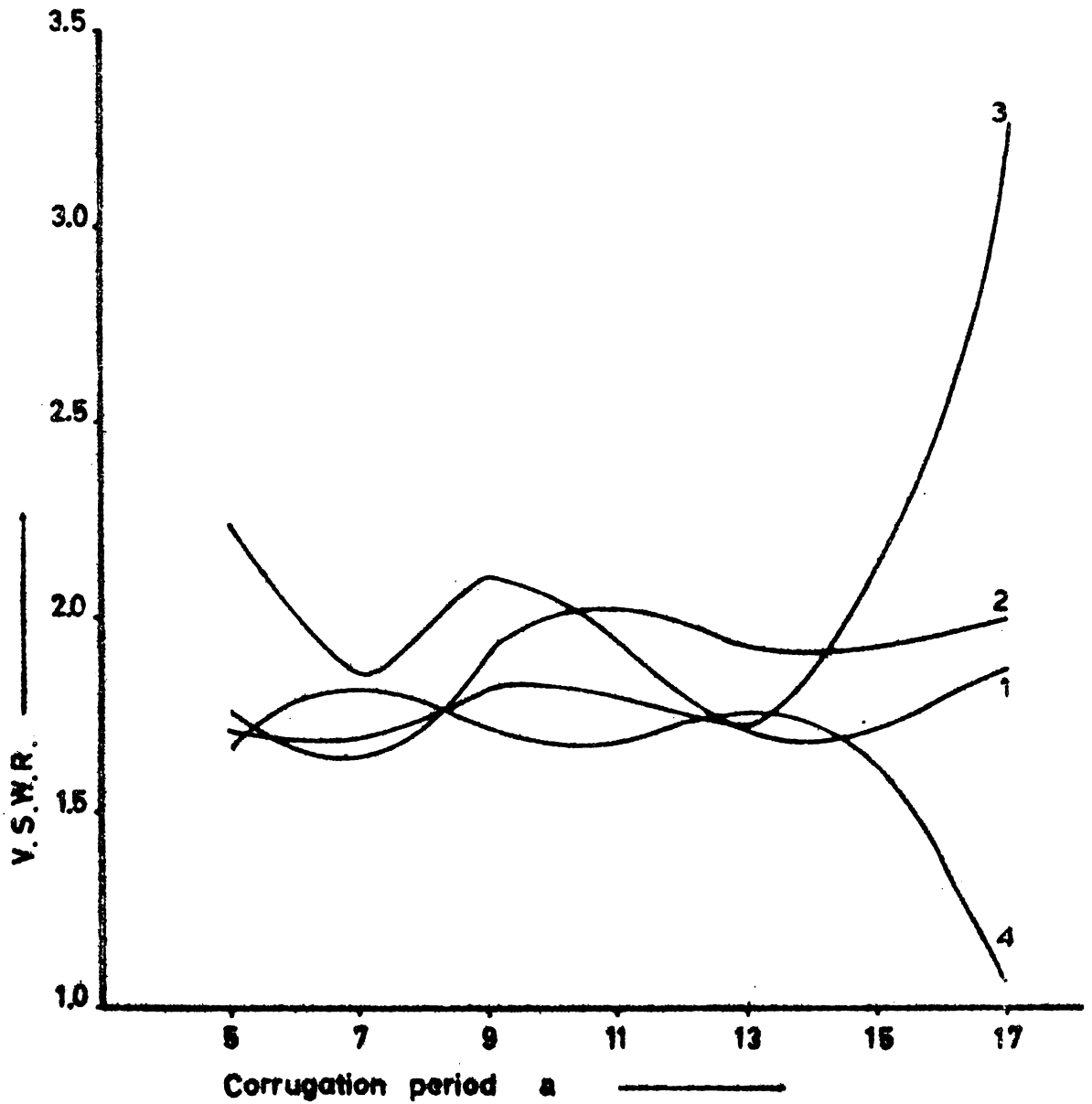


Fig. 4.1(iv)(a) Variation of VSWR with corrugation period 'a', when flanges are kept at the aperture.  $2\beta = 90^\circ$ , Horn -  $H_3$ . 1 - 8.7 GHz; 2 - 9.4 GHz, 3 - 10.15 GHz, 4 - 11.05 GHz.

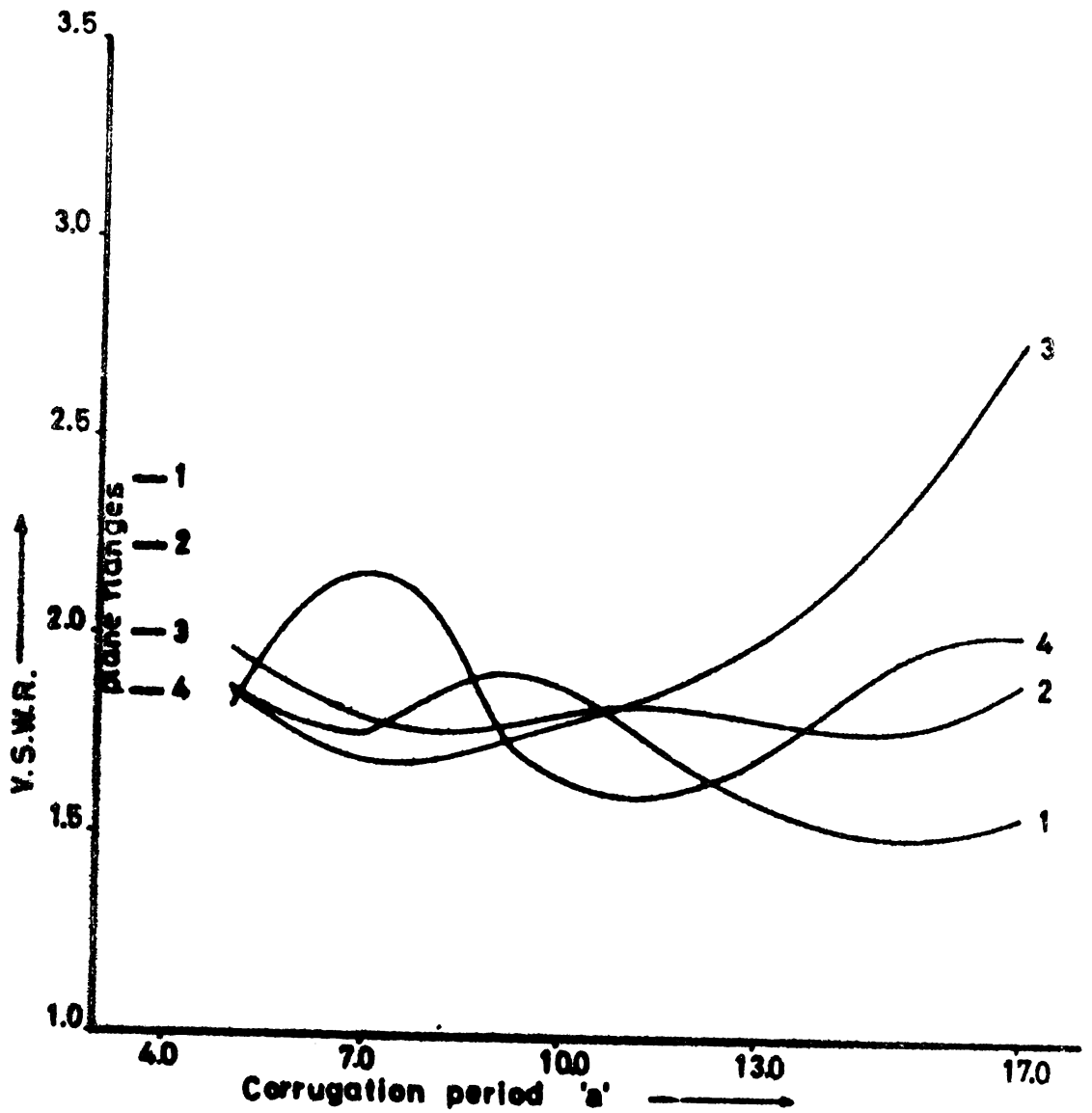


Fig.4.1(iv)(b) Variation of VSWR with corrugation period 'a', when the flanges are kept at the 0-position.  $2\beta = 90^\circ$ , Horn -  $H_3$ . 1 - 8.7 GHz, 2 - 9.4 GHz, 3 - 10.15 GHz, 4 - 11.05 GHz.

## 4.2 On-axis Power Density

On-axis power density is defined as the power radiated along the axis of the antenna system. In a symmetric radiation pattern, the on-axis power density is usually the power density corresponding to the main lobe peak. This is measured with a probe kept at the axis of the antenna system at a large distance ( $> 2D^2/\lambda$ ) from the transmitter.

Optimum position (O-position) is the flange position corresponding to a maximum value of on-axis power density.

Minimum position (N-position) is the flange position corresponding to a minimum value of on-axis power density.

### 4.2(i) Dependence of On-axis Power Density on Flange Position

It is observed that the on-axis power density is very strongly dependent on the position of the flanges relative to the horn aperture. As the flanges are moved back from the aperture, the on-axis power density fluctuates between sharp maxima and minima. At certain positions, the power density along the axis falls to zero value. There are other positions which give very large axial power density.

Figs.4.2(i)(a) - (d) are graphs showing the variation of on-axis power density with respect to change in flange position. The dependence of VSWR on flange position was discussed in sec.4.1(i). It was seen that the VSWR depends very strongly on the flange position. Hence a comparison between the changes in VSWR and on-axis power density, due

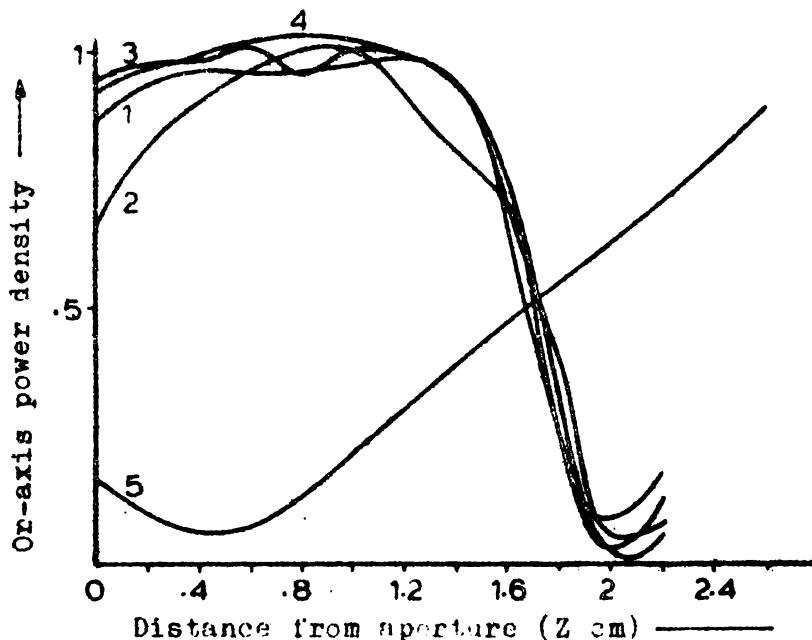


Fig.4.2(i)(a) Variation of On-axis power density with flange position.  $2\beta = 90^\circ$ , Horn -  $H_3$ , Frequency = 8.7 GHz, 1 -  $N = 8$ , 2 -  $N = 11$ , 3 -  $N = 14$ , 4 -  $N = 19$ , 5 - Plane flanges.

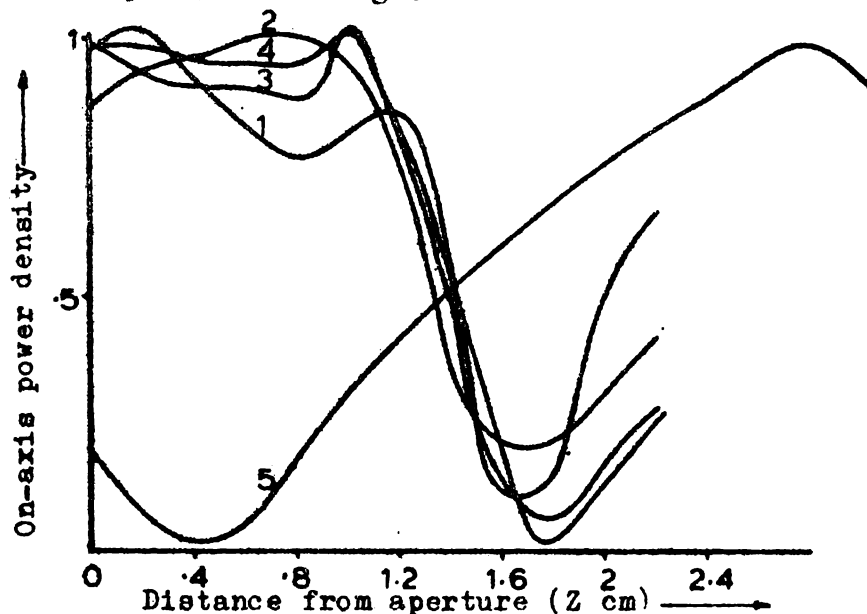


Fig.4.2(i)(b) Variation of On-axis power density with flange position.  $2\beta = 90^\circ$ , Horn -  $H_3$ , Frequency = 9.4 GHz, 1 -  $N = 8$ , 2 -  $N = 11$ , 3 -  $N = 14$ , 4 -  $N = 19$ , 5 - Plane flanges.

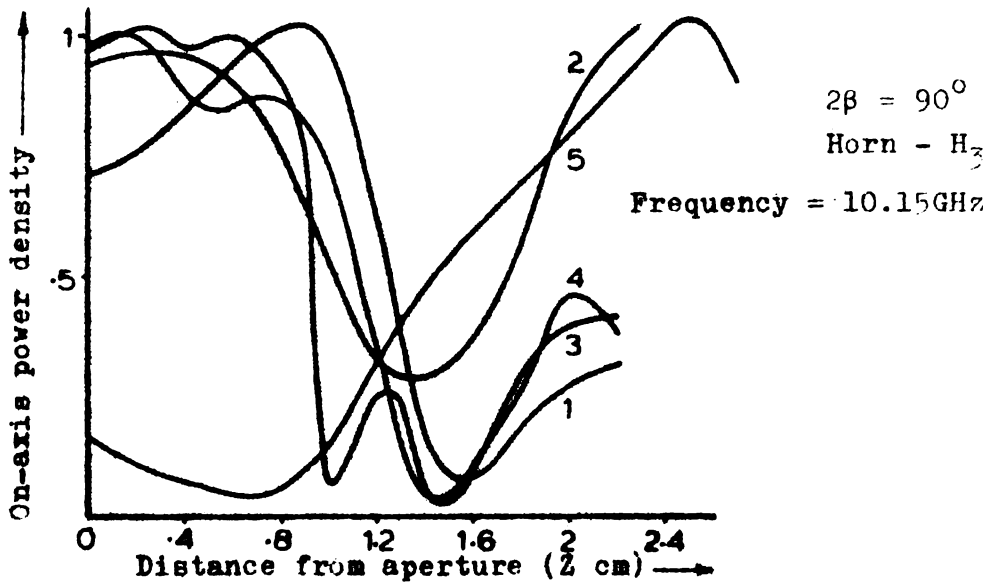


Fig.4.2(1)(c) Variation of On-axis power density with flange position. 1 -  $N = 8$ , 2 -  $N = 11$ , 3 -  $N = 14$ , 4 -  $N = 19$ , 5 - Plane flanges.

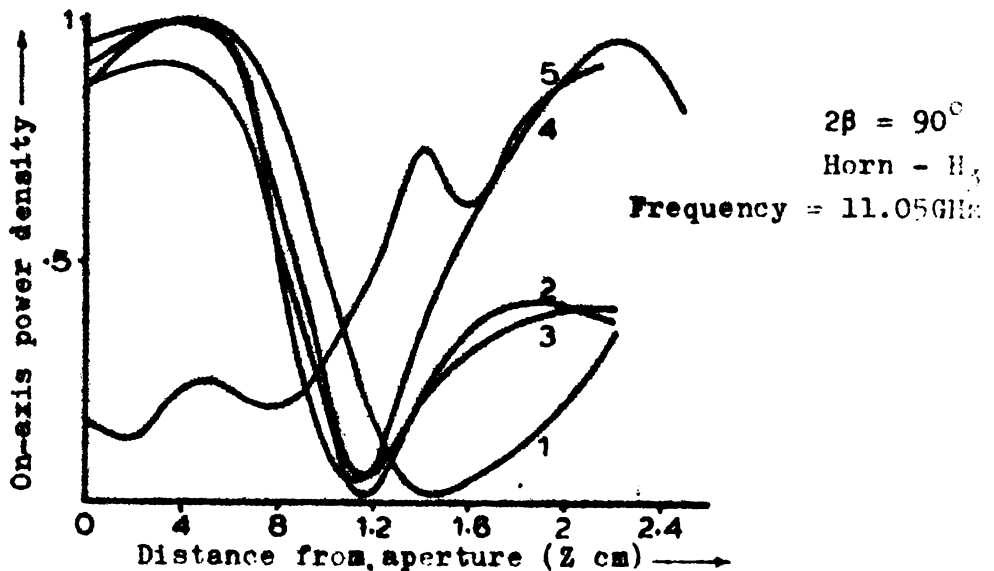


Fig.4.2(1)(d) Variation of On-axis power density with flange position. 1 -  $N = 8$ , 2 -  $N = 11$ , 3 -  $N = 14$ , 4 -  $N = 19$ , 5 - Plane flanges.

to changes in flange position is made. It is observed that the general trend in the case of corrugated flanges is such that the VSWR variations follow the on-axis power density changes  $180^\circ$  out of phase. That is, to say, when the on-axis power density is a maximum, the VSWR is a minimum, and when the on-axis power density is a minimum, the VSWR is a maximum. The maximum and minimum values of these does not fall exactly at the same point, but the general trend is such that, they are spaced close together. This is clear from Figs.4.2(i)(e) - (h). It may be noted that it is very advantageous in a practical system to have a very low VSWR at the 0-position where the beam is well focused and directed along the axis of the system.

This result may be compared to that obtained with plane flanges. In this case the VSWR minimum does not generally agree with an on-axis power density maximum. This is clear from Figs.4.2(i)(i) and (j). This is a definite advantage that the corrugated flanges possess over the plane flanges.

Figs.4.2(i)(k) shows the changes in the radiation pattern with respect to the flange position variation, compared with VSWR and On-axis power density variations. A detailed study of the changes in beam shape and radiation pattern are made in sec.4.3.

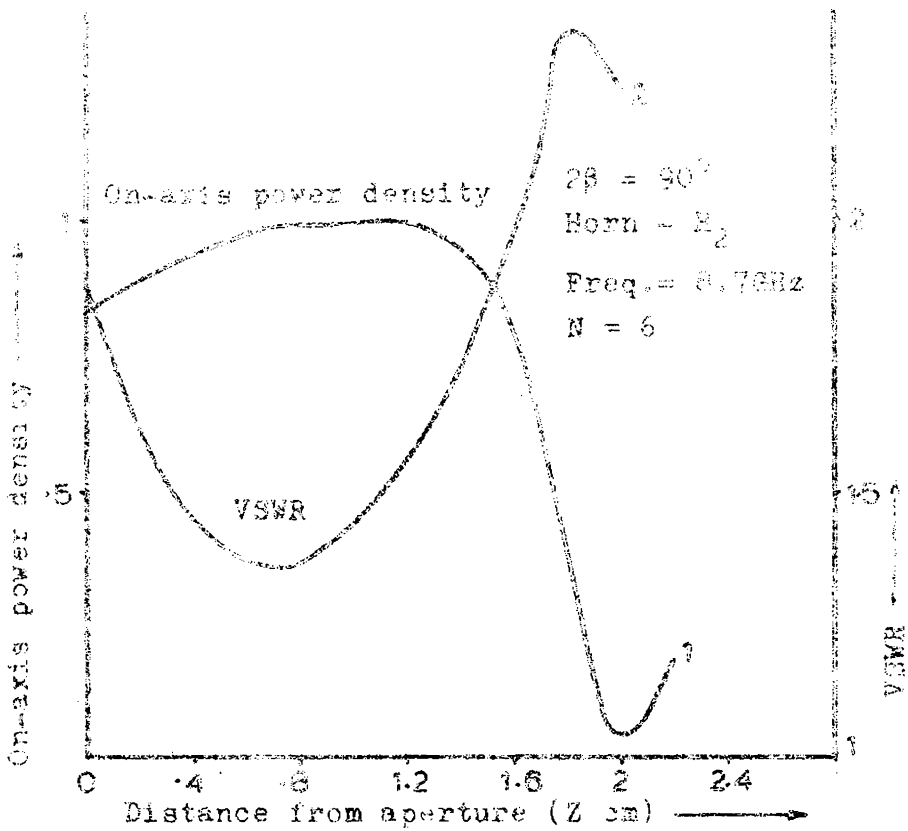


Fig.4.2(i)(e) Comparison between the effects of flange position on the VSWR and On-axis power density.

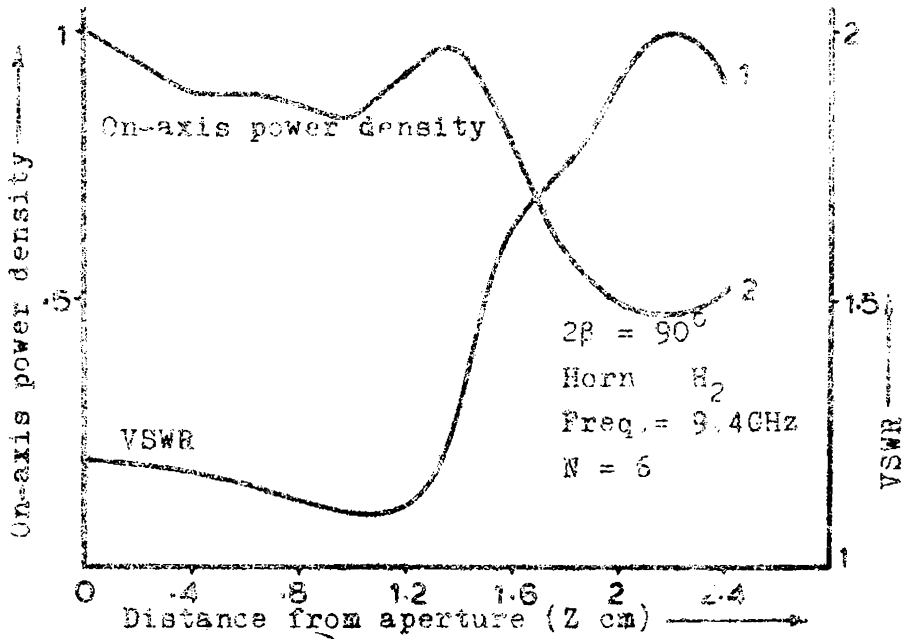


Fig.4.2(i)(f) Comparison between the effects of flange position on the VSWR and On-axis power density.

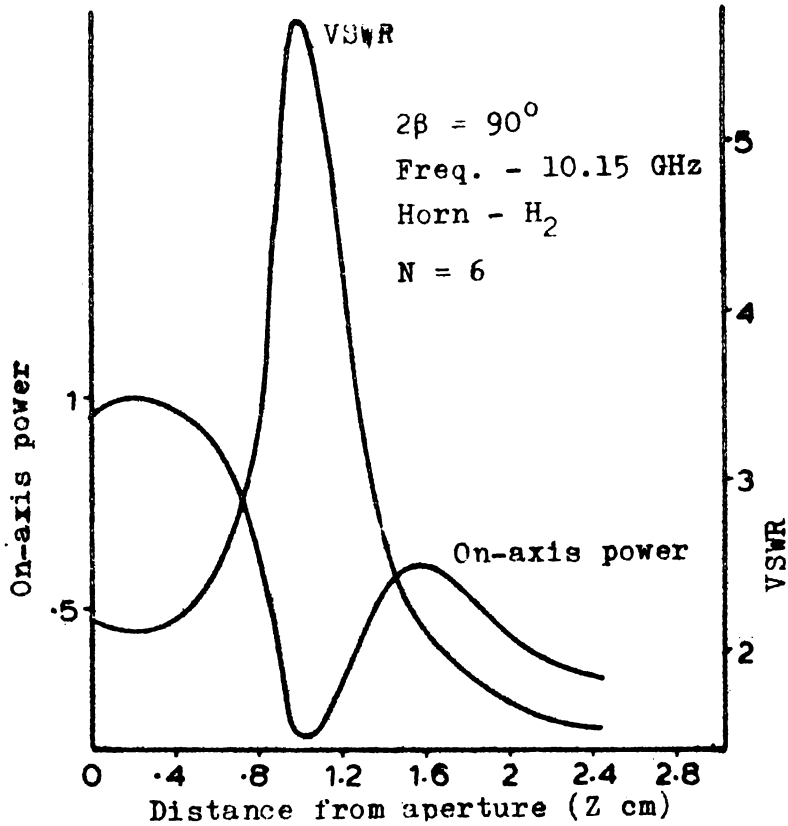


Fig.4.2(i)(g) Comparison between the effects of flange position on the On-axis power density and VSWR.

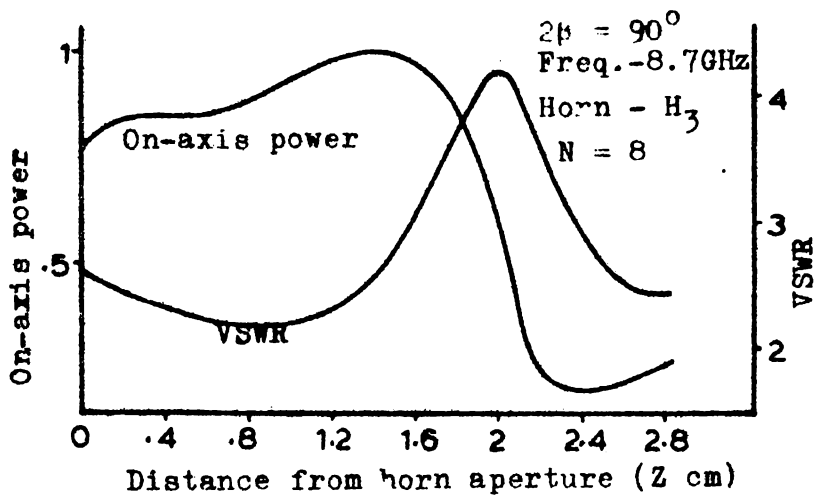


Fig.4.2(i)(h) Comparison between the effects of flange position on the On-axis power density and VSWR.

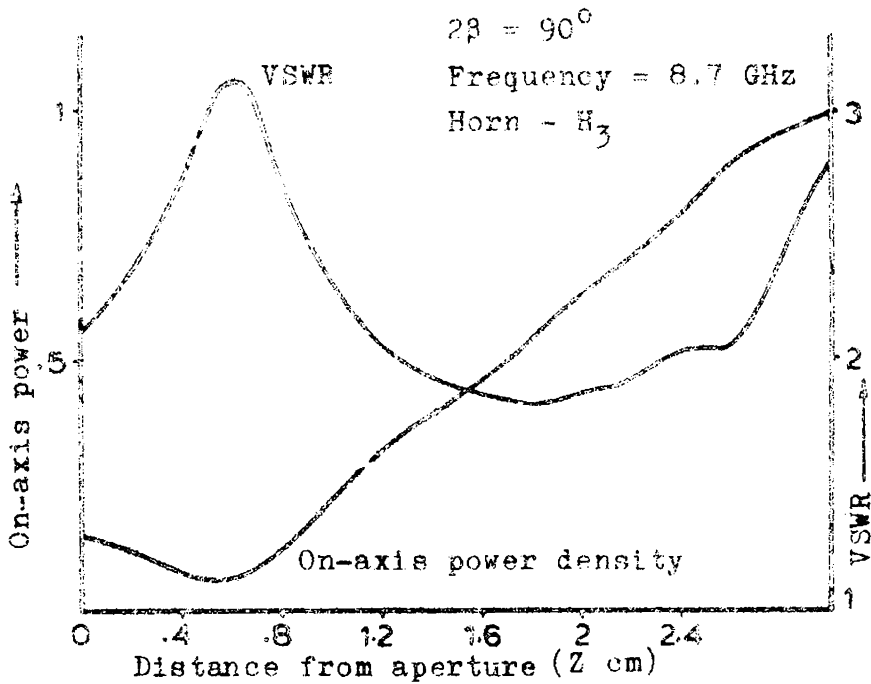


Fig.4.2(i)(i) Comparison between the effects of flange position on the On-axis power density and VSWR when plane flanges are employed.

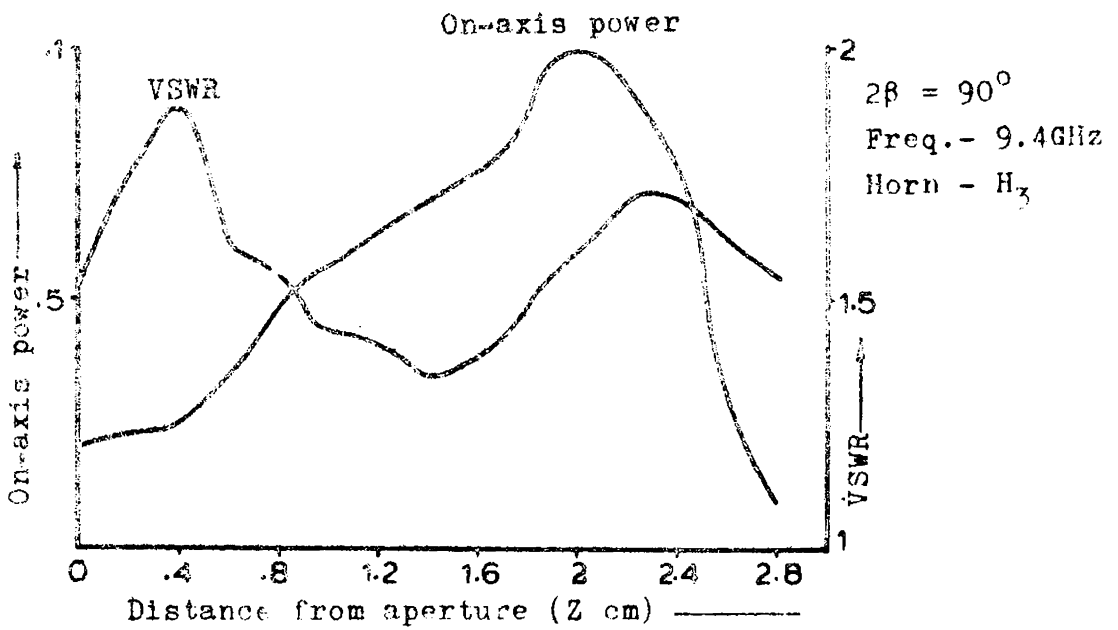


Fig.4.2(i)(j) Comparison between the effects of flange position on the On-axis power density and VSWR when plane flanges are employed.

#### 4.3(i) Effect of Flange Position on Beamshape

It is observed that the corrugated flanges have a large effect on the beam shape of the system. For any flange angle, as described in sec.4.1 and sec.4.2, there are many different positions relative to the horn aperture, where the flanges can be kept. The radiation pattern was recorded at each of these positions. This change in radiation pattern which occurs was referred in sec.4.2(i) also. Fig.4.2(i)(k) shows the typical changes that would occur in the beamshape. Here for convenience, the radiation pattern is shown in polar co-ordinates.

It was found that for all flange angles and flanges, when the flanges are kept at the aperture of the system, the radiated beam was narrower than the natural beam of the sectoral horn. As the flanges are pulled back, the beam shape undergoes large variations. At O-position described earlier, the beam is very narrow, and is pointed along the axis of the system. When the flanges are moved away from the O-position, the beam broadens and finally splits into two major lobes with zero intensity along the axis. These changes are shown in Fig.4.3(i)(a). It is evident from the figure that at 1.5 cms from the aperture, an O-position occurs, since we get a very narrow main lobe. At 3 cms, the main lobe has vanished. Hence this is an M-position.

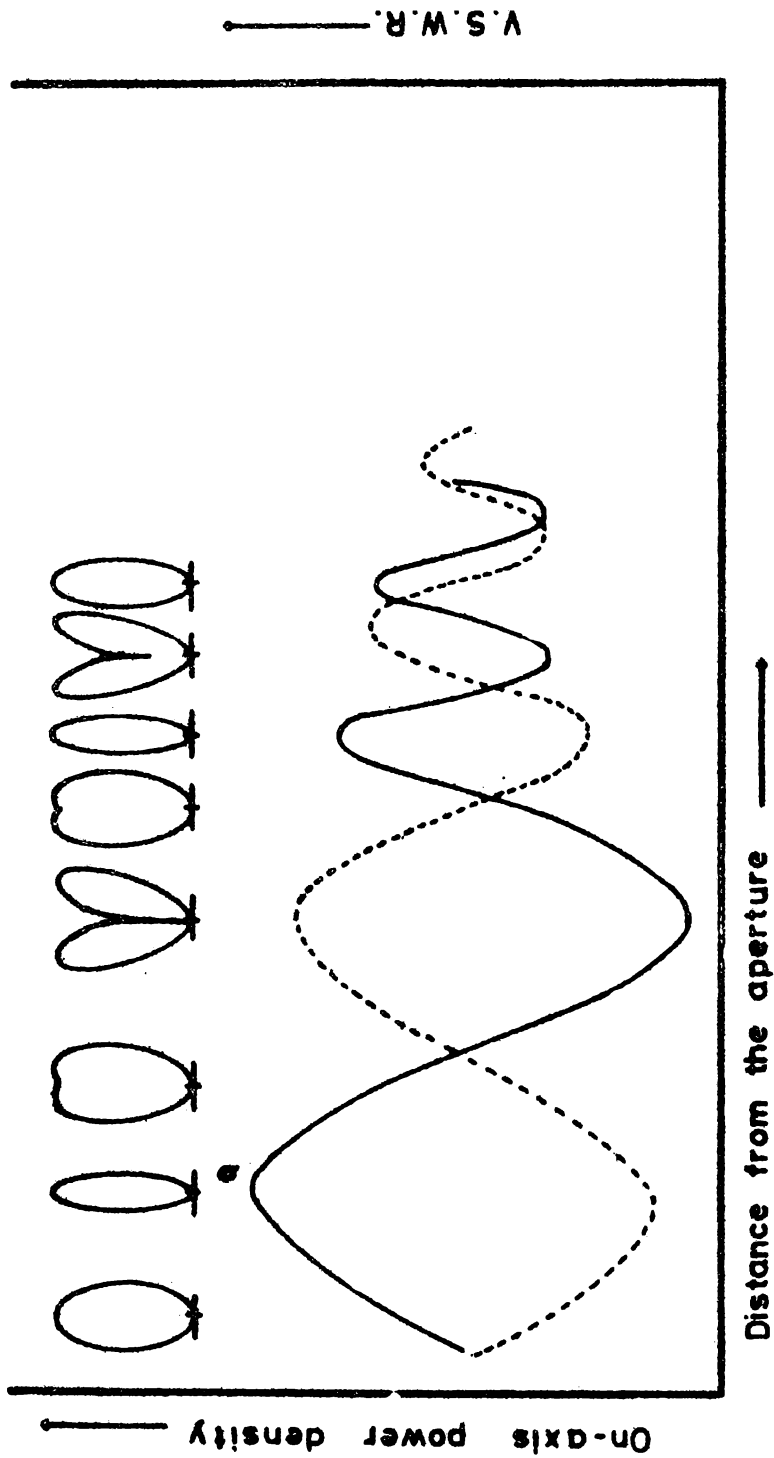
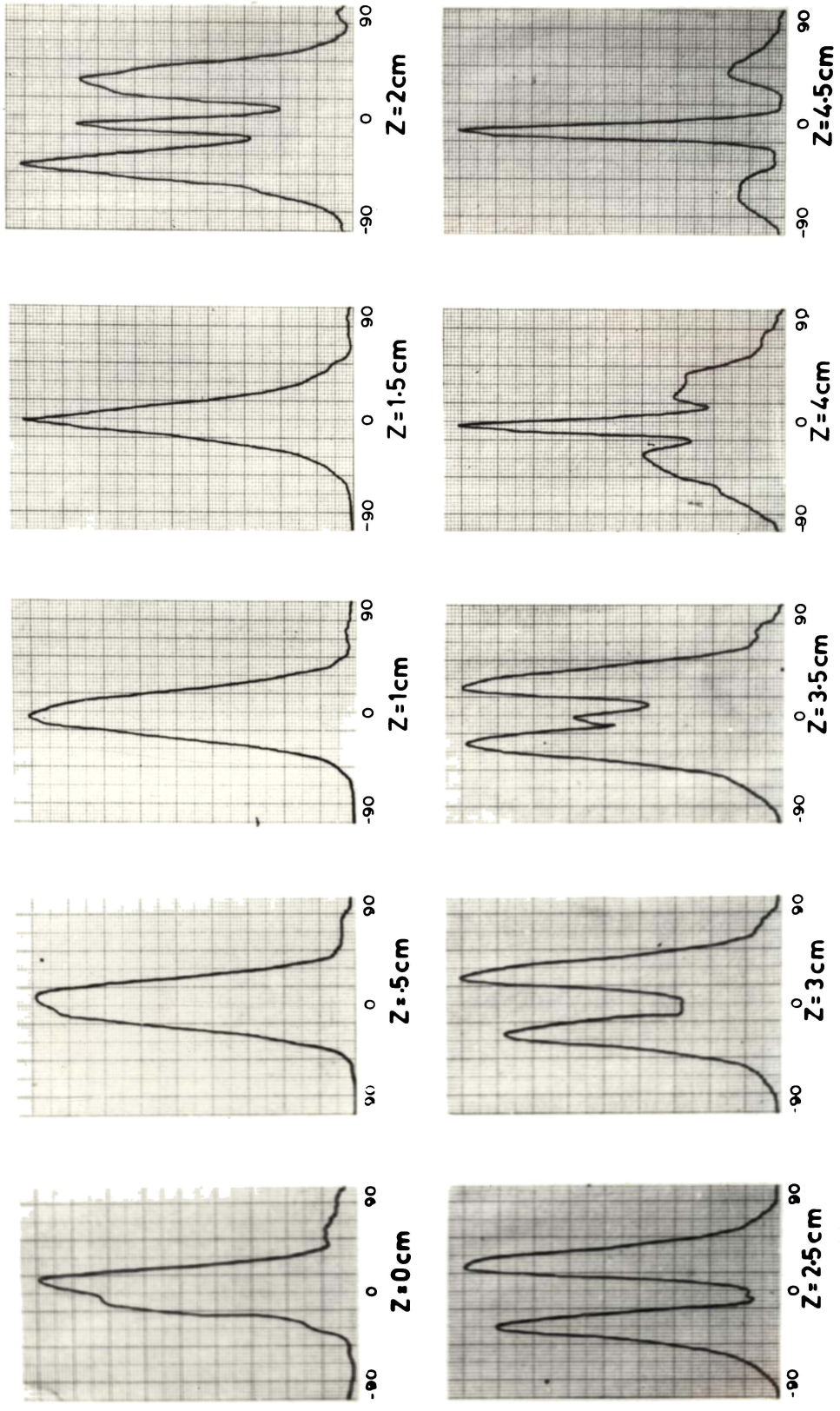
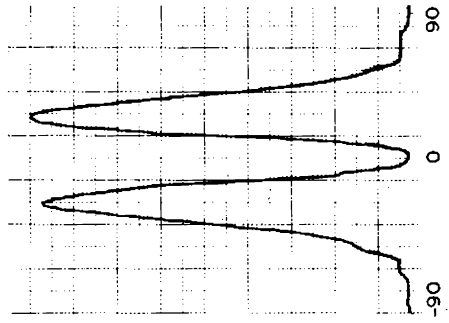


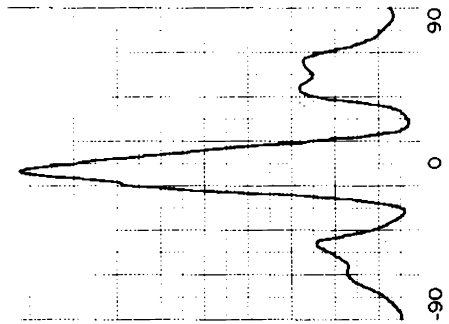
Fig.4.2(i)(k) Typical changes that occur in the radiation pattern, On-axis power density, and VSWR as the distance of the flanges from the aperture is varied.



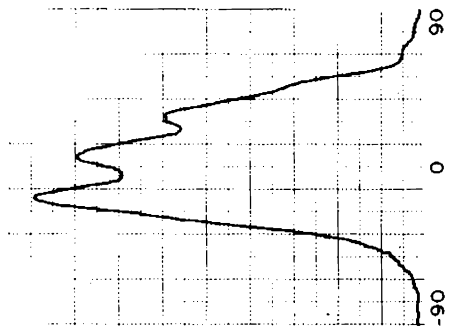
**Fig. 4.3(i)(a)** Variation in beam shape due to changes in flange position.  $2\beta=90^\circ$ , Horn -H<sub>3</sub>, Frequency = 8.7 GHz, N=11.



M-position (2.6 GHz)



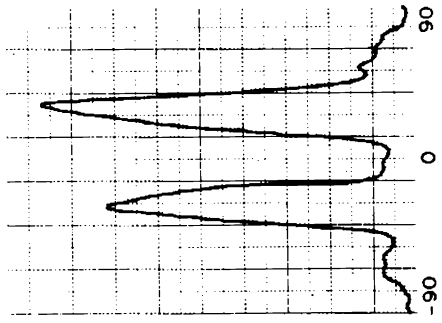
O-position (2.6 GHz)



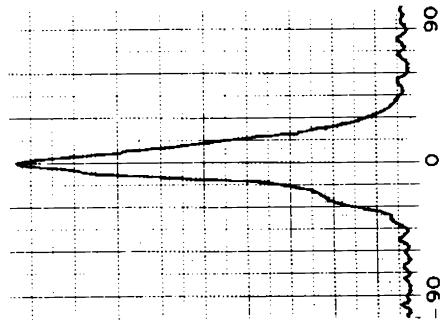
Aperture (2.6 GHz)



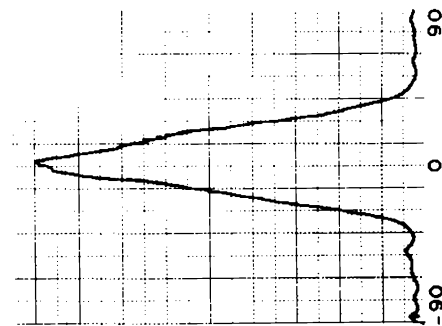
Natural (2.6 GHz)



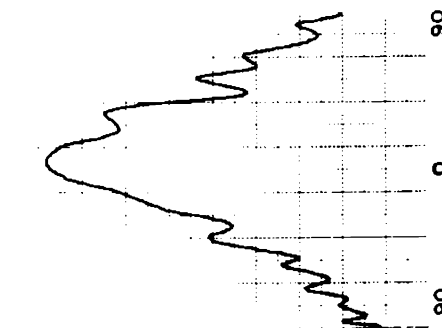
M-position (4.2 GHz)



O-position (4.2 GHz)



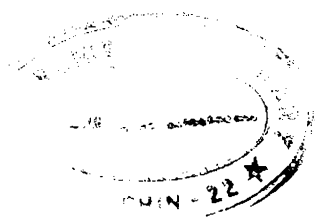
Aperture (4.2 GHz)



Natural (4.2 GHz)

Fig 4.3(i)(b) Effect of corrugated flanges on the beam shape in the S-band.

$2\beta = 120^\circ$ , Horn-S<sub>1</sub>, Flange-6 (N=11).



G 2963 -

The effect of corrugation parameters on the beam shape was also studied in detail. But since it is more easy to compare and interpret, it has been presented as a function of gain in the next section.

#### 4.4 Antenna Gain

The antenna gain was estimated using the technique described in sec.3.4. Since in a rectangular aperture antenna, the radiation pattern in either of the principal planes can be modified independent of the pattern in the other plane, our attempts to modify the E-plane radiation pattern of H-plane sectoral horns, do not affect the H-plane pattern. Hence the H-plane gain remains constant. Since the antenna gain is given by,

$$G = \frac{G_E G_H}{\pi} \text{ or,}$$

$$G_{dB} = G_E \text{ dB} + G_H \text{ dB} - 20 \text{ Log}_{10} \pi$$

Hence for comparison purposes, the E-plane gain alone need be considered.

##### 4.4(i) Dependence of E-plane Gain on Flange Position

Table 4.4(i)(I) gives the (uncorrected) gain of the different sectoral horns used in this study. As the flanges are kept at different positions relative to the horn aperture, the beam shape undergoes drastic changes. These

Table 4.4(i)(I)

Natural E-plane Gain of the various sectoral horns used in this study

Horn	Gain dB	
	8.7 GHz	11.05 GHz
H <sub>1</sub>	5.3	6.5
H <sub>2</sub>	4.9	6.3
H <sub>3</sub>	5.4	6.4

Table 4.4(i)(II)

Modified E-plane Gain when the flanges are kept at the aperture.  $2\beta = 90^\circ$

'a'	Gain dB	
	8.7 GHz	11.05 GHz
17	14.9	14.8
13	14.3	12.7
9	14.3	14.7
7	15.7	17.1
5	15.3	16.7
Plane	13.3	14.3

changes in beam shape causes corresponding changes in antenna gain. This variation in antenna gain as the position of the flanges relative to the horn aperture is varied is shown in Fig.4.4(i)(a). Here the peaks correspond to the maximum positions. The first peak, which corresponds to the highest gain also corresponds to the 0-position. The dip in the gain curve corresponds to a minimum position.

Tables 4.4(i)(II),(III) and (IV), give the values of the gain for different sets of flanges, at different frequencies and flange positions. Data from three positions only are presented. These are the aperture, optimum, and minimum. The corrugated flanges yield higher gain than plane flanges as is evident from tables 4.4(i)(II),(III) and (IV). Figs.4.4(i)(b),(c) and (d), show the variation of gain with respect to the corrugation period at different positions. In these graphs, the gain obtained with plane flanges of identical overall size is shown as a reference level for comparison. This gain enhancement while using corrugated flanges is mainly due to the reduction in side lobe levels. This reduction in E-plane side lobe level is predicted by theory, as well. The corrugated conducting surface is known to reduce the fringing electric fields near the extreme edges of the flange elements. The corrugations also help to introduce a systematic fall in the intensity of excitation as one

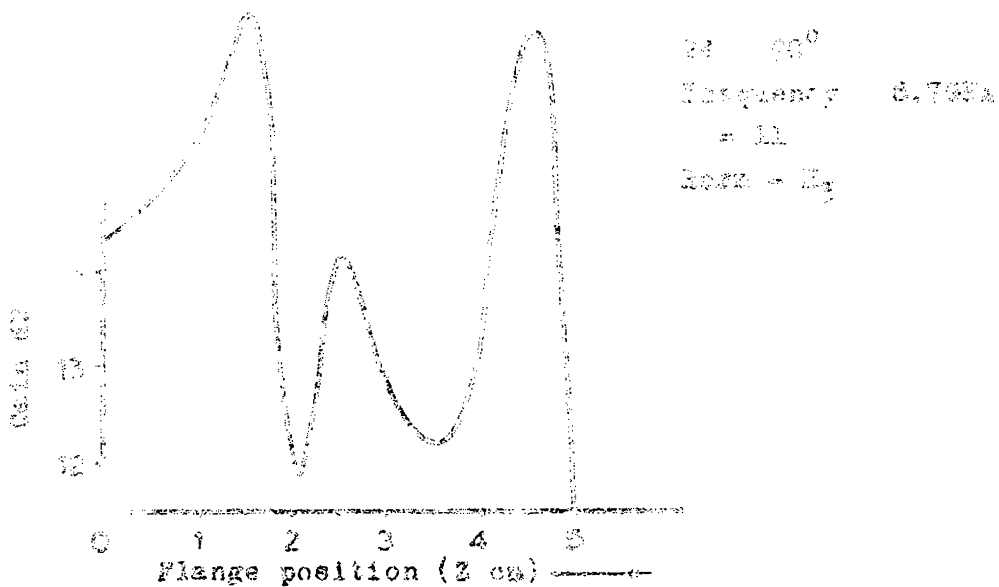


Fig. 4.4(i)(a) Variation of E-plane gain with flange position relative to Horn aperture.

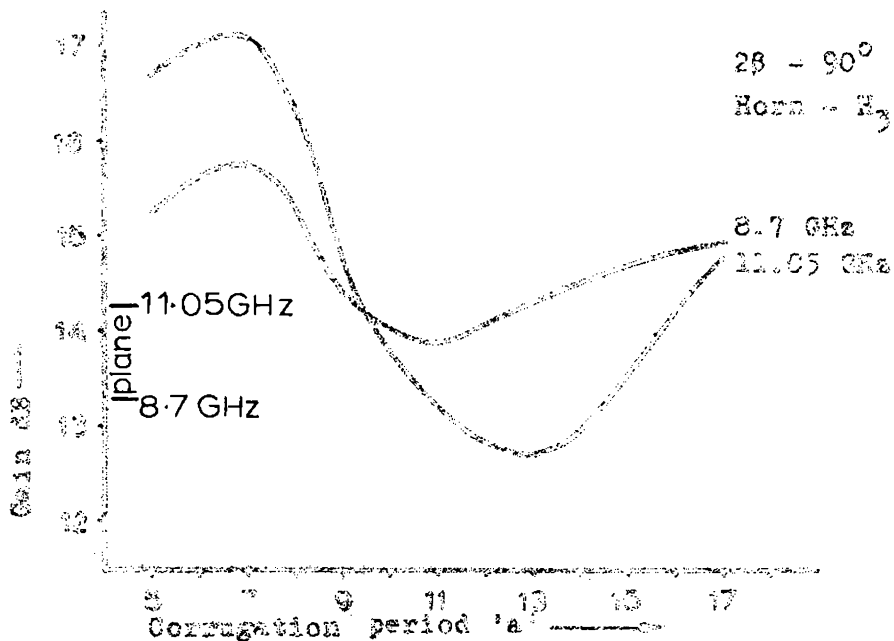


Fig. 4.4(i)(b) Variation of E-plane gain with corrugation period 'a' when the flanges are kept at the horn aperture.

Table 4.4(i)(III)

Modified E-plane Gain when the flanges are kept at the optimum.  $2\beta = 90^\circ$

'a'	Gain dB	
	8.7 GHz	11.05 GHz
17	15.7	14.6
13	17.8	17.6
9	16.1	17.3
7	17.2	18.1
5	18.3	18
Plane	13.6	14.5

Table 4.4(i)(IV)

Modified E-plane Gain when the flanges are kept at the minimum.  $2\beta = 90^\circ$

'a'	Gain dB	
	8.7 GHz	11.05 GHz
17	13.1	13.7
13	14.1	12.1
9	14.3	13.6
7	15	14.8
5	14.5	15.3
Plane	12.8	13.6

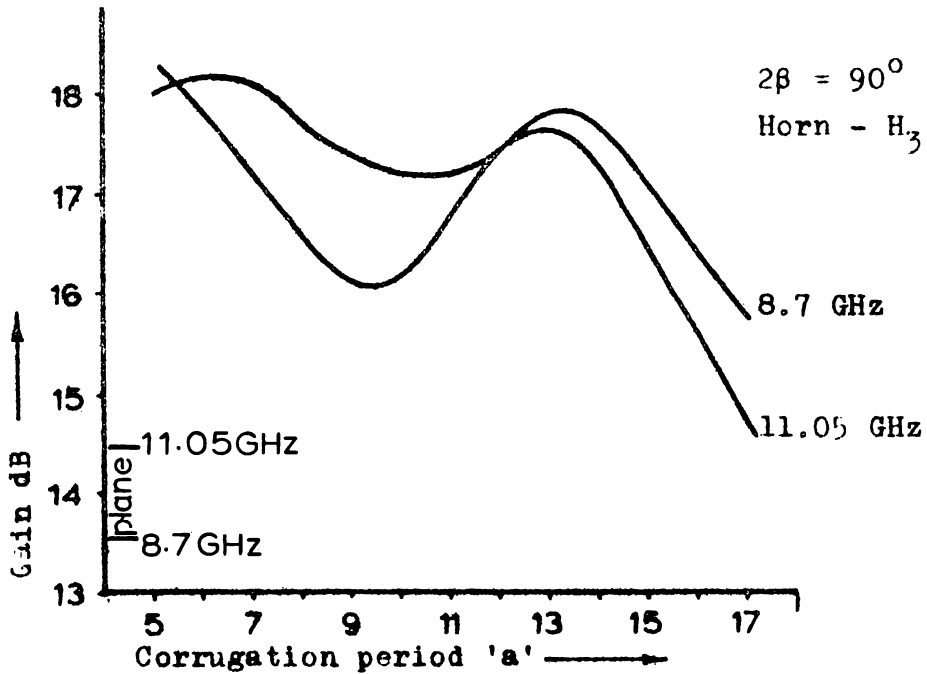


Fig.4.4(1)(c) Variation of E-plane gain with corrugation period 'a' when the flanges are kept at the 0-position.

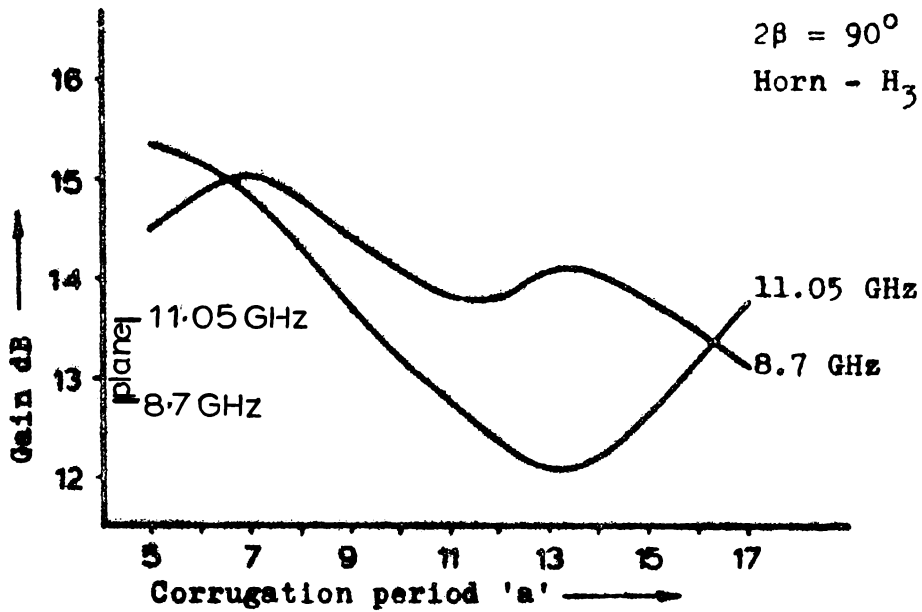


Fig.4.4(1)(d) Variation of E-plane gain with corrugation period 'a' when the flanges are kept at the M-position.

goes to the flange edges. This corresponds to the taper in the aperture field intensity obtained in the E-plane of corrugated horns, which also effects a major reduction in side lobe levels and an increase in gain.

#### 4.4(ii) Dependence of E-plane Gain on Flange Angle

The variation in E-plane gain for changes in the included angle is described in this section. The flanges were kept at the 0-position only. Fig.4.4(ii)(a) gives the graphs showing the variation of E-plane gain for changes in the included angle  $2\beta$ . From these curves it can be seen that,

- 1) The gain reduces as the flange angle increases
- 2) As the corrugation period decreases, the gain increases.

The first is mainly due to the fact that, the horn aperture radiates like an open ended waveguide in the E-plane, and hence has a certain directivity. Therefore as the flange angle increases, flanges move out towards regions of lower field intensity, whereby their excitation is reduced. The second effect will be discussed in detail in the next section.

#### 4.4(iii) Dependence of E-plane gain on corrugation period

The variation of E-plane gain as a function of the corrugation period is described in this section. The flanges

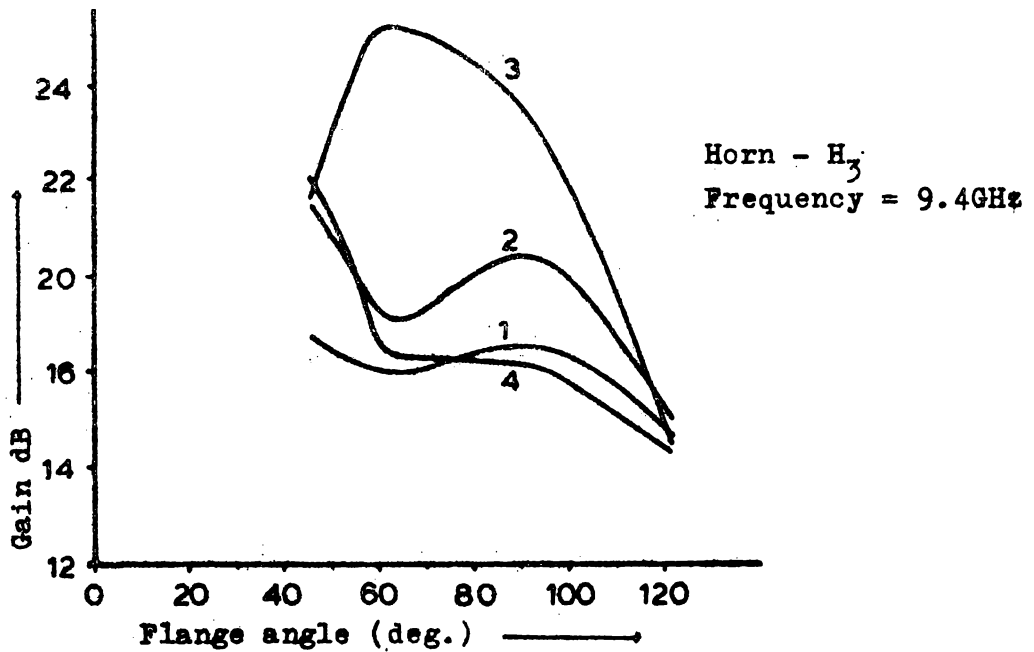


Fig. 4.4(ii)(a) Variation of E-plane gain with flange angle.  
1 -  $N = 6$ , 2 -  $N = 8$ , 3 -  $N = 11$ , 4 - Plane flange.

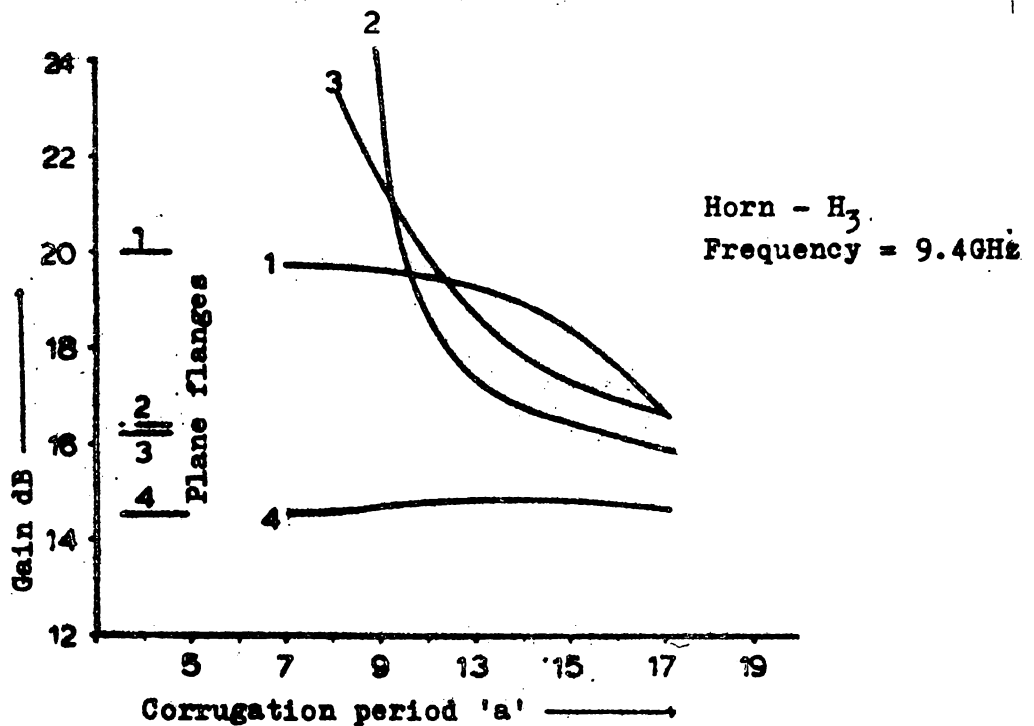


Fig. 4.4(iii)(a) Variation of E-plane gain with corrugation period.  
for different flange angles. 1 -  $2\beta = 45^\circ$ ,  
2 -  $2\beta = 60^\circ$ , 3 -  $2\beta = 90^\circ$ , 4 -  $2\beta = 120^\circ$ .

were kept at the 0-position only. Different sets of flanges with different spacings between corrugations were attached to the horn and the gain measurements were made using the technique described earlier. The results have been presented in graphical form in Fig.4.4(iii)(a). It can be seen that as the corrugation period reduces, or the number of corrugations increases, the gain increases. This is explained in terms of the behaviour of corrugated conducting surfaces. As the corrugation period decreases, the surface reactance becomes such that it will not support surface waves. Hence the decay of current across the flange surface becomes more rapid and current at the flange edges falls low. This reduces the fringing electric fields, which results in a lower side lobe level and an increased gain. Another interesting observation is that for larger included angles, the variation in gain is very small, as is evident from curve 4 corresponding to  $120^{\circ}$ , in Fig.4.4(iii)(a). The explanation given in sec.4.4(ii) is valid for this phenomenon also.

In the figure, the gain corresponding to an equivalent plane flange of different included angles is given for comparison.

#### 4.5 Half Power Beam Width

The results of the investigations described in earlier sections clearly show that, as the flange parameters are varied, many changes occur in the radiation characteristics

Some of these had been discussed in detail already. Another important parameter is the half power beam width (HPBW). The main lobe beam width controls the directivity, and to a large extent, the gain of the antenna system. The effect of corrugated flanges on the half power beam width is described in this section.

#### 4.5(i) Dependence of HPBW on Flange Angle

The variation of HPBW as a function of flange angle is considered. In this study, the flanges were kept only at the 0-position. Fig.4.5(i)(a) shows the variation in HPBW for changes in flange angle. The variation in HPBW for an equivalent plane flange is also shown for comparison.

#### 4.6 Corrugated Flange Mounted Sectoral Horn as a Circularly Polarised Radiator

When a linearly polarised radiation is incident on a periodic corrugated metallic surface, with the E-vector inclined at  $45^\circ$  to the corrugations, it is resolved into two components, one perpendicular and the other parallel to the corrugations. By a proper choice of the corrugation geometry it is possible to make the two components equal in magnitude and get them reflected from the surface such that one component is delayed by  $90^\circ$  behind the other. This means that the reflected radiation would be circularly polarised.

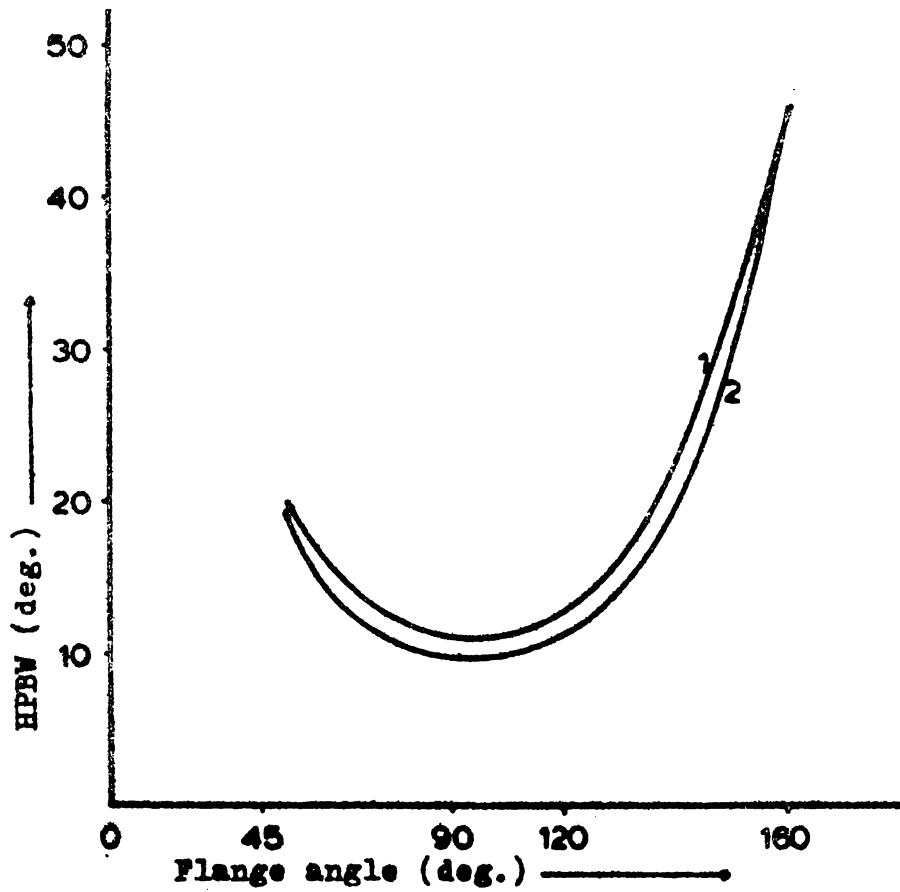


Fig. 4.5(1)(a) Variation of HPBW with flange angle.  
 Frequency = 9.4 GHz, Horn -  $H_1$ ,  
 1 - Plane, 2 -  $N = 11$ .

The possibility of employing such a corrugated flange system to obtain a circularly polarised radiated beam was investigated. Different sets of flanges were made with varying corrugation parameters. All these flanges were fabricated such that the slots are inclined at  $45^\circ$  to the E-vector when attached to the sectoral horn.

#### 4.6(i) Effect of Flange Position on the Axial Ratio of the System

The effect of flange position on the axial ratio of the system was studied. As the flange position is varied, the axial ratio changes. Here the axial ratio mentioned is that corresponding to the main lobe maximum.

The TE and TM reflection coefficients for a corrugated surface depends on the angle of incidence: <sup>(100)</sup> Hence to maintain their value equal at all points on the flange surface, the corrugation parameters had to be varied, as one moves across the flange surface. Since the slot depth was the easiest to alter, it was changed slowly across the flange surface. In other words, the slot depth  $h_1$  and  $h_2$  at two opposite edges of the flange were made different. Fig.4.6 (i)(a) shows the geometry of this type of flanges. Table 3.1(II) gives the different parameters of the flanges used in this study.

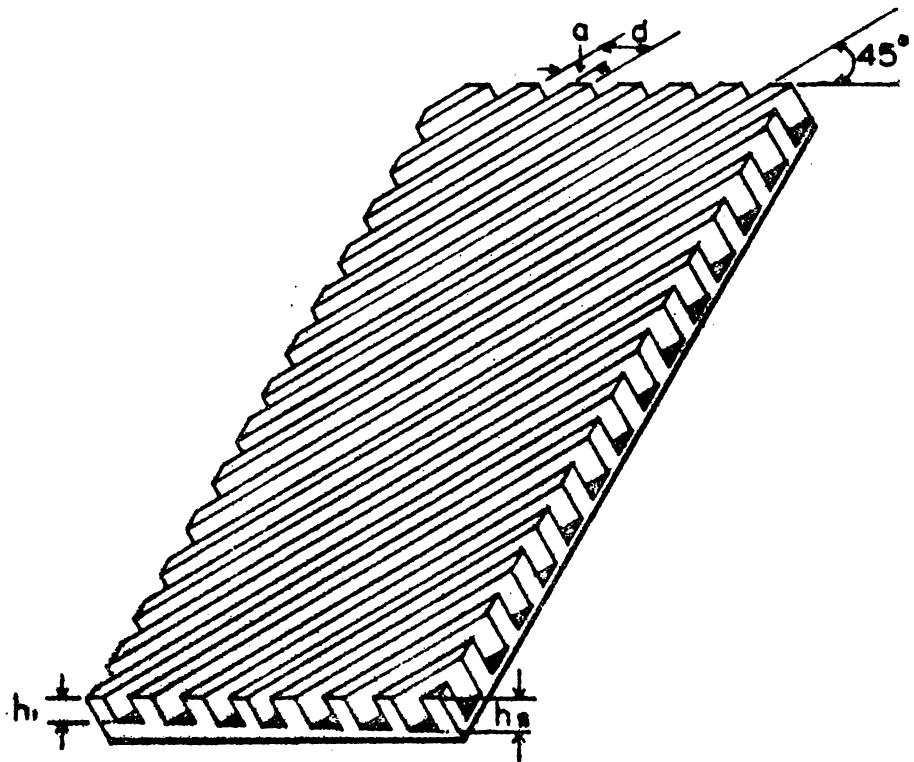


Fig.4.6(1)(a) Geometry of the inclined corrugated flange.

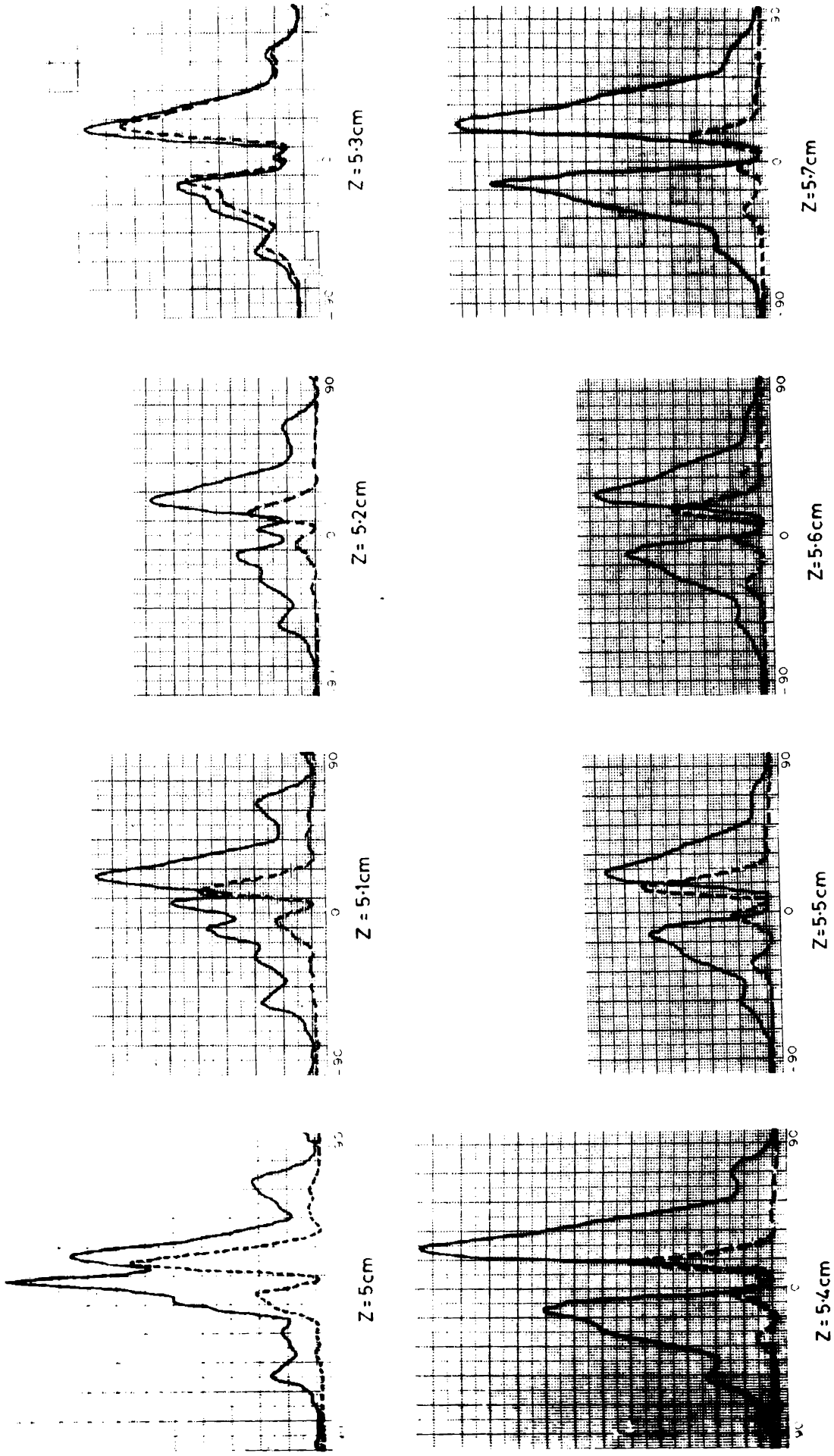


Fig. 4-6(i)(b) Parallel and orthogonal plane patterns due to inclined corrugated flanges.  
 $2\beta = 90^\circ$ , Horn  $-H_{11}$ , Frequency = 9.4 GHz, Flange -11. — Parallel - - - - Orthogonal

Fig.4.6(i)(b) shows the parallel and orthogonal plane pattern for this type of flanges. It may be noted that at  $Z = 5.3$  cms, a circularly polarised radiation is obtained. The axial ratio is 0.4 dB.

In this chapter the results of the experimental investigations carried out, have been reported. Theoretical explanations for these observed phenomena are next attempted and these are presented in chapter V.

## CHAPTER V

### THEORY OF THE CORRUGATED FLANGE MOUNTED SECTORAL HORN

5.0 In this chapter, the radiation from a corrugated flange mounted sectoral horn has been theoretically analysed on the basis of the line source theory.<sup>(7,18)</sup> This is reported in this chapter. Numerical calculations are presented and the results are compared with experimental values.

#### 5.1 Line Source Theory as Applied to Plane Flanges

Owen and Reynolds<sup>(7)</sup> proposed the line source theory to explain the effect of flanges on the radiation pattern of sectoral horns. In their theory, they made the simplifying assumption that the aperture of the sectoral horn can be treated as a linear radiator. The flanges are excited by the primary radiator, and hence the flange edges act as secondary radiators, whose amplitude and phase depends on the flange width, flange angle, and flange position. Fig.5.1(a) is a schematic of the flange mounted sectoral horn. Here,  $A$  is the horn aperture,  $M$  is the distant point, the field at which point we are interested in,  $\theta$  is the bearing angle, the point  $M$  makes with horn axis at the aperture,  $2\beta$  is the flange angle. Fig.5.1(b) is the geometry of the system.

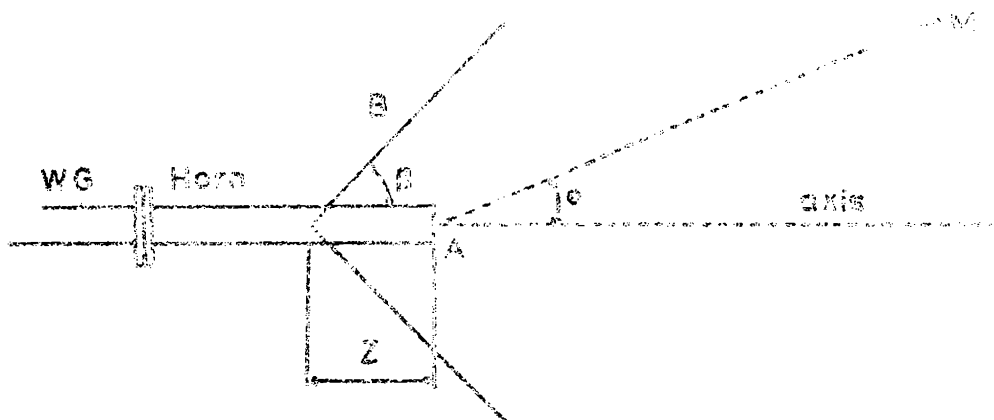


Fig.5.1(a) Schematic diagram of the flange mounted sectoral horn. A is the horn aperture,  $\epsilon$  is the bearing angle, B is the flange width.

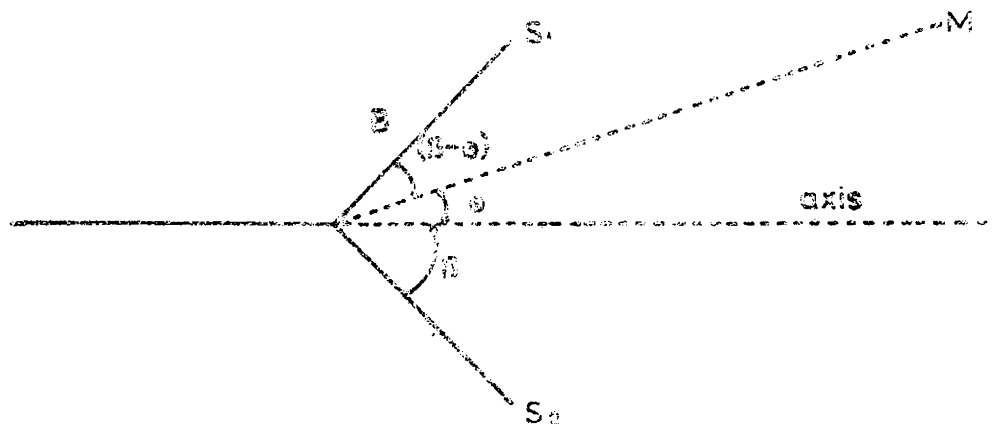


Fig.5.1(b) Geometry of the plane flange mounted sectoral horn.  $S_1$  and  $S_2$  are the secondary sources.

$S_1$  and  $S_2$  are the flange edges, which act as secondary sources,  $k$  is the amplitude of excitation of the secondary source, with respect to the primary aperture amplitude which is taken as unity.

Let  $\epsilon_1$  and  $\epsilon_2$  be the relative phase of the secondary radiators,  $S_1$  and  $S_2$ . Hence,

$$\epsilon_1 = \frac{2\pi B}{\lambda} \cos(\beta - \theta) \quad (1)$$

$$\epsilon_2 = \frac{2\pi B}{\lambda} \cos(\beta + \theta) \quad (2)$$

$$\text{Hence, } \epsilon_2 - \epsilon_1 = \frac{4\pi B}{\lambda} \sin \beta \sin \theta \quad (3)$$

The resultant  $\bar{R}$  of the fields due to the radiation from these two secondary radiators is given by,

$$|\bar{R}|^2 = k^2 + k^2 + 2k^2 \cos(\epsilon_2 - \epsilon_1) \quad (4)$$

$$|\bar{R}|^2 = 4k^2 \cos^2\left(\frac{\epsilon_2 - \epsilon_1}{2}\right) \quad (5)$$

$$\text{Hence, } |\bar{R}| = 2k \cos\left[\left(\frac{2\pi B}{\lambda}\right) \sin \beta \sin \theta\right] \quad (6)$$

The resultant power due to this field and the field due to the primary horn aperture at the point  $M$  is given by,

$$P_\theta = 1 + |\bar{R}|^2 + 2\bar{R} \cos\left(\frac{\epsilon_2 + \epsilon_1}{2} - \phi\right) \quad (7)$$

$$P_{\theta} = 1 + 4k \cos\left(\frac{2\pi B}{\lambda} \sin \beta \sin \theta\right) \left[ \cos\left(\frac{2\pi B}{\lambda} \cos \beta \cos \theta + \varphi\right) + k \cos\left(\frac{2\pi B}{\lambda} \sin \beta \sin \theta\right) \right] \quad (8)$$

$P_{\theta}$  gives the power distribution at M.

## 5.2 Corrugated Flange Mounted Sectoral Horn

Fig.5.2(a) is a schematic representation of the corrugated flange mounted sectoral horn.  $\theta$  is the bearing angle an arbitrary point 'M' in the far field makes with the axis of the horn.  $2\beta$  is the flange angle.  $Z$  is the distance between the aperture of the horn and the position where the flanges are kept. The corrugation period  $n\lambda$  is the separation between two adjacent fins. Here the fin thickness is considered to be vanishingly small even though it has a finite value.

Here also, as in the previous case, the major assumption is that the aperture of the primary horn can be considered as linear radiator. However, in actual case, the primary horn radiates like an open ended waveguide in the E-plane. The errors introduced by the inaccuracies of this assumption will be discussed later.

Fig.5.2(b) shows the geometry of the system. Here 'O' is the horn aperture.  $S_p$  is the 'p'th element on the flange surface.  $B_p$  is the distance of the  $p^{\text{th}}$  element from the horn aperture, O.

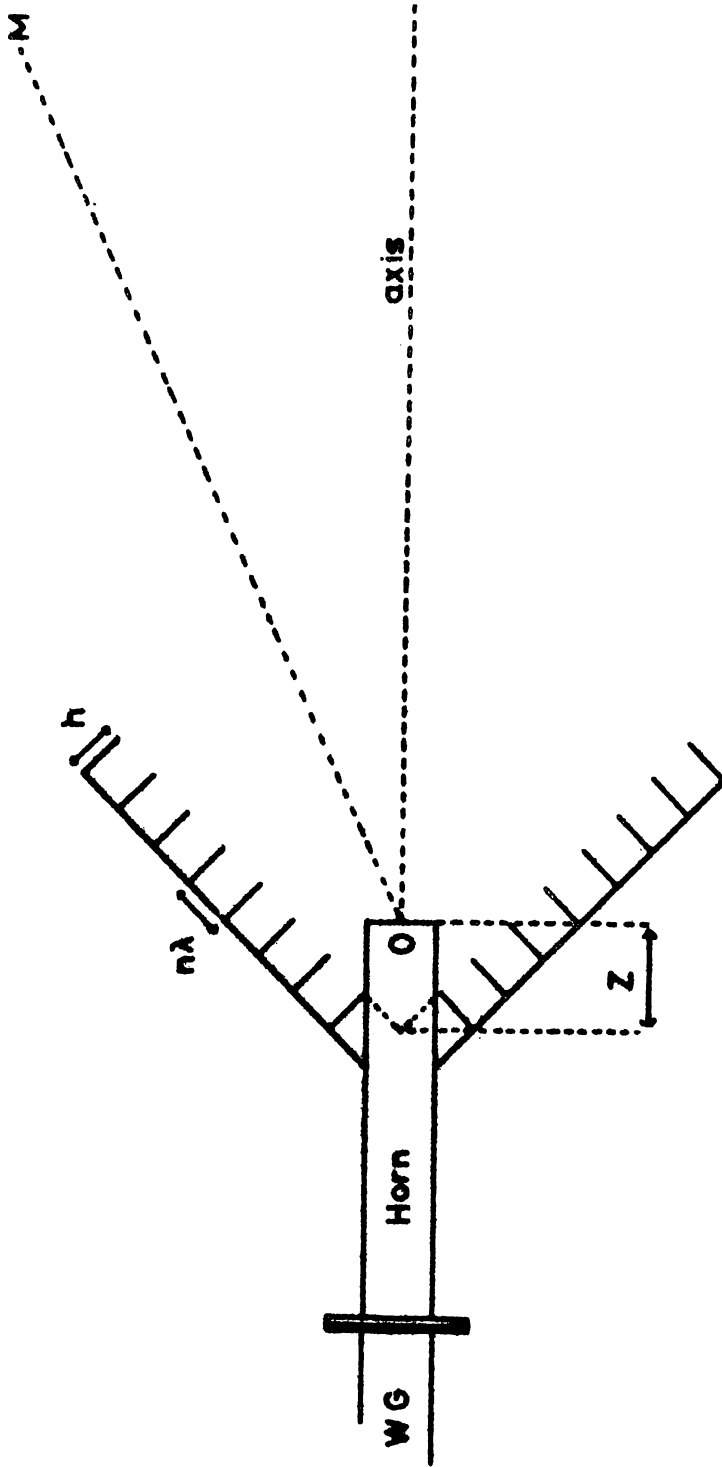


Fig.5.2(a) Schematic representation of the corrugated flange mounted sectoral horn.  $O$  is the horn aperture.  $M$  is a point in the far field.

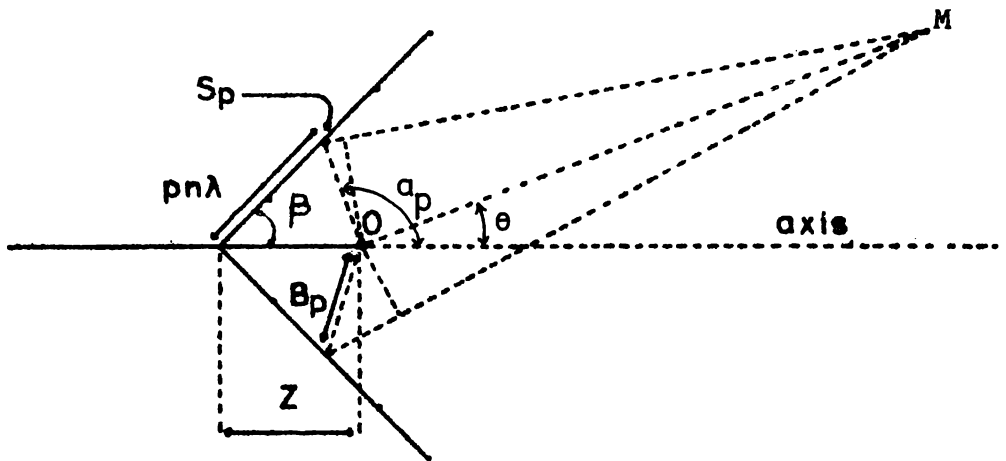


Fig.5.2(b) Geometry of the corrugated flange mounted sectoral horn.  $O$  is the horn aperture.  $S_p$  is the  $p^{\text{th}}$  element on the flange surface.  $B_p$  is the distance of the  $p^{\text{th}}$  element from the horn aperture.  $Z$  is the distance between the point where the flanges are kept and the horn aperture.

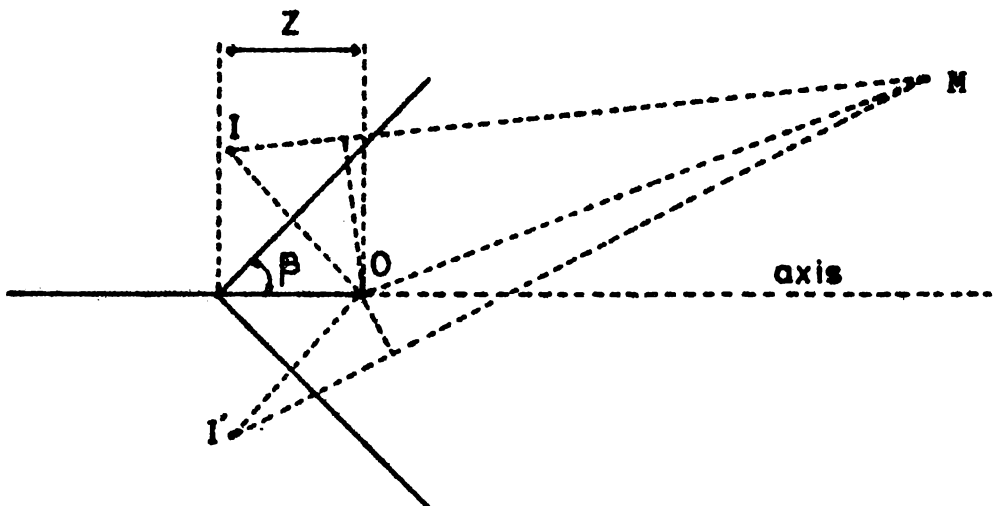


Fig.5.2(c) Geometry of the flange mounted sectoral horn.  $O$  is the horn aperture.  $I$  and  $I'$  are the images of  $O$  cast by the flange elements.

The tips of the fins on the flange surface are assumed to be excited by the primary horn. The amplitude and relative phase of these sources, with respect to the aperture, varies from element to element. These elements, in their turn, re-radiate this absorbed energy. The radiation from these elements adds up with the direct radiation from the horn. Let there be  $N$  fins on each flange element. Hence, there will be  $2N$  secondary radiators in total. The amplitude of excitation of these secondary radiators are taken to be proportional to  $1/B_p^2$ .

From Fig.5.2(b) and (c), it can be seen that,

$$B_p = \left[ Z^2 + \left( pn\lambda - \frac{h}{\tan \beta} \right)^2 - 2Z \left( pn\lambda - \frac{h}{\tan \beta} \right) \cos \beta \right]^{\frac{1}{2}} \quad (1)$$

When the radiation from the  $p^{\text{th}}$  element reaches the point  $M$ , the path difference between these waves and the radiation from the primary horn would be,

$$OM - (OS_p + S_pM) = \left[ Z^2 + \left( pn\lambda - \frac{h}{\tan \beta} \right)^2 - 2Z \left( pn\lambda - \frac{h}{\tan \beta} \right) \cos \beta \right]^{\frac{1}{2}} [1 - \cos (\alpha_p - \theta)] \quad (2)$$

Hence, the phase difference  $\eta_p$  of the radiation from the  $p^{\text{th}}$  element, and that from the horn aperture, as it reaches the point  $M$ , is given by,

$$\eta_p = \frac{2\pi}{\lambda} \left[ Z^2 + \left( pn \lambda - \frac{h}{\tan \beta} \right)^2 - 2Z \left( pn \lambda - \frac{h}{\tan \beta} \right) \cos \beta \right]^{\frac{1}{2}} \times [1 - \cos(\alpha_p - \theta)] \quad (3)$$

i.e.,

$$\eta_p = \frac{2\pi}{\lambda} B_p [1 - \cos(\alpha_p - \theta)] \quad (4)$$

By a similar argument, the relative phase of the  $p^{\text{th}}$  element on the second flange element,  $\eta'_p$  is given by,

$$\eta'_p = \frac{2\pi}{\lambda} B_p [1 - \cos(\alpha_p + \theta)] \quad (5)$$

The amplitude of these radiators is taken to be  $k/B_p^2$ , where  $k$  is a constant, the value of which was estimated by Butson and Thomson.<sup>(18)</sup> The vector sum of the radiation from all these elements give the resultant contribution due to them. Let  $K$  be the amplitude of this resultant, and  $\phi$  be the relative phase of this resultant.

$$K = \left\{ \left[ \frac{k}{B_1^2} \sin \eta_1 + \frac{k}{B_2^2} \sin \eta_2 + \dots + \frac{k}{B_N^2} \sin \eta_N \right]^2 + \left[ \frac{k}{B_1^2} \cos \eta_1 + \frac{k}{B_2^2} \cos \eta_2 + \dots + \frac{k}{B_N^2} \cos \eta_N \right]^2 \right\}^{\frac{1}{2}} \quad (6)$$

The relative phase is given by,

$$\varphi = \tan^{-1} \frac{\left[ \frac{k}{B_1^2} \sin \eta_1 + \frac{k}{B_2^2} \sin \eta_2 + \dots + \frac{k}{B_N^2} \sin \eta_N \right]}{\left[ \frac{k}{B_1^2} \cos \eta_1 + \frac{k}{B_2^2} \cos \eta_2 + \dots + \frac{k}{B_N^2} \cos \eta_N \right]} \quad (7)$$

The expression for K in (6) can be written in the form,

$$K = \left\{ \left[ \sum_{p=1}^N \frac{k}{B_p^2} \sin \eta_p \right]^2 + \left[ \sum_{p=1}^N \frac{k}{B_p^2} \cos \eta_p \right]^2 \right\}^{\frac{1}{2}} \quad (8)$$

and,  $\varphi$  in (7) as

$$\varphi = \tan^{-1} \left[ \frac{\sum_{p=1}^N (\sin \eta_p / B_p^2)}{\sum_{p=1}^N (\cos \eta_p / B_p^2)} \right] \quad (9)$$

By a similar argument, the corresponding values,  $K'$  and  $\varphi'$  for the second flange element are given by,

$$K' = \left\{ \left[ \sum_{p=1}^N \frac{k}{B_p^2} \sin \eta'_p \right]^2 + \left[ \sum_{p=1}^N \frac{k}{B_p^2} \cos \eta'_p \right]^2 \right\}^{\frac{1}{2}} \quad (10)$$

and,

$$\varphi' = \tan^{-1} \frac{\sum_{p=1}^N (\sin \eta'_p / B_p^2)}{\sum_{p=1}^N (\cos \eta'_p / B_p^2)} \quad (11)$$

The vector sum of these two fields gives the total contribution from the fins. This resultant is given by,

$$\bar{E} = K \angle \varphi + K' \angle \varphi'$$

$$E = [(K \sin \varphi + K' \sin \varphi')^2 + (K \cos \varphi + K' \cos \varphi')^2]^{\frac{1}{2}} \quad (12)$$

This is multiplied by an overall space directivity factor

$(\frac{\cos \theta}{\cos \beta} - 1)$  to satisfy the limiting conditions.

Hence,

$$E_{\theta} = \left\{ [(K \sin \varphi + K' \sin \varphi')^2 + (K \cos \varphi + K' \cos \varphi')^2] \left[ \frac{\cos \theta}{\cos \beta} - 1 \right]^{\frac{1}{2}} \right\} \quad (13)$$

$$\varepsilon = \tan^{-1} \frac{K \sin \varphi + K' \sin \varphi'}{K \cos \varphi + K' \cos \varphi'} \quad (14)$$

where  $\varepsilon$  is the relative phase of  $E$ . For values of  $\theta$ , such that  $(\frac{\cos \theta}{\cos \beta} - 1) < 0$ ,  $E_{\theta}$  values will be imaginary and hence will be ignored.

In the flanges constructed for this study, the slot width  $n\lambda$  is of the order of 0.25 to 0.5  $\lambda$ . Hence propagation inside the slots is possible. This causes the images I and I' to be formed. From Fig.5.2(c) the relative phase,  $\delta$ , of the image 'I' can be calculated to be,

$$\delta = \frac{2\pi}{\lambda} 2Z \sin \beta \sin (\beta - \theta) \quad (15)$$

By a similar argument,  $\delta'$ , the relative phase of  $I'$ , can be calculated to be,

$$\delta' = \frac{2\pi}{\lambda} 2Z \sin \beta \sin (\beta + \theta) \quad (16)$$

Now we can vectorially add the contribution from  $O$ ,  $I$ , and  $I'$ . This gives the amplitude as,

$$E'_\theta = \left\{ 3 + 2 \cos(\delta - \delta') + 2[\cos \delta(1 + \cos(\delta - \delta')) + \sin \delta \sin(\delta - \delta')] \right\}^{\frac{1}{2}} \quad (17)$$

Its phase is,

$$\epsilon' = \tan^{-1} \frac{\sin \delta + \sin \delta'}{1 + \cos \delta + \cos \delta'} \quad (18)$$

The resultant field distribution at the point  $M$  due to the contribution from all the radiators is the vector sum of the fields given by the expressions, (12), (13), (16) and (17). We are interested only in the amplitude of the resultant. This is given by,

$$P_\theta = \left\{ [E_\theta \sin \epsilon + E'_\theta \sin \epsilon']^2 + [E_\theta \cos \epsilon + E'_\theta \cos \epsilon']^2 \right\} \times (1 + \cos \theta) \quad (19)$$

Here the term  $(1 + \cos \theta)$  is taken as the common directivity factor for the directional antenna systems.

### 5.3 Results of the Theoretical Calculations

The radiation pattern given by equation 5.2(19) was calculated using a TDC 316 computer. The results are presented in this section. This is divided into two parts, part one giving the calculated on-axis power density, and the second part giving the calculated radiation pattern. These results are compared with the experimental values.

#### 5.3(i) On-axis Power Density as a Function of the Flange Position

Here the variation of the on-axis power density as the distance of the flanges from the horn aperture is varied, is presented. In equation 5.2(19), putting the value of  $\theta = 0$  gives the power density along the axis of the system. It has been observed that the computed values of  $P_{\theta}$ , for different values of 'z', fluctuates between maxima and minima. This fluctuation is shown in Fig.5.3(i)(a) and (b). In these figures, the dotted lines corresponds to the theoretical values. The experimental results are shown as solid lines for comparison. The curves presented corresponds to normalised values. It can be seen that there is fairly good agreement between theory and experiment.

#### 5.3(ii) Computed Radiation Patterns

The antenna patterns computed using equation 5.2(19) are presented here. In this expression,  $P_{\theta}$  was calculated for different values of  $\theta$  given by

— Experimental  
 - - - Theoretical

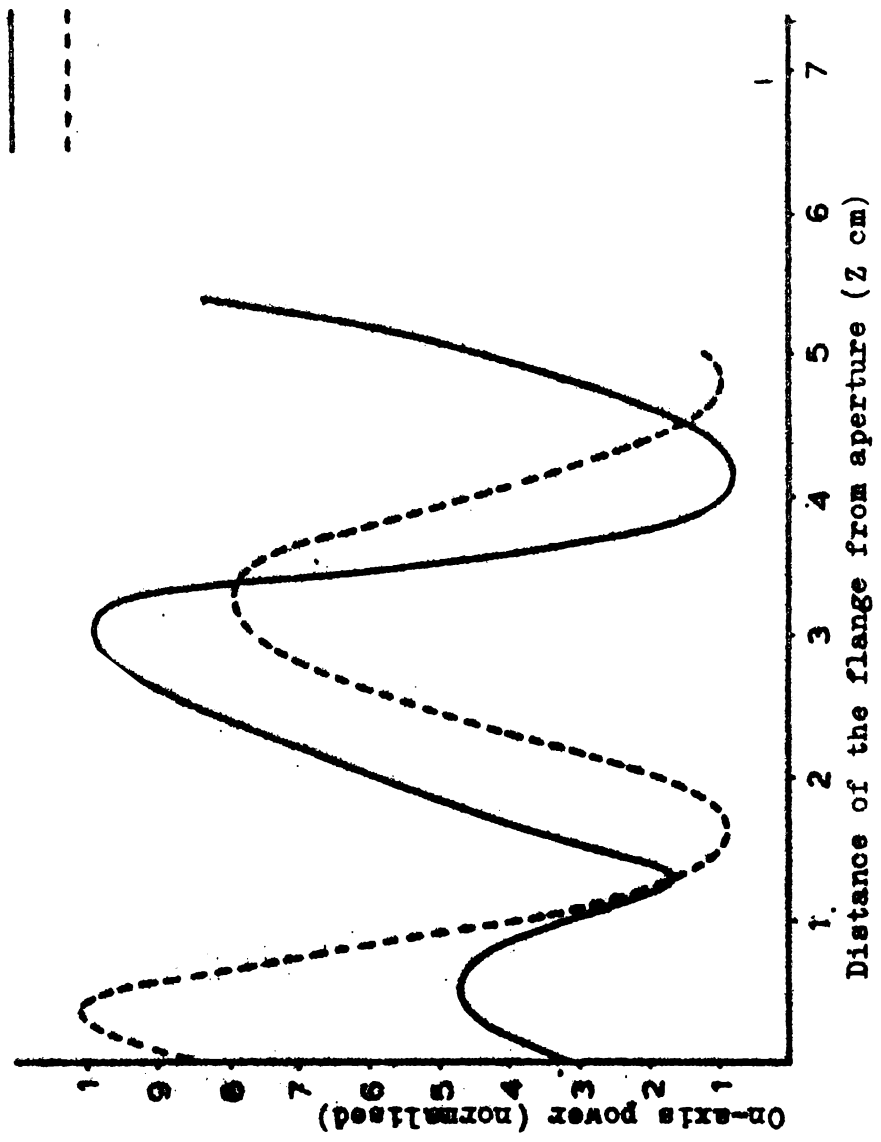


Fig.5.3(1)(a) Variation of On-axis power density with flange position.  $2\beta = 90^\circ$ , Frequency = 9.4 GHz,  $N = 6$ .

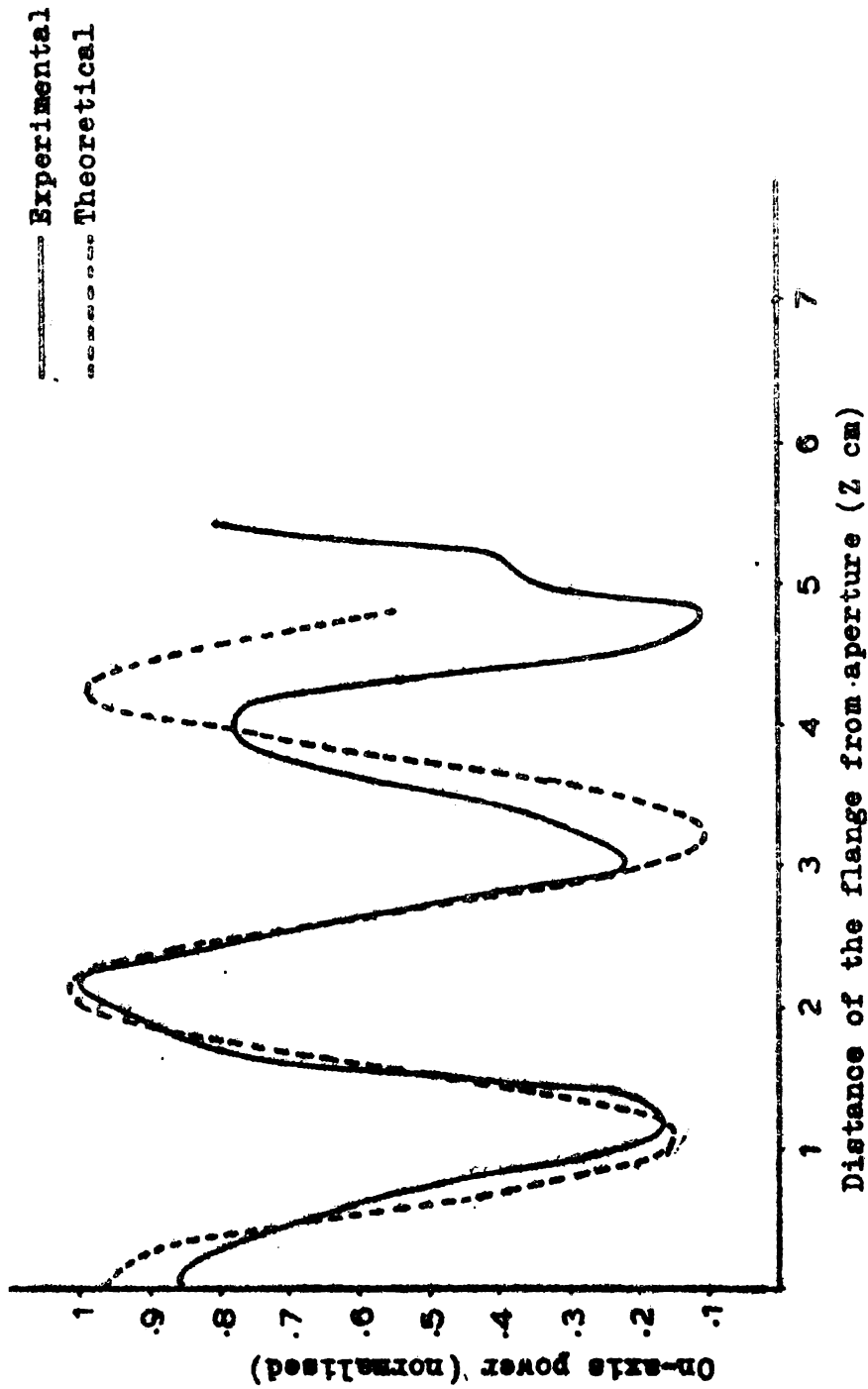


Fig.5.3(1)(b) Variation of On-axis power density with flange position.  
 $2\beta = 120^\circ$ , Frequency = 9.4 GHz,  $N = 6$ .

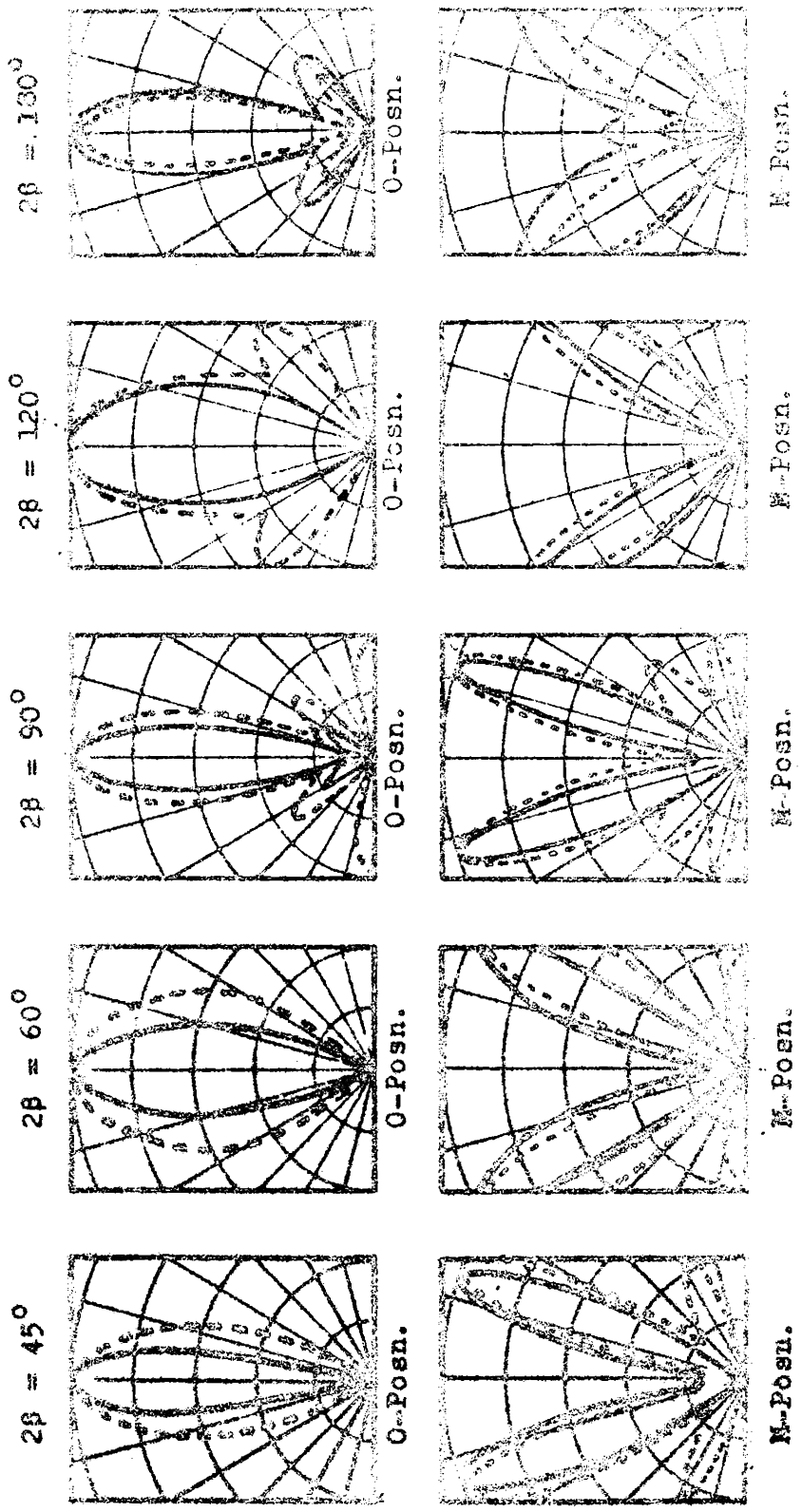


Fig. 5.3(11)(a) The radiation patterns due to the corrugated flanges.  
 Frequency = 9.4 GHz,  $N = 6$ .  
 Experimental. Theoretical.

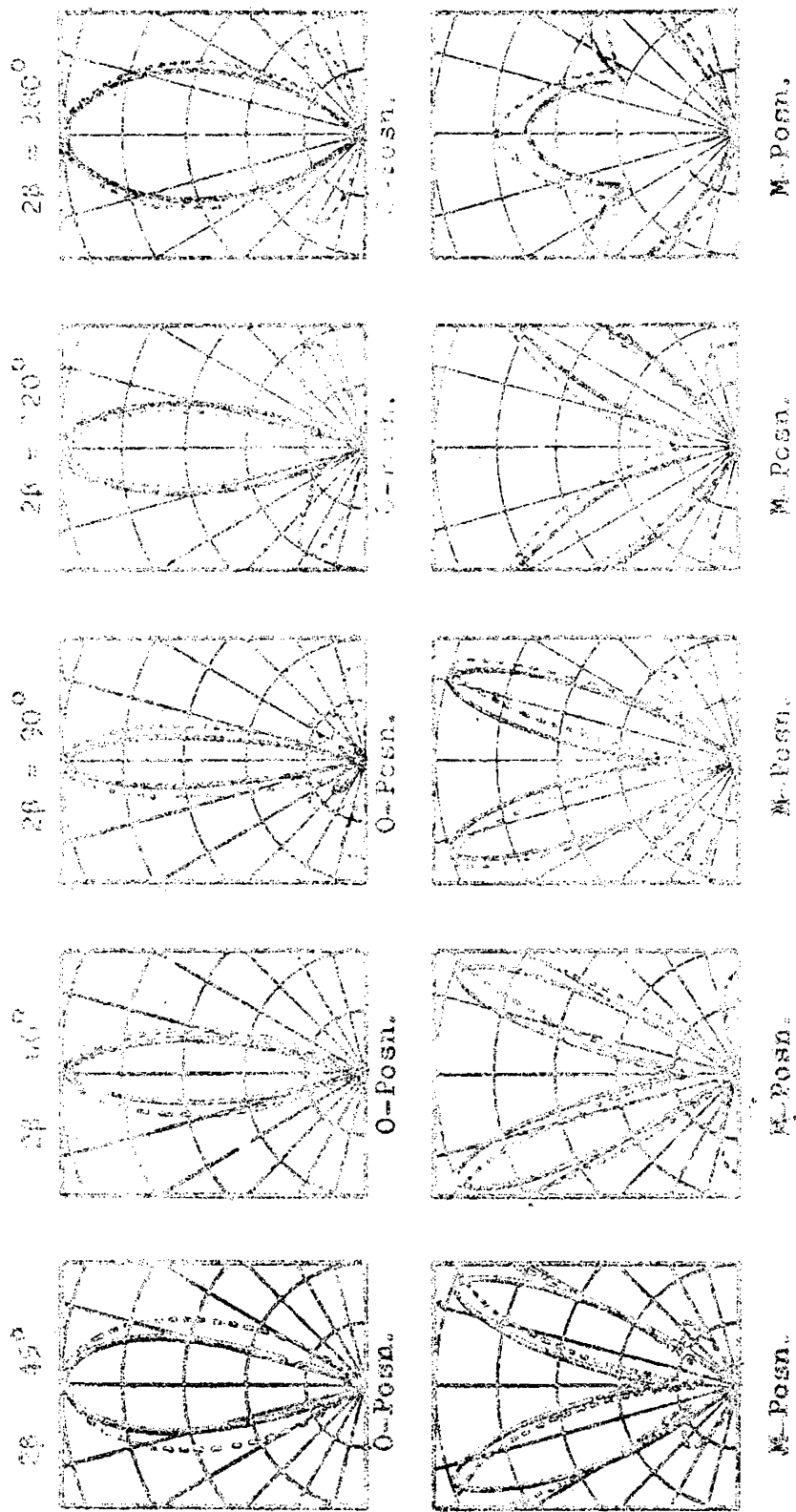


Fig. 5.3(1a)(b) The radiation patterns due to the corrugated flanges.  
 Frequency = 9.4 GHz,  $N = 11$ .

$\theta = 0^\circ, 5^\circ, 10^\circ, \dots, 90^\circ$  From these values, the patterns were plotted manually. These are shown in Fig.5.3(ii)(a). It may be noted from these figures that, there is good agreement between theory and experiment.

The small differences between theory and experiment is due to the inadequacy of the approximations made in the theory. This is discussed in detail in the next chapter.

Expressions were derived for the radiation pattern of the corrugated flange mounted sectoral horn, on the basis of the model proposed by Owen and Reynolds.<sup>(7)</sup> Numerical computations were made, and the results are presented. These are compared with experimental values. As can be seen from the data presented good agreements between theoretical and experimental values are obtained.

The effect of the inclined corrugated flanges, reported in Section 4.6, can be explained in terms of the TE and TM polarised wave reflection. A linearly polarised wave, with E-vector inclined at  $45^\circ$  to the corrugations, can be resolved into two equal components, one with the E-field and the other with the H-field parallel to the corrugations. The TE wave is totally reflected from the top of the corrugations. The reflection coefficient for the TM wave can be derived in terms of the surface parameters. This exhaustive theoretical analysis has been left out from the present work for future investigations.

## CHAPTER VI

### CONCLUSIONS

6.0 The results of the exhaustive experimental investigations and their theoretical explanations are given in chapters 4 and 5 respectively. In this chapter, the conclusions drawn from those results are presented. Suggestions for carrying out further investigations related to the work reported in this thesis are given at the end of this chapter.

#### 6.1 Inferences from the Experimental Investigations

The effect of various parameters on the VSWR of the system had been described in sections 4.1(i) through 4.1(iv). From these studies it is seen that by carefully controlling the flange parameters, the value of VSWR can be maintained low throughout the desired frequency band. It is observed that in most cases, the flanges brought down the VSWR of the system below that of the uncorrected VSWR of the horns used.

The variation in on-axis power density, due to changes in the flange parameters are described in sec.4.2. Here the effect of plane and corrugated flanges are compared. It is seen that whereas the corrugated

flanges give a fairly good match at 0-positions, plane flange does not. This is one of the major advantages that the corrugated flanges possess over the plane flange.

It is observed that the corrugated flanges possess good control on the beam shape. A narrow main lobe, broad beam, or a beam **with** a null along the axis can be obtained. Such patterns are needed in many applications. For example, a very narrow beam is needed in radar tracking systems, a broad beam with sharp fall off near the edges is needed for illuminating deep paraboloids, and a null along the axis is ideally suited for illuminating cheese mirrors.

The dependence of the E-plane gain on various flange parameters, are described in sections 4.4(i) through 4.4(iii). The results are compared with those obtained with plane flanges. It is observed that the corrugated flanges give a higher antenna gain.

It is observed that by a proper choice of the corrugation geometry, corrugated flanges can be used to obtain a circularly polarised beam with a linearly polarised primary horn.

From the experimental investigations carried out, it has been observed that corrugated flanges are very effective in beam shaping of sectoral horn antennas. They are much superior to the plane flanges in performance.

The performance of the corrugated flanges show that they behave similar to the behaviour of corrugated surfaces employed in corrugated horns.

## 6.2 Line Source Theory as Applied to Corrugated Flanges

The results of the theoretical computations carried out, show that there is fairly good agreement between theory and experiment. However, in certain cases, especially in the side lobe directions, there exists some difference between theory and experiment. This is due to the inadequacy of the approximations made in the theoretical model. The main causes of error are the assumption that the horn radiates like an isotropic linear radiator. This assumption is not valid in a strict sense. However for small included angles, the error due to the assumption that the primary horn radiation pattern is omnidirectional can be small. The error due to the finite width of the E-plane aperture increases as the bearing angle increases. This is the reason for the larger discrepancies in the side lobe directions.

However, the general trend is such that the system yields to theoretical analysis based on the line source theory.

## 6.3 Suggestions for Further Work

The studies reported here have opened the following interesting topics for further investigations.

A more accurate theoretical model can be developed, taking into consideration the primary horn radiation pattern in the E-plane. The edge diffractions from the E-plane edges of the primary horn also has to be taken into consideration.

The possibility of developing a circularly polarised antenna using the flange technique has to be considered in detail. The preliminary results reported in sec.4.6(i) are very encouraging.

The asymmetric corrugated flanges had not been included in the present study. This has to be studied in detail especially for offset feeding of paraboloids.

Another possible direction to work is the use of an asymmetric corrugated flange system to develop a frequency scannable antenna.

Effect of dielectric material in the corrugations will be an interesting problem for further investigations.

The observations made and the conclusions drawn therein are indicating wide scope for incorporating corrugated flange system as feed horns for fine adjustments of antenna parameters. The potentiality of the flange system to be used as an 'antenna trimmer' for delicate adjustment of its characteristics is a feature which may find wide applications in modern antenna techniques.

## APPENDIX I

### DESIGN AND DEVELOPMENT OF A MICROWAVE ANECHOIC CHAMBER FOR ANTENNA MEASUREMENTS

#### A.I.0 Introduction

One of the major projects in which the author participated and involved for quite some time was the design and fabrication of a microwave anechoic chamber. Most of the antenna measurements reported in this thesis were performed inside this chamber.

An anechoic chamber is an artificially simulated 'free-space environment', in which r.f. propagation studies can be performed without any interaction from other objects. This essentially consists of a large room, the interior surfaces of which are covered with some electromagnetic wave absorbing material with good absorption at the frequencies of interest. To avoid any possible coupling with the outer environment, a metallic lining is also put on the exterior. Since human beings present inside the chamber can cause appreciable reflection and scattering, operators cannot remain inside the chamber while taking measurements. This means that the turn-table etc. inside the chamber, have to be equipped with remote control devices.

The design details and specifications of the chamber are described in the following sections.

### A.I.1 Absorbing Material

Microwave absorbing material forms the most important part of the anechoic chamber, since the performance of a chamber is directly related to it. The average reflectivity of a chamber can never be less than that of the absorbing material used in its construction.

The earlier anechoic chambers were made by placing a 'space cloth' one quarter wavelength in front of a conducting surface.<sup>(54)</sup> This gives very good absorption but is highly frequency sensitive. Later, animal hair impregnated with rubber was developed. Animal hair is a good absorber, for electromagnetic waves. When it is spun, it traps large volumes of air inside and thus a good absorber was developed. Another version is polyurethane foam based, with some microwave absorbing material in powder form dispersed inside it.

In this chamber, indigenecously available material of the last type is employed. The material has been cut into pyramidal or wedge shape. The following types of material were employed:

- 1) Small pyramids of base 7.6 cms and height 15.2 cms. These are used on the ceiling, side walls, a major portion of the back wall, and a portion of the floor.

- 2) Larger pyramids of base 15.2x15.2 cms and height 45.7 cms. These are used on that portion of the back wall which takes the full impact of the main beam (target area) from where the reflections are most likely to occur.
- 3) Wedges of base width 10.2 centimeters and height 5.1 cms. These are used to cover less important regions of the chamber, like the surfaces of the tapered section.
- 4) Layered flat absorber. The absorber types described in 1, 2 and 3 achieve a slow transfer from a low absorber density to a high absorber density by means of its physical shape. Such a slow transfer is essential to reduce the surface reflections. However any of the designs described above cannot be used on the floor space where the operator has to stand and walk (walkways), for obvious reasons. Here we use 'layered flat absorbers'. Here, the absorber content in a flat foam sheet is slowly varied in such a way that there is gradually increasing gradient of absorber density, as the energy penetrates into the material. This is achieved by stacking a large number of absorbant sheets

with varying absorber content. Such a flat layered sheet with five layers and a total thickness of 15.2 cms is used on the walkways.

- 5) Flat absorber. This is a densely packed absorber material of thickness 5.1 cms. This has been put beneath all the above mentioned types to increase the effective absorption.

Prior to sticking these materials inside the chamber, their reflectivity was measured. The "Arch method" of testing the absorber material was employed to measure the absorber reflectivity. Fig.A.I.1(a) shows the experimental set up. Here separate transmitting and receiving horns are employed. These are arranged along an arc of a circle, pointing towards the absorber kept at its centre. The reflected power  $P_r$  is noted. The absorber is replaced with a metallic sheet of the same dimensions and the reflected power  $P_o$  is noted as the reference level. From these the reflectivity is calculated as,

$$R \text{ dB} = 10 \text{ Log}_{10} \left( \frac{P_r}{P_o} \right)$$

The advantage of this method is that the reflectivity at different angles of incidence can be measured. The 15.2 cms high pyramids with a 5.1 cms thick flat absorber on the back and a metallic surface behind had a reflectivity of -35 dB. This was considered fairly sufficient. The wedge absorber

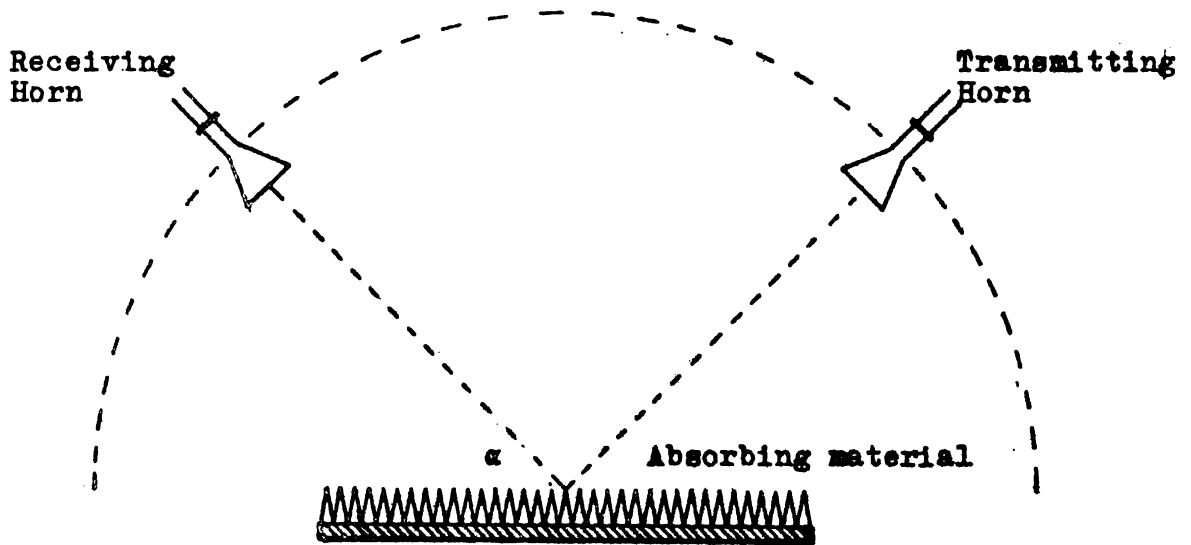


Fig.A.I.1(a). The experimental set up for the 'Arch method' used to test absorber samples.  $\alpha$  is the angle of incidence.

had a slightly higher reflectivity, but, since the wedges were used to cover only the tapered portion, this is acceptable.

The power rating of the absorber is not an important parameter when used inside an anechoic chamber, since the radiated power density is very small. Hence practically no heating will occur.

Polyurethane foam is inflammable. Hence while making the absorber it was specially treated to impart fire retardent properties.

#### A.I.2 Design of the Chamber

##### a) Scattering from rough periodic surface

The inside of an anechoic chamber lined with pyramidal absorbers constitutes a periodic rough surface. In treating such a surface the diffraction from the pyramids have to be considered. The finger pitch of the pyramids governs the scattering by it. The following discussion is based on a paper by Green<sup>(91)</sup>, in which he discusses in detail the scattering from the inside of an anechoic chamber.

Fig.A.I.2(a) is a schematic representation of the surface. 's' is the finger pitch of the surface. 'S' is the source. 'P' is a distant field point, the scattered field at which point we are interested in. The radius vector from the origin to the (i,k)<sup>th</sup> scatterer is,

$$\bar{r} = \hat{x} is + \hat{y} ks$$



When a plane wave is incident, the unit vector in its direction of propagation is,

$$\hat{n}_1 = \hat{y} \sin \theta_1 - \hat{z} \cos \theta_1$$

The phase of the incident field at the scatterer relative to the origin is,

$$\varphi_{(i,k)} \text{ (incident)} = -\beta \hat{n}_1 \cdot \vec{r} = -\beta ks \sin \theta_1$$

$\beta$  is the wave number.

Considering the scattering towards a distant field point 'P',

$$\hat{n}_2 = \hat{y} \sin \theta_2 + \hat{z} \cos \theta_2$$

The phase of the scattered field from the  $(i,k)^{\text{th}}$  scatterer, relative to that from the origin is

$$\begin{aligned} \varphi_{(i,k)} \text{ (scattered)} &= \beta \hat{n}_2 \cdot \vec{r} \\ &= \beta ks \sin \theta_2 \end{aligned}$$

Hence the total phase difference at P is,

$$\begin{aligned} \varphi_{(i,k)} \text{ (total)} &= \varphi_{(i,k)} \text{ (incident)} + \varphi_{(i,k)} \text{ (scattered)} \\ &= \beta ks (\sin \theta_2 - \sin \theta_1) \end{aligned}$$

To produce a constructive interference, between scattered energy from different scatterers,

$$\sin \theta_2 - \sin \theta_1 = \pm n \frac{\lambda}{s}$$

where  $n$  is any integer.

As shown in Fig.A.I.2(b), the incident field may be considered to be from an arbitrary direction  $(\theta_1, \varphi_1)$  and scattered to a direction  $(\theta_2, \varphi_2)$ . In this case,

$$\begin{aligned}\hat{n}_1 &= -\hat{x} \sin \theta_1 \cos \varphi_1 - \hat{y} \sin \theta_1 \sin \varphi_1 - \hat{z} \cos \theta_1 \\ \hat{n}_2 &= \hat{x} \sin \theta_2 \cos \varphi_2 + \hat{y} \sin \theta_2 \sin \varphi_2 + \hat{z} \cos \theta_2\end{aligned}$$

Hence,

$$\begin{aligned}\varphi(i, k) &= \beta (\hat{n}_2 \cdot \bar{r} - \hat{n}_1 \cdot \bar{r}) \\ &= \beta i s (\sin \theta_1 \cos \varphi_1 + \sin \theta_2 \cos \varphi_2) + \\ &\quad \beta k s (\sin \theta_1 \sin \varphi_1 + \sin \theta_2 \sin \varphi_2)\end{aligned}$$

So that the scattered field from the different scatterers may add constructively,

$$\begin{aligned}\sin \theta_1 \cos \varphi_1 + \sin \theta_2 \cos \varphi_2 &= \pm n_1 \frac{\lambda}{s} \\ \sin \theta_1 \sin \varphi_1 + \sin \theta_2 \sin \varphi_2 &= \pm n_2 \frac{\lambda}{s},\end{aligned}$$

when  $\theta_1 = \theta_2$  and  $\varphi_1 = \varphi_2$ ,

$$\tan \varphi_1 = n_2/n_1$$

The frequencies at which back scattering can occur is,

$f = c\sqrt{n_1^2 + n_2^2}/2s \sin \theta$ , where  $c$  is the velocity of light.  $f$  will be lowest when  $\theta_1 = \pi/2$  and either  $n_1 = 1$   $n_2 = 0$ , or  $n_1 = 0$  and  $n_2 = 1$ .

Hence the lowest frequency is,

$$f_{\min} = c/2s \sin \theta_1.$$

In this chamber,  $s = 7.6$  cms and this corresponds to an  $f_{\min}$  of 1.97 GHz. Below this frequency, specular reflection occur.

#### b) Design of the enclosure

For antenna measurements, the antenna under test has to be illuminated by a plane wavefront.<sup>(29)</sup> Although this is achievable only with an infinitely large separation between the transmitting and receiving antennas,  $2D^2 / \lambda$  is taken as a practical minimum safe limit, where  $D$  is the aperture of the test antenna, and  $\lambda$  is the operating wavelength. The actual length of the chamber must be more than this, since the test antenna will be put in the 'quiet zone' of the chamber, which occurs at some distance from the chamber walls. This chamber has a total length of 7.2 mtrs. Hence an effective propagation length of about 6 mtrs is obtained. At X-band this corresponds to approximately  $10 \lambda$  (30 cms) aperture diameter. This is the largest size of the antenna which is expected to be tested in this chamber.

Microwave absorbers perform at their best at normal incidence and when the angle of incidence becomes greater than  $60^\circ$ , their performance degrades sharply.<sup>(57)</sup> This imposes a minimum limit on the width of the chamber. Hence the length to width ratio was chosen to be 2. This ensures that the angle of incidence at regions more prone to the main lobe is less than  $60^\circ$ . The width of the chamber is 3.6 mtrs.

A tapered geometry was adopted in the design of the chamber due to two reasons. Firstly, from the economic view point, the quantity of the absorbing material must be low. Secondly, for a given material specification, the tapered geometry gives a quieter quiet zone. This is explained in Fig.A.I.2(c) and (d). In a rectangular chamber, the radiation from the source and its images (though of a very small intensity, this may not be negligible when a highly uniform wavefront is needed) combine at the quiet zone, and this produces intensity maxima and minima across the quiet zone. In the case of a tapered chamber, if the source is kept at the apex of the tapered section, the images coincide with the source and hence the fluctuation in amplitude at the quiet zone will be eliminated.<sup>(57)</sup> Even if the source is kept not exactly at the apex, the fluctuation in amplitude would be very much less than that in the case of a rectangular chamber. The tapering started exactly half way across the chamber.

As mentioned earlier, this chamber is shielded for avoiding external interference. A metallic lining was put behind the absorbing material. This shield or lining prevents any coupling between the interior and exterior of the chamber. An iron shield would provide both plane wave and magnetic shielding. In this case, only a plane wave shielding was required and hence aluminium sheets were employed for

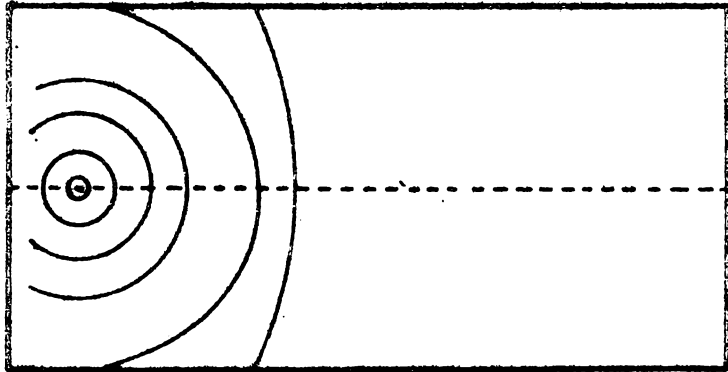


**Fig.A.I(2)(c)** Propagation of the wavefront in a rectangular chamber.

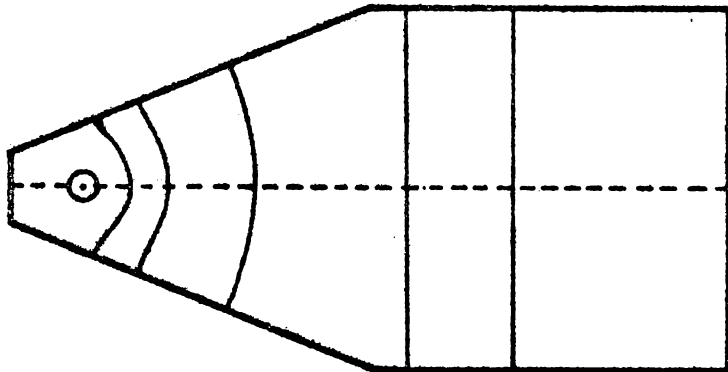


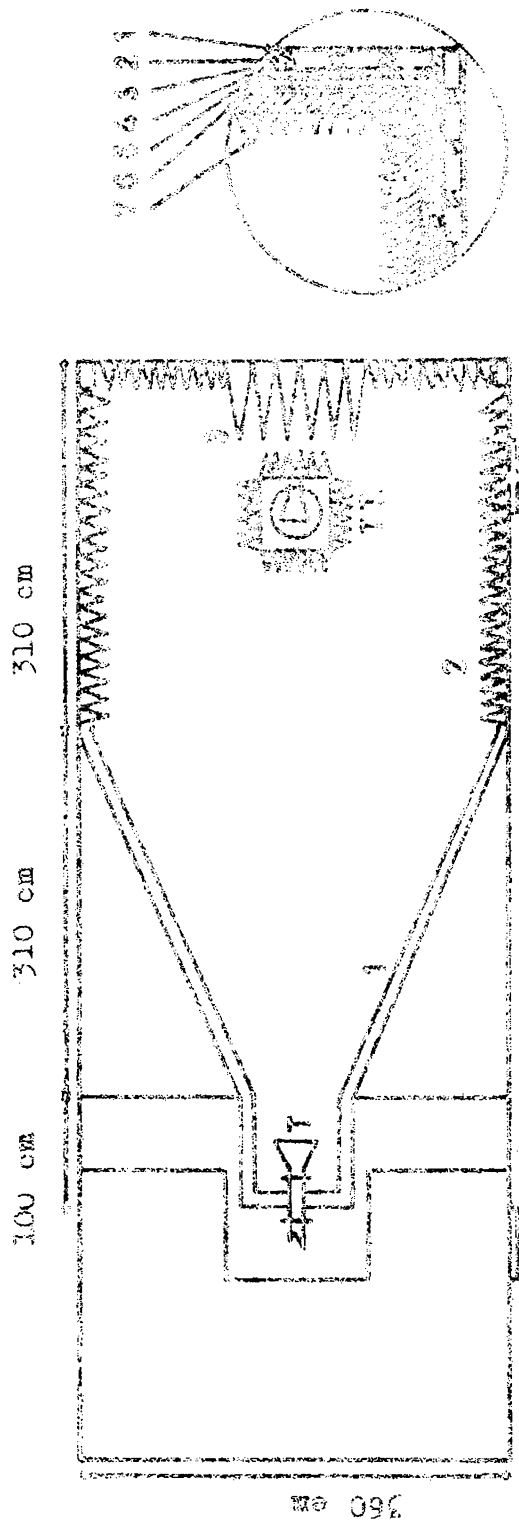
**Fig.A.I(2)(d)** Propagation of the wavefront in a tapered chamber.

shielding. 18 Gauge Aluminium sheets were paved over the plywood walls of the chamber throughout.

### A.I.3. Construction of the Chamber

The anechoic chamber was constructed inside a large rectangular hall 9.1 mtrs x 7.3 mtrs. One portion of the hall, 7.2 mtrs x 3.6 mtrs, was separated by a wooden partition for the anechoic chamber. Inside this, the anechoic chamber with the tapered portion was constructed using wooden frame work. Aluminium sheets were nailed on to the wooden framework for the shield. Over the aluminium sheets, water resistant 12 mm plywood boards were fixed. Absorbing material was stucked on to the surface of the plywood using commercial adhesives. As mentioned earlier, the tapered portion was covered with wedges and the walkways with flat layered material. The area at the centre of the back wall (target area) was covered with large pyramids.

A door at the rectangular end of the chamber provides access to the antenna turn-table etc., kept inside the chamber. The tapered portion ends in another small rectangular portion, inside which the transmitter is kept. This arrangement helps to keep the transmitter exactly at the apex of the tapered portion, as shown in Fig.A.I.3(a). This also helps to provide easy access to the transmitter.



(a)

(b)

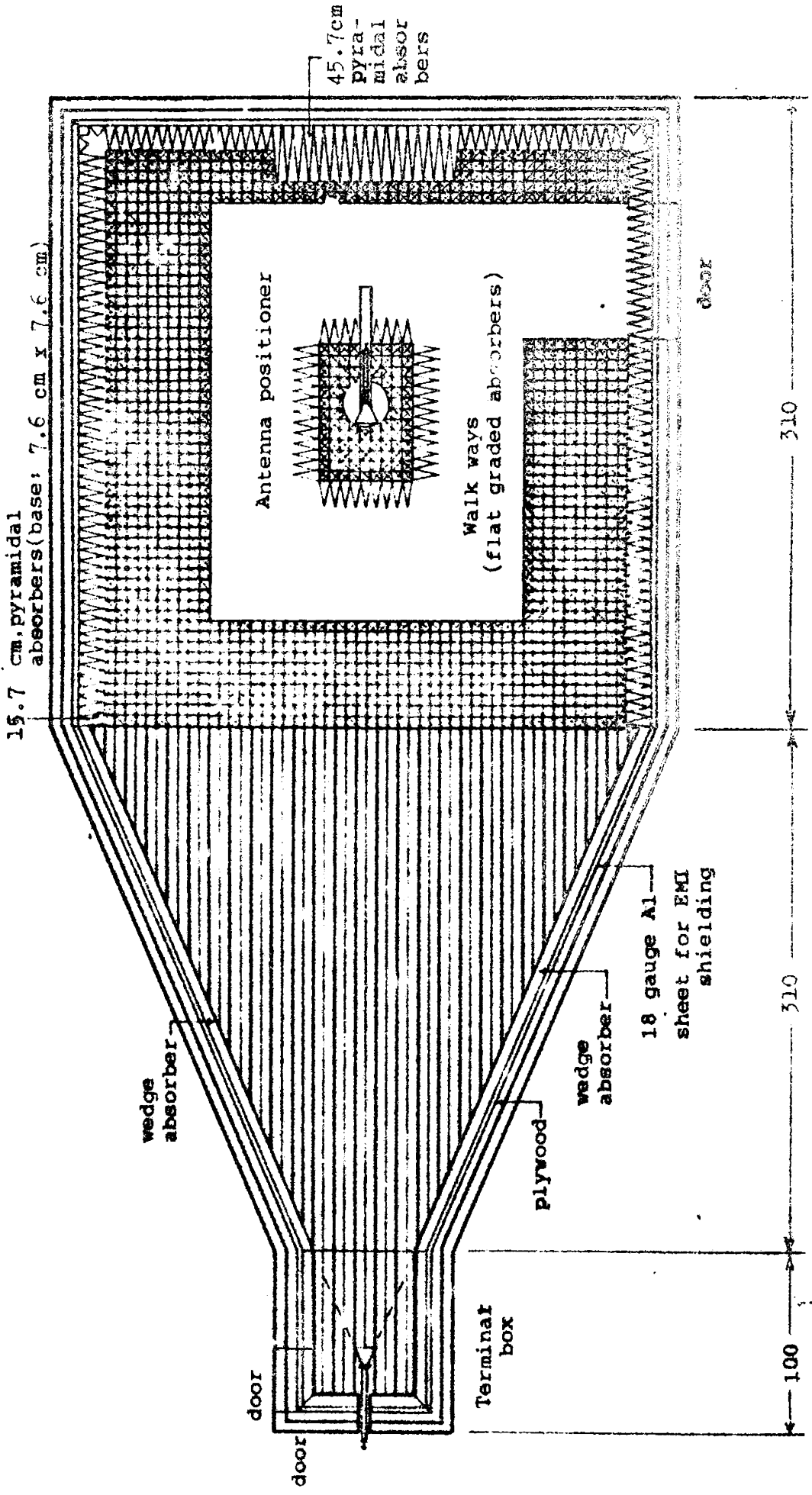
FIG. A.I.3

- (a) Construction of the anechoic chamber: T.T. is the transmitter, T.T. is the turn-table. 1 - Wedge absorber, 2 - Small pyramids, 3 - Large pyramids.
- (b) Structure of the walls. 1 - Outer plywood lining, 2 - Wooden structure, 3 - Plywood lining, 4 - Aluminium sheet (shield), 5 - Water resistant plywood lining, 6 - Flat absorber, 7 - Pyramids.

360 cm

COCHIN UNIVERSITY MICROWAVE ANECHOIC CHAMBER

[VIEW FROM THE TOP]



(All dimensions are in cm.)

FIG. A13 (c)

An incandescent lamp, hanging from the ceiling at the rectangular end provides sufficient light inside. Care was taken to avoid possible reflections from the lamp fittings. An exhaust duct was connected through a hole at one of the top corners. The position of the hole was so chosen to be one from where there was not the possibility of any reflections occurring. A powerful exhaust fan at the other end of the duct, draws the air from the chamber and pushes out. This provides a light and uniform air current through the chamber, which keeps the chamber fresh and dust free.

#### A.I.4 Instrumentation

As mentioned earlier an antenna turn-table with full remote control facility forms the major instrument. Its important features are:

1. An electrically driven platform, over which the antenna under test is to be attached. The platform rotates at a very uniform rate of 1 rpm. Limit switches are put at intervals to programme the turn table to stop after a predetermined angle of rotation. There is also provision to let the platform to rotate continuously.

2. There are brush and ring contacts to connect the antenna under test to the recording instruments. This was incorporated to prevent the cables from twisting and breaking.

3. A position indicator showing the exact azimuthal position of the rotating platform. This mainly consists of a highly linear, wire wound, potentiometer, the shaft of which rotates in synchronisation with the platform. The potential across the wiper terminals is directly proportional to the angle through which the platform has rotated.

4. Cables running between the control room and the turn-table. Shielded cables running through metallic conduit pipes are used to eliminate noise pickup. The power cables running to the motor are well isolated from those carrying signal, to reduce power-line interference.

5. Control room set up. The control panel for the turn-table, transmitter, measuring instruments, recorder etc., are situated inside the control room.

a) Turn-table control panel. This has the following provisions:

- i) Motor ON/OFF. This incorporates a relay starter with overload protection etc.
- ii) Direction of rotation indicator. This gives visual indication about the sense of rotation of the turn-table platform.
- iii) Position indicator. This includes the stabilised D.C. supply for the position indicator circuit, meter calibrated to read directly the angle through which the platform has rotated, jacks

for coupling the position information to recorder etc.

- iv) Signal level monitor. This contains a sensitive microgalvanometer to which the signal received by the receiving antenna is fed. This monitor is used for initial aligning and for a quick check of the transmitter and the receiver. This monitor can be removed and the signal can be fed to the recorder while taking actual measurements.
  - v) Limit switch control. This is used to preprogramme the rotation of the platform through any fixed angle, depending on the settings on the turn-table.
- b) Microwave source and power supply. The microwave source feeding the transmitter and its power supply are situated in the control room.
- c) Recording and measuring instruments. The pattern recorder is situated in the control room. An HP Model 7047A X-Y recorder is used for pattern recording. This is a fast recorder with a high sensitivity of 20 microvolts per cm. The signal received by the antenna under test is directly fed to the recorder. The radiated power of about 30 mW is sufficient to enable straight

reception. In the case of weak signals, heterodyne reception can be employed. Other measuring instruments like power meter, VSWR meter etc. are also kept in the control room.

#### A.I.5 Evaluation

The quality of an anechoic chamber depends on the quietness of its quiet zone. Quiet zone is the region inside the anechoic chamber, where the field distortion due to radiation reflected from walls, floor, and ceiling are said to be below a certain specified minimum. The quiet zone is generally a sphere centred at the test stand.

The merit of the quiet zone is specified as that value where the reflected ray from any surface bounded by the chamber is less than the direct ray by a specified amount expressed in dB.

The performance of this anechoic chamber was evaluated after its construction. The antenna pattern comparison technique, the most widely accepted and versatile of the several techniques<sup>(62)</sup> was used for evaluating the quiet zone reflectivity.

In this method, two identical pyramidal horns are taken. One is used as the transmitter and the other is mounted on the turn-table, kept exactly at the centre of the design quiet zone. Its pattern is recorded. This is the

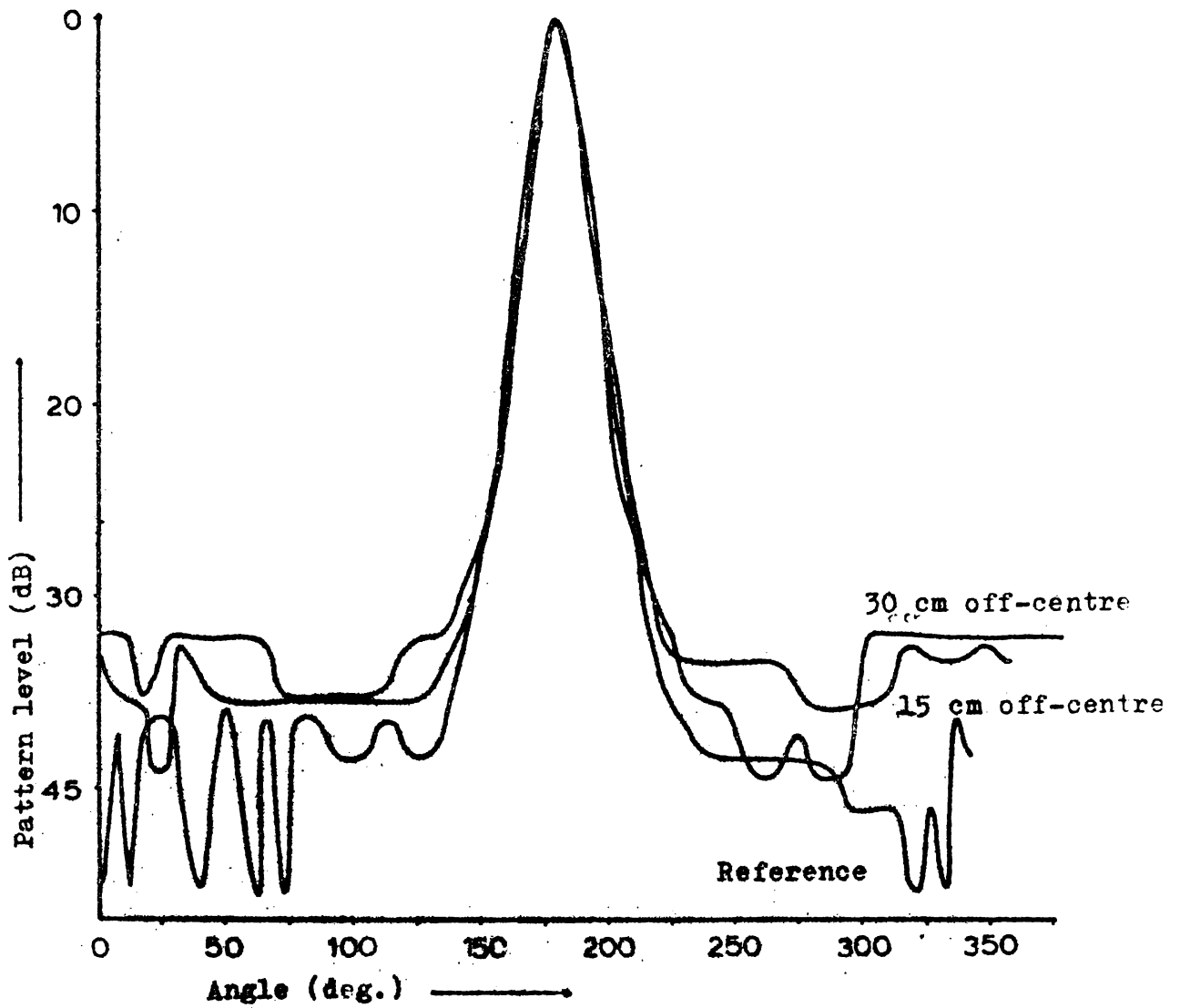


Fig.A.I.5(a) Radiation patterns recorded for the pattern comparison method of evaluation.

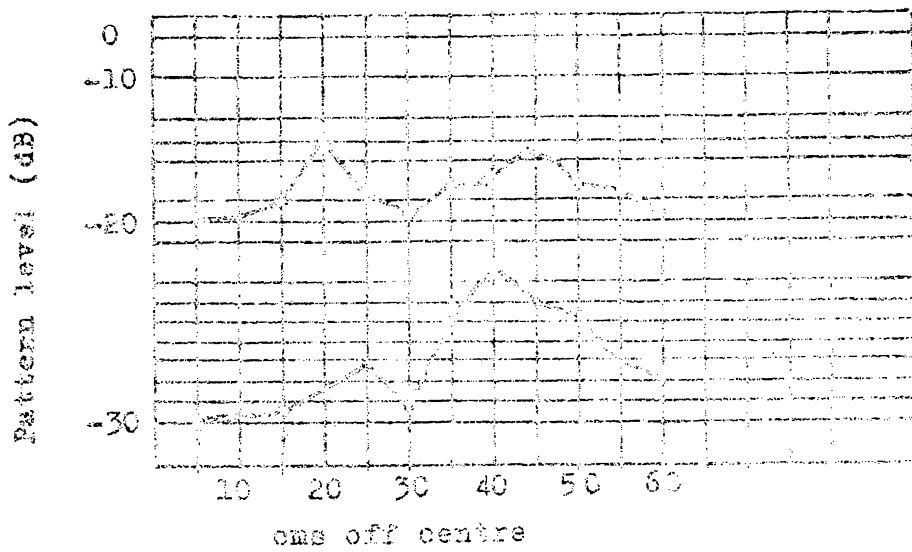


Fig.A.I.5(b) The deviation at each reference-pattern level radial distance between chamber centre point.

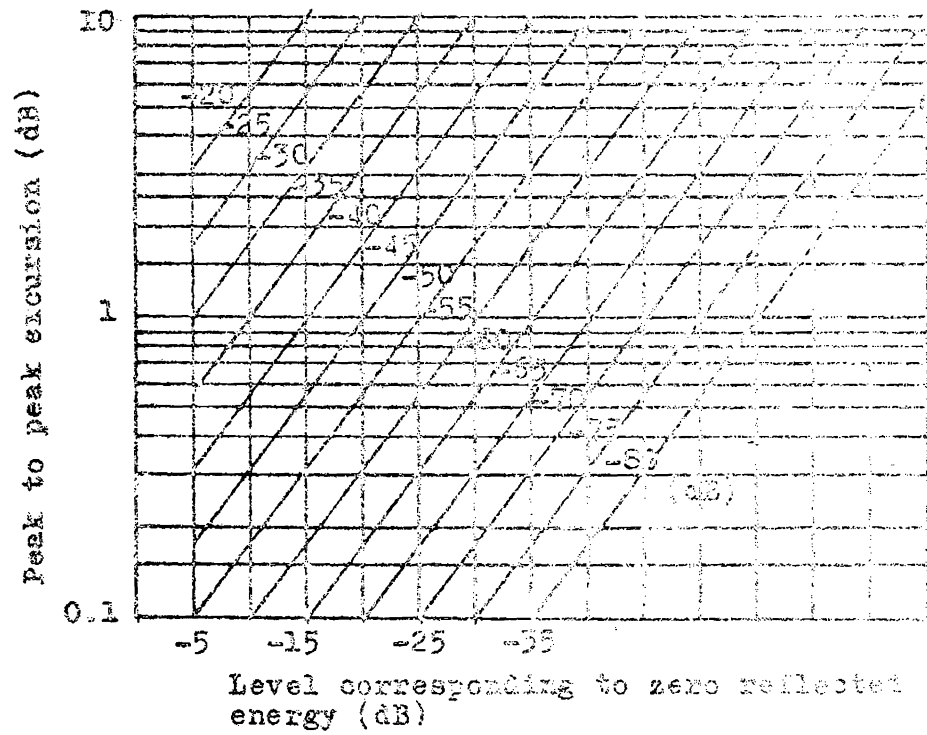


Fig.A.I.5(c) The standard curve used for determining reflectivity of quiet zone. (Reference: 25, 99).

reference pattern. Now the turn-table is moved to another closeby position along a longitudinal or transverse axis. The radiation pattern at this new position is superimposed over the reference pattern. A large number of such patterns are plotted. Fig.A.I.5(a) shows some of the plotted patterns. At specified pattern levels, say -15dB, -20dB etc., the difference between the reference pattern and the pattern at the other position is measured. This deviation is plotted as a function of the distance of the new position from the reference position. Fig.A.I.5(b) is the plotted deviation curve. The peak to peak magnitude of this deviation curve is noted at different pattern levels. The chamber reflectivity corresponding to this is obtained from Fig.A.I.5(c), which is taken from published literature.<sup>(25)</sup>

The measurements were conducted and reflectivity of the chamber was estimated to be -32dB in the X-band. This is in par with the standard values of good anechoic chambers<sup>(99)</sup> and is quite adequate for the measurements planned in this chamber.

## APPENDIX II

### DEVELOPMENT OF A MICROWAVE ABSORBING MATERIAL

A.II.0 Microwave absorbing material finds wide applications ranging from lining the interior of anechoic chambers to making terminations and antenna guard-rings. Both the mechanical and electrical properties of the material depends on the specific use to which it is put to. Material which is used to line the interior of anechoic chambers is generally foam based. This is done to reduce the density of the material, whereby first surface reflections can be reduced. Generally polyurethane foam is used as the base material. Only very few companies are manufacturing this type of material in India. Hence a major part of the internal requirement is met through import. Another factor worth noting is that, polyurethane foam is a costly material. Again, in moist warm environment, this material deteriorates fast. All these factors prompted the present investigation, where the possibility of employing natural rubber foam as the base material for microwave absorbers has been studied. Apart from being a satisfactory base material, rubber itself is an absorber of microwave energy. Another advantage is the longer life period of the rubber foam compared to that of the polyurethane foam.

### A.II.1 Preparing the Material

As mentioned earlier, foamy material is used for lining the interior of microwave anechoic chambers. Carbon is a microwave absorbing material. Graphite, which is an allotropic form of carbon is also an absorber of microwaves. Another type of absorber, which introduce magnetic losses, are the ferrites. In the present study, only carbon and graphite were used.

Natural rubber latex, after removing the preservatives, is mixed with carbon and graphite in the required proportion and certain setting agents. The mixture is ground to a smooth paste in a grinding mill. This is then poured in the moulds and steamed in a steam chamber. When the curing is complete, this is taken out, removed from the mould, and dried.

The amount of absorber which can be added to the latex is limited, since the addition of 'fillers' to the latex impairs the foaming and curing. Generally, the maximum amount of material that can be added to the latex is equal to the weight of the latex. In other words, the mixture contains 50 percent by weight latex, and all the additives constitutes the rest 50 percent. The ratio, by weight, of carbon to graphite was varied. Table A.II(I) gives the percentage composition, by weight, of carbon and graphite in the different absorber samples prepared for the study.

Table A.II(I)

## Composition of absorber samples used

Sample Number	Composition percentage		
	Latex	Carbon	Graphite
1	50	00	50
2	50	10	40
3	50	20	30
4	50	30	20
5	50	40	10
6	50	50	00

### A.II.2 Testing the Samples

The absorption coefficient of the various samples was measured using a laboratory setup. For this, the absorber samples were introduced into a waveguide test bench circuit and measurements carried out using the slotted line. Fig. A.II.2(a) shows the schematic diagram of the test setup.

The absorber samples were cut into pyramidal shape. Care was taken to see that the dimensions of all the pyramids were identical. This was introduced into a waveguide, shorted at one end, as shown in fig.A.II.2(a). This is connected to a microwave test bench and the VSWR measured. From the VSWR, the absorption coefficient of the samples can be calculated.<sup>(12)</sup> Let 's' be the VSWR. The reflection coefficient corresponding to this VSWR is given by,

$$R = \frac{(s-1)}{(s+1)}$$

From this the absorption coefficient 'A' can be obtained as,

$$A = 1-R$$

The absorption was measured at different frequencies in the X- and S-bands. Table A.II(II) gives the different values of absorption coefficients of the samples at different frequencies.

Fig.A.II.2(b) shows the variation of absorption coefficient as the composition of the material is varied.

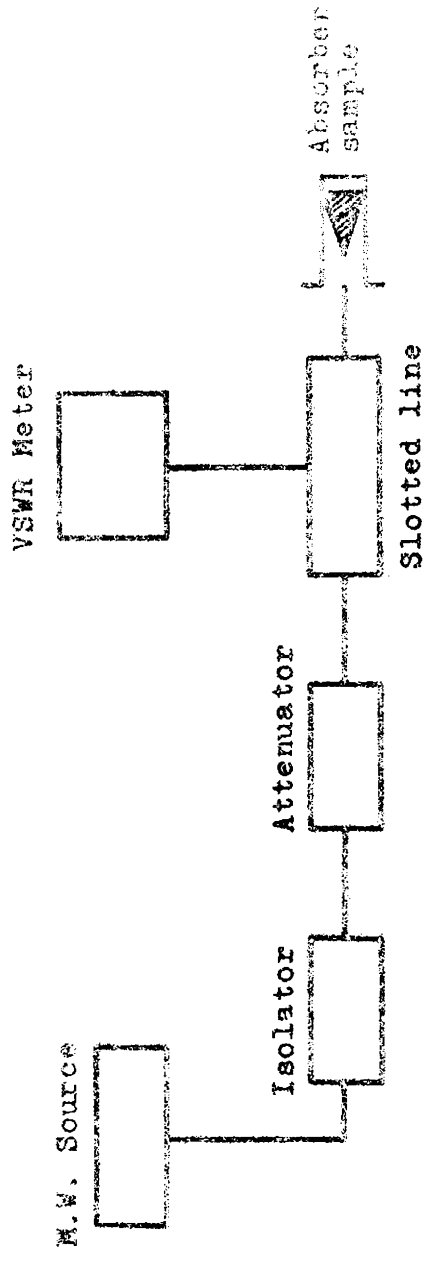


Fig. A.II.2(a) Experimental set up used to measure the absorption coefficient of the different absorber samples.

Table A.II(II)

Measured values of absorption coefficient  
for different samples

Sample Number	Frequency GHz	Absorption coefficient
1	2.5	0.41
	3.9	0.41
	4.2	0.46
	9.3	0.42
2	2.5	0.52
	3.9	0.51
	4.2	0.65
	9.3	0.45
3	2.5	0.48
	3.9	0.42
	4.2	0.64
	9.3	0.54
4	2.5	0.58
	3.9	0.75
	4.2	0.79
	9.3	0.62
5	2.5	0.67
	3.9	0.86
	4.2	0.95
	9.3	0.78
6	2.5	0.63
	3.9	0.79
	4.2	0.80
	9.3	0.73

It can be seen from fig.A.II.2(b) that the sample no.5 gives the maximum absorption at all frequencies. .

The sample materials were sent to other laboratories for test reports and comments. Extracts from one such report we received from Bharat Electronics Limited, Ghaziabad is given below:

"The three samples A, B and C have been tested by us for transmission attenuation in wave guides of 4 to 6 GHz range. Sample 'A' appears reasonably good with an attenuation of 5 dB over 40 mm of thickness whereas sample 'B' and 'C' have poor attenuation of the order of 3 and 1 dB respectively over 30 mms. When sample 'A' is formed into the pyramidal shape customary for Anechoic Chambers, the two way attenuation over the larger depth may render this material suitable for Anechoic Chamber Applications. In case you are able to identify any such indigenous absorber materials suitable for Anechoic Chamber Application, I shall be grateful to receive details of such materials".

Here the sample marked as A is the same as sample No.5.

Sample No.6 is marked as B and sample No.3 as C.

It can be seen from table A.II(I) that sample No.5 contains 50% latex, 40% carbon, and 10% graphite. The

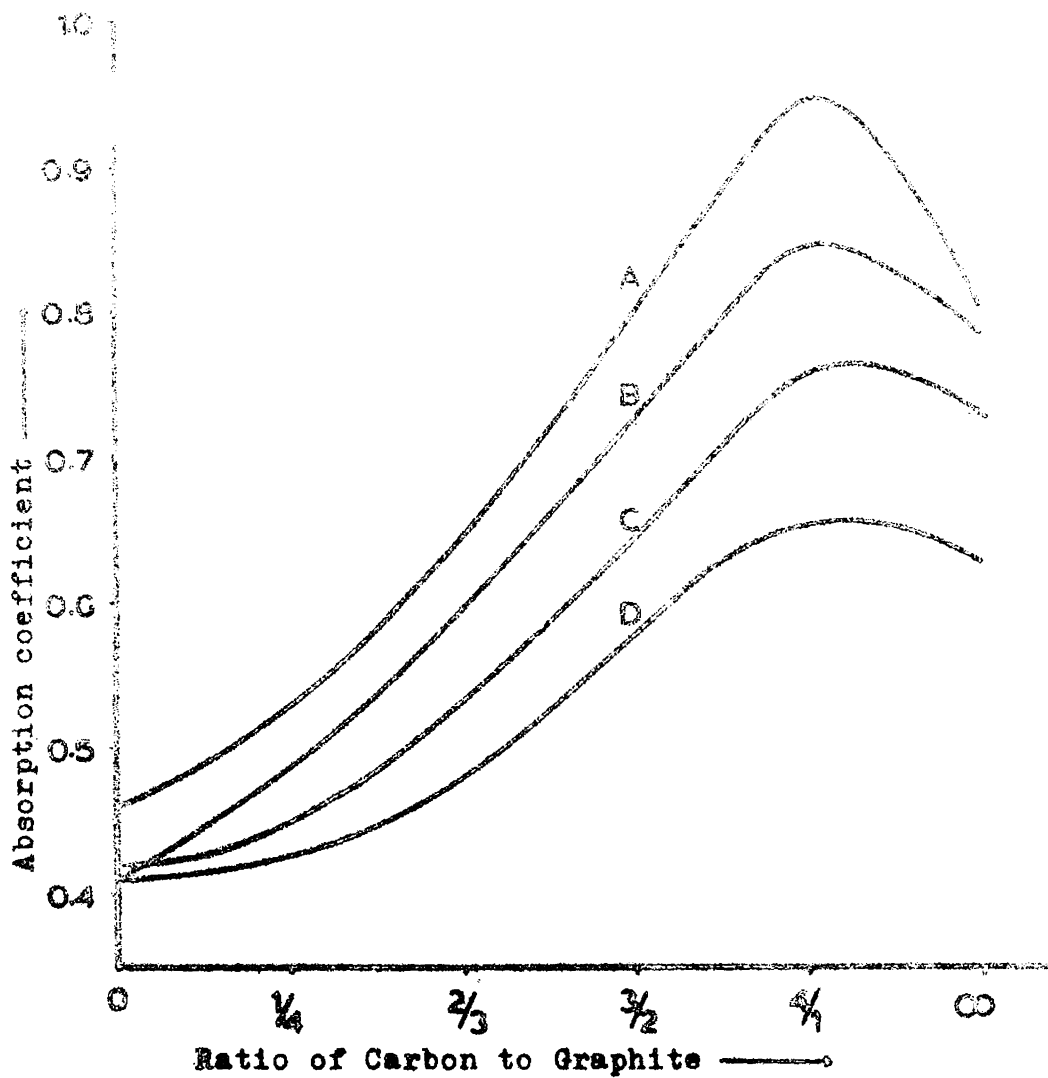


Fig.A.II(2)(b) Variation of absorption coefficient with the composition of the material for different frequencies. A - 4.2 GHz, B - 3.9 GHz, C - 9.3 GHz, D - 2.5 GHz.

mechanical properties of this material are ideally suited for cutting them into pyramids to cover the interior of microwave anechoic chambers. Developing a proper production technique, this material can be produced in mass scale to provide a standard microwave absorber material for applications like, interior lining of anechoic chambers, dummy loads, absorber screens and antenna shrouds.

## REFERENCES

1. W.L. Barrow and F.D. Lewis, "The sectoral electromagnetic horn", Proc. IRE, vol.27, pp.41-50, 1939.
2. W.L. Barrow and L.J. Chu, "Theory of the electromagnetic horn", Proc. IRE, vol.27, pp.51-64, Jan. 1939.
3. G.C. Southworth and A.P. King, "Metal horns as directive receivers of ultra short waves", Proc. IRE, vol.27, pp.95-102, Feb.1939.
4. L.J. Chu and W.L. Barrow, "Electromagnetic horn design", Trans. AIEE, vol.58, pp.333-338, Jul.1939.
5. L.J. Chu, "Calculation of radiation properties of hollow pipes and horns", J.Appl.Phys., vol.11, pp.603-610, Sep.1940.
6. N.M. Rust, "The phase correction of horn radiators", J.Inst.Elec.Eng., vol.93, pt.III A, pp.50-51, Mar.-May 1946.
7. A.R.G. Owen and L.G. Reynolds, "The effect of flanges on the radiation patterns of small horns", J.Inst.Elec. Eng., vol.93, pp.1528-1535, 1946.
8. D.R. Rhodes, "An experimental investigation of the radiation pattern of electromagnetic horn antennas", Proc.IRE, vol.36, pp.1101-1105, Sep.1948.
9. C.W. Horton, "On the theory of the radiation patterns of electromagnetic horns of moderate flare angles", Proc.IRE, vol.37, pp.744-749, Jul.1949.

10. S. Silver, "Microwave antenna theory and design",  
McGraw-Hill Book Company, New York, 1949.
11. C.G. Montgomery, "Techniques of microwave measurements",  
McGraw-Hill Book Company, New York, 1949.
12. H.M. Barlow and A.L. Cullen, "Microwave measurements",  
Constable and Company, London, 1950.
13. A.P. King, "The radiation characteristics of conical  
horn antennas", Proc.IRE, vol.38, pp.249-251,  
Mar.1950.
14. Marvin G. Schorr and Fred J. Beck Jr., "Electromagnetic  
field of the conical horn", J.Appl.Phys., vol.21,  
pp.795-801, Aug.1950.
15. W.C. Jakes Jr., "Gain of electromagnetic horns", Proc.  
IRE, vol.39, pp.160-162, Feb.1951.
16. E.H. Braun, "Gain of electromagnetic horns", Proc. IRE,  
vol.41, pp.109-115, Jan.1953.
17. E.H. Braun, "Some data for the design of electromagnetic  
horns", IEEE Trans. Antennas Propagat., vol.AP-4,  
pp.29-31, Jan.1956.
18. P.C. Butson and G.T. Thomson, "The effect of flanges on  
the radiation patterns of waveguides and sectoral  
horns", J.Inst.Elec.Eng., vol.106, pt.B, pp.422-426,  
1959.
19. A.E. Booth, "Microwave data tables", Iliffe and Sons Ltd.,  
London, 1959.

20. S. Hariharan and K. Gopalakrishnan Nair, "An experimental investigation of the change in radiation patterns in the Fresnel's region of sectoral electromagnetic horn antennas due to shorting grills", J.Inst.Telecom.Engrs., vol.7, pp.189-196, 1961.
21. James J. Epis, "Compensated electromagnetic horns", Microwave J., vol.4, pp.84-89, May 1961.
22. E.A. Jasik, "Antenna engineering hand book", McGraw-Hill Book Company, New York, 1961.
23. S. Hariharan and K. Gopalakrishnan Nair, "Impedance matching of sectoral electromagnetic horn antennas by shorting grills", J.Inst.Telecom.Engrs.,vol.8, pp.246-251, 1962.
24. D.R. Rhodes, "The optimum line source for the best mean square approximation for a given radiation pattern", IEEE Trans. Antennas. Propagat., vol.AP-11, pp.440-446, Jul.1963.
25. E.F. Buckley, "Outline of evaluation procedures for microwave anechoic chambers", Microwave J., vol.6, pp.69-75, Aug.1963.
26. Tingye Li, and R.H. Turrin, "Near zone field of the conical horn", IEEE Trans.Antennas.Propagat., vol.AP-12, pp.800-802, Nov.1964.

27. P.M. Russo, R.C. Ruddock and L. Peters Jr., "A method for computing E-plane patterns of horn antennas", IEEE Trans.Antennas.Propagat., vol.AP-13, pp.219-224, Mar.1965.
28. T.S. Chu and R.A. Semplak, "Gain of electromagnetic horns", Bell Syst.Tech.J., vol.44, pp.527-537, Mar. 1965.
29. "Test procedure for antennas", Institute of Electrical and Electronics Engineers, New York, 1965.
30. A.H. LaGrone and G.F. Roberts, "Minor lobe suppression in a rectangular horn antenna through the utilisation of a high impedance choke flange", IEEE Trans. Antennas.Propagat., vol.AP-14, pp.102-104, Jan.1966.
31. J.S. Yu, R.C. Ruddock and L. Peters Jr., "Comprehensive analysis for E-plane of horn antennas by edge diffraction theory", IEEE Trans. Antennas.Propagat., vol.AP-14, pp.138-149, Mar.1966.
32. A.J. Simmons and A.F. Kay, "The scalar feed- a high performance feed for large paraboloidal reflectors", IEEE Conf.Publ.21, pp.213-217, 1966.
33. V.H. Rumsey, "Horn antennas with uniform power patterns around their axes", IEEE Trans.Antennas.Propagat., vol.AP-14, pp.656-658, Sep.1966.
34. R.E. Lawrie and L. Peters Jr., "Modification of horn antennas for low side lobe levels", IEEE Trans. Antennas.Propagat., vol.AP-14, pp.605-610, Sep.1966.

35. B.V. Rao and K.K. Reddy, "A study of microwave horn and lens antennas", J.Inst.Telecom.Engrs., vol.13, pp.390-399, 1967.
36. K.G. Nair and G.P. Srivastava, "Beam shaping of H-plane sectoral horns by metal flanges", J.Inst.Telecom.Engrs., vol.13, pp.76-82, Feb.1967.
37. E.C. Jordan, "Electromagnetic waves and radiating systems", Prentice-Hall of India, New Delhi, 1967.
38. E.V. Jull, "On the behaviour of electromagnetic horns", Proc.IEEE, vol.56, pp.106-108, Jan.1968.
39. K.G. Nair, V.K. Koshy and G.P. Srivastava, "E-plane sectoral horns yield to flange technique", Int.J.Electronics, vol.24, pp.93-98, 1968.
40. K.G. Nair, V.K. Koshy and G.P. Srivastava, "A theoretical study of the asymmetric excitation of conducting flanges by a primary aperture antenna and the consequent radiation patterns", Int.J. Electronics, vol.24, pp.497-500, 1968.
41. K.G. Nair, G.P. Srivastava, S.B. Singh and V.K.Koshy, "A study of the effect of the relative position of metal flanges on the radiation pattern of H-plane sectoral horn", Int.J.Electronics, vol.25, pp.153-164, 1968.

42. V.K. Koshy, S.B. Singh, K.G. Nair and G.P. Srivastava, "Effect of asymmetry in amplitude of excitation of secondary sources by a primary aperture antenna", *Int.J.Electronics*, vol.25, pp.289-291, 1968.
43. M.A.K. Hamid, "Diffraction by a conical horn", *IEEE Trans.Antennas.Propagat.*, vol.AP-16, pp.520-528, Sep.1968.
44. K.G. Nair, G.P. Srivastava and S.B. Singh, "Some effects of metal flanges on the radiation pattern of H-plane sectoral horns", *J.Inst.Telecom. Engrs.*, vol.14, pp.352-358, 1968.
45. V.K. Koshy, K.G. Nair and G.P. Srivastava, "An experimental investigation of the effect of conducting flanges on the H-plane radiation patterns of E-plane sectoral horns", *J. Inst.Telecom.Engrs.*, vol.14, pp.519-527, 1968.
46. K.G. Nair, G.P. Srivastava and S. Hariharan, "Sharpening of E-plane radiation patterns of E-plane sectoral horns by metallic grills", *IEEE Trans.Antennas. Propagat.*, vol.AP-17, pp.91-93, Jan.1969.
47. S.B. Singh, K.G. Nair and G.P. Srivastava, "Experimental confirmation of the effect of asymmetric flanges on the radiation pattern of aperture antennas", *Int.J.Electronics*, vol.26, pp.173-177, 1969.

48. K.G. Nair, G.P. Srivastava and S. Hariharan, "Effect of conducting grills on the E-plane radiation patterns of E-plane sectoral horns", Int.J. Electronics, vol.26, pp.561-572, 1969.
49. P.J.B. Clarricoats, "Analysis of spherical hybrid modes in a corrugated conical horn", Electron. Lett., vol.5, pp.189-190, May 1969.
50. P.J.B. Clarricoats and P.K. Saha, "Radiation from wide flare angle scalar horns", Electron.Lett., vol.5, pp.376-378, Aug.1969.
51. J.S. Yu and R.C. Ruddock, "H-plane pattern of a pyramidal horn", IEEE Trans.Antennas.Propagat., vol.AP-17, pp.651-652, Sep.1969.
52. M.E.J. Jeuken, "Experimental radiation pattern of the corrugated conical horn antenna with small flare angles", Electron.Lett., vol.5, pp.484-485, Oct.1969.
53. M.E.J. Jeuken and C.W.Lambrechtse, "Small corrugated conical horn antenna with wide flare angle", Electron. Lett., vol.5, pp.489-490, Oct.1969.
54. Steven Galagan, "Understanding microwave absorbing materials and anechoic chambers - Part I", Microwaves, pp.38-41, Dec.1969.
55. R.E. Collin and F.J. Zucker, "Antenna theory - Part I", McGraw-Hill Book Company, New York, 1969.

56. R.E. Collin and P.J. Zucker, "Antenna theory - Part II", McGraw-Hill Book Company, New York, 1969.
57. Steven Galagan, "Understanding microwave absorbing materials and anechoic chambers - Part II", *Microwaves*, pp.44-49, Jan.1970.
58. M.S. Narasimhan and B.V. Rao, "Hybrid modes in corrugated conical horns", *Electron.Lett.*, vol.6, pp.32-34, Jan.1970.
59. K.G. Nair, "A modified theory for the radiation pattern of an aperture antenna and two secondary sources excited by the primary", *Int.J.Electronics*, vol.28, pp.459-462, 1970.
60. R.Baldwin and P.A. McInnes, "Surface wave excitation from a corrugated horn", *Electron.Lett.*, vol.6, pp.259-260, Apr.1970.
61. Steven Galagan, "Understanding microwave absorbing materials and anechoic chambers - Part III", *Microwaves*, pp.47-50, Apr.1970.
62. Steven Galagan, "Understanding microwave absorbing materials and anechoic chambers-Part IV", *Microwaves*, pp.69-73, May 1970.
63. V.K. Koshy, K.G. Nair and G.P. Srivastava, "Analysis of radiation from a flanged aperture antenna", *IEEE Trans.Antennas.Propagat.*, vol.AP-18, pp.407-411, May 1970.

64. B. Mac A. Thomas, "Prime focus one and two hybrid mode feeds", *Electron. Lett.*, vol.6, pp.460-461, Jul.1970.
65. M.S. Narasimhan and B.V. Rao, "Diffraction by a wide flare angle corrugated conical horn", *Electron. Lett.*, vol.6, pp.469-471, Jul.1970.
66. E.V. Jull, "Finite range gain of sectoral and pyramidal horns", *Electron. Lett.*, vol.6, pp.680-681, Oct.1970.
67. Seymore B. Cohn, "Flare angle changes in a horn as a means of pattern control", *Microwave J.*, vol.13, pp.41,42,44,46, Oct.1970.
68. Eugen I. Neuhldorf, "The phase centre of horn antennas", *IEEE Trans. Antennas.Propagat.*, vol.AP-18, pp.753-760, Nov.1970.
69. Gordon J. King, "The practical aerial hand book", Newnes-Butterworths, London, 1970.
70. M.S. Narasimhan and B.V. Rao, "Modes in a conical horn - a new approach", *Proc.Inst.Elec.Eng.*, vol.118, pp.287-292, Feb.1971.
71. V.K. Koshy, K.G. Nair and G.P. Srivastava, "Gain improvement of flanged sectoral horn antennas by flange angle variations", *Ind.J.Pure.Appl.Phys.*, vol.9, pp.476-478, Jul.1971.

72. M.S. Narasimhan and B.V. Rao, "Reflection from conical horns with large flare angles", IEEE Trans. Antennas.Propagat., vol.AP-19, pp.678-681, Sep.1971.
73. P.J.B. Clarricoats and P.K. Saha, "Propagation and radiation behaviour of corrugated feeds - pt.1 Corrugated waveguide feed", Proc.Inst.Elec.Eng., vol.118, pp.1167-1176, Sep.1971.
74. P.J.B. Clarricoats and P.K. Saha, "Propagation and radiation behaviour of corrugated feeds - pt.2 Corrugated conical horn feed", Proc.Inst.Elec. Eng., vol.118, pp.1177-1186, Sep.1971.
75. J.K.M. Jansen, H.E.J.Jeuken and C.W. Lambrechtse, "The scalar feed", Arch. Elec.Ubertagung., vol.26, pp.22-30, Jan.1972.
76. Harry E. Thomas, "Hand book of microwave techniques and equipment", Prentice-Hall Inc., Englewood Cliffs, New Jersey, 1972.
77. Mooto Mizuzawa, Fumio Takeda and Shin-ichi Betsudan, "Radiation characteristics of a corrugated conical horn", Electron.Commun.Japan., vol.56B, pp.42-47, Jan.1973.
78. E.V. Jull, "Errors in the predicted gain of pyramidal horns", IEEE Trans.Antennas.Propagat.,vol.AP-21, pp.25-31, Jan.1973.

79. M.S. Narasimhan, "Corrugated conical horns with arbitrary corrugation depth", Radio.Electron.Eng., vol.43, pp.188-192, Mar.1973.
80. John L. Kerr, "Short axial length broad band horn", IEEE Trans.Antennas.Propagat., vol.AP-21, pp.710-715, Sept.1973.
81. Carl A. Mentzer and Leon Peters Jr., "Properties of cut off corrugated surfaces for corrugated horn design", IEEE Trans.Antennas,Propagat., vol.AP-22, pp.191-196, Mar.1974.
82. M.S. Narasimhan, "Corrugated conical horn feed as space feed for phased array illumination", IEEE Trans. Antennas.Propagat.,vol.AP-22, pp.720-722, Sep.1974.
83. R. Baldwin and P.A. McInnes, "Corrugated conical horns for use as microwave feeds", Proc.Inst.Elec.Eng., vol.122, pp.465-469, May 1975.
84. G.P. Srivastava, K.K. Bhan and R. Baldwin, "Experimental study of a flange mounted waveguide as a device for square radiation pattern", IEEE Trans.Antennas. Propagat., vol.AP-24, pp.242-244, Mar.1976.
85. K.G. Nair, K. Mohanachandran and K.T. Mathew, "Beam shaping of sectoral horn antennas by dielectric flanges", Ind.J.Radio.Space.Phys., vol.5, pp.254-256, Sep.1976.

86. Gordon R. Ebbeson, "TM polarised electromagnetic scattering from fin corrugated periodic surfaces", J. Opt. Soc.Am., vol.66, pp.1363-1367, Dec.1976.
87. K.G. Nair and K.T. Mathew, "Effect of flanged sectoral horn primary feeds on the radiation patterns of secondary reflector antennas", J.IETE, vol.23, pp.148-149, 1977.
88. E.V. Jull, J.W. Heath and G.R. Ebbeson, "Gratings that diffract all incident energy", J.Opt.Soc.Am.,vol.67, pp.557-560, Apr.1977.
89. K.G. Nair and P.A. Mathews, "Metallic flanges on sectoral horns as corner reflectors", IEEE Trans.Antennas. Propagat., vol.AP-25, pp.431-435, May 1977.
90. C. Dragone, "Characteristics of a broad band microwave corrugated feed: a comparison between theory and experiment", Bell.Syst.Tech.J., vol.56, pp.869-888, Jul-Aug.1977.
91. H.E. Green, "Some aspects of radio anechoic chambers", Elec.Eng.Trans., pp.18-19, 1977.
92. A.J. Terzouli, J.H. Richmond and L. Peters Jr., "The VSWR of E-plane dihedral horns", IEEE Trans. Antennas.Propagat., vol.AP-26, pp.236-239, Mar.1978.
93. A.J. Terzouli and L. Peters Jr., "The VSWR of E-plane dihedral corrugated horn", IEEE Trans.Antennas.Propagat., vol.AP-26, pp.239-243, Mar.1978.

94. Glenn F. Engen, "Advances in microwave measurement science", Proc. IEEE, vol.66, pp.483-507, Apr.1978.
95. Ernest E. Donaldson, William R. Free, Douglas W. Robertson, and Jimmy A. Woody, "Field measurements made in an enclosure", Proc. IEEE, vol.56, pp.464-472, Apr.1978.
96. W.H. Kummer and E.S. Gillespie, "Antenna measurements - 1978", Proc. IEEE, vol.66, pp.483-507, Apr.1978.
97. James W. Heath and Edward V. Jull, "Perfectly blazed reflection gratings with rectangular grooves", J. Opt.Soc.Am., vol.68, pp.1211-1217, Sep.1978.
98. K.K. Bhan, S. Ghosh and G.P. Srivastava, "Study of control of beam width of radiation pattern of a waveguide using inclined slotted flanges", IEEE Trans. Antennas. Propagat., vol.AP-26, pp.447-453, May 1978.
99. K.K. Srivastava, "Anechoic chambers (design evaluation and measurements)", Proc.IEEE Workshop on Design, Measurements and Evaluation of Microwave Antenna Systems, New Delhi, Sep.28-30, 1978.
100. E.V. Jull, "Reflection circular polarisers", Electron. Lett., vol.15, pp.423-424, Jul.1979.
101. K. Ito, N. Aziaawa and N. Goto, "Circularly polarised printed array composed of strips and slots", Electron. Lett., vol.15, pp.811-812, Dec.1979.

## LIST OF PUBLICATIONS

1. "Beam shaping and impedance matching of electromagnetic horn antennas using corrugated flanges", Ind. J. Radio. Space. Phys., vol.8, pp.24-28, Feb. 1979.
2. "Metal flanges with more parameters for beam shaping", IEEE Trans. Antennas. Propagat., vol.AP-27, pp.708-711, Sep. 1979.
3. "Microwave absorber using Rubber and Carbon", Ind. J. Pure. Appl. Phys., vol.18, pp.216-218, Mar. 1980.
4. "Fabrication of an antenna turn table with remote control system for anechoic chamber investigations", Communicated to the Journal of the Institution of Engineers.

## INDEX

- Absorbing material 137,146, 157,158
- Absorption coefficient 160
- Anechoic chamber 54,115,118, 121,136,141,148,153, 156,157,158,163,165
- Antenna 14
- Antenna characteristics 74
- Antenna gain 58,68,100
- Aperture efficiency 26
- Arch method 139
- Attenuator 64
- Axial ratio 69,70,111
  
- Baldwin, R 39
- Barrow, W.L. 20,30,31
- Beam elimination 44
- Beam shape 96,100,133
- Beck, F.J. 33
- Bearing angle 68,115
- Bhan, K.K. 48
- Braun, E.H. 33
- Butson, P.C. 24,42,43,75,122
  
- Chu, L.J. 20,30,31,32,34
- Choke slot 37
- Choke flange 42
- Clarricoats, P.J.B. 37,38, 39,40
- Cohn, S.B. 47
- Corrugated horn 26,106
- Corrugated flanges 27,51,66 74,92,96,109,111,132, 133,135
- Corrugated surface 37
- Corrugation-depth 56
  - inclined 56
  - period 56,86,106,108
  - straight 56
  - tips 78
  
- Dipole 18
- Directional antenna 58
- Directional coupler 62,66
  
- Effective area 33
- Epis, James, J. 34
- E-plane aperture 53
  
- Field equations 14
- Flanges - dielectric 46
  - metallic 43,51
  - slotted 46
  - positioner 75
  - surface 111,118,121
  - technique 24
  - width 115
  - width asymmetry 43
- Flange angle 75,83,96,106, 109,115
- Flare angle 53,54
- Frequency meter 62,64,66
  
- Gain 58,67,68,74,106,108
- Grill system 45
- Gunn-diode 49
  - oscillator 49,62,66
  - power supply 49,62,66
  
- Half power beam width 67,69,74 108,109
- Hamid, M.A.K. 35
- Hariharan, S, 45
- Hertz, H 14,15
- Horn antenna - conical 21
  - pyramidal 21,67 124
  - sectoral 21,23,51, 66,68,86,115, 133
- Horton, L.W. 32
- H-plane aperture 53
- Huygens principle 31
  
- Impedance 64
- Integration - pattern 58,68
  - numerical 68
- Intensity pattern 58,68,69
- Isolator 62,64,66

- Jakes, W.C. 33  
 Jansen, J.K.M. 38  
 Jeuken, N.E.J. 38,39  
 Jull, E.V. 35
- Kay, A.F. 37,38  
 Kerr, J.L. 36  
 King, A.P. 20,31,32  
 Kirchhoffs formula 32  
 Kirchhoff-Huygen's method 40  
 Koshy, V.K. 44,45  
 Klystron oscillator 47
- La Grone, A.H. 42  
 Lambrechtse, L.W. 38  
 Lawrie, R.E. 37  
 Li, Tingye 34  
 Linear radiator 115,118  
 Line Source Theory 42,115  
 Lobe - main 69,96,109,111,  
           133  
       - side 69  
 Logarithmic curvature 36
- Mac A. Thomas 40  
 Marconi antenna 17  
 Mathew, K.T. 47  
 Mathews, P.A. 46  
 Maxwell, J.C. 14  
 McInnes, P.A. 39  
 Mentzer, C.A. 40  
 Microstrip antenna 19  
 Microwave diode 61  
 Minimum position 43,83,89  
 Modal expansion 38  
 Mode filter 20  
 Monopole antenna 17  
 Muelhdorf, E.I. 36
- Nair, K.G. 43,44,45,46,47  
 Narasimhan, M.S. 36,38,39  
 Numerical Integration 65
- On-axis power density 64,66,  
           74,75,89,92,126,132
- Optimum - horn 33  
           - position 43,83,89  
 Owen, A.R.G. 24,42,43
- Parabolic reflector 16  
 Pattern integration 58,68  
 Peters, L. 37,40  
 PIF diode 49  
       -modulator 61,66,67  
 Plane flanges 51,74,92,108,109,  
           132,133  
 Polarisation 69  
 Power pattern 68,69
- Quiet zone 60,145,146,153
- Radiation - characteristics 58,108  
           - Intensity 67  
           - pattern 58,63,68,74,  
                     89,92,96,100,115,  
                     126  
 Rao, B.V. 35,36,38  
 Receiver 67  
       - antenna 58,60,61
- Reciprocity theorem 60  
 Rectangular chamber 146  
 Reddy, K.K. 35  
 Reflectivity 139,141,153,156,163  
 Resonant cavity 49  
 Resultant power 117  
 Reynolds, L.G. 24,42,43  
 Rhodes, D.R. 32  
 Roberts, G.F. 42  
 Ruddock, R.C. 35,36  
 Rumsey, V.H. 35  
 Russo, P.M. 34
- Saha, P.K. 38,40  
 Scalar feed 37  
 Schorr, M.G. 33  
 Shorting plunger 49  
 Simmons, A.J. 37  
 Singh, S.B. 44  
 Semplak, R.A. 34  
 Slotted line 64,66  
 Slot - depth 83  
       - width 72,78

Space directivity factor 124  
Southworth, G.C. 31  
Srivastava, G.P. 43, 46  
Surface reactance 37

Thomson, G.T. 24, 42, 43, 75,  
122  
Transmission line 64  
Transmitter, 58, 60, 61, 63, 64,  
69, 89, 148, 152, 153  
Turn-table 54, 57, 58, 62, 66,  
136, 150, 151, 152, 153,  
156  
Turrin, R.H. 34

VSWR 64, 66, 74, 75, 78, 83,  
86, 92, 132, 160  
VSWR meter 67, 70, 153

Wave guide 49, 64, 118, 160  
Waveguide flanges 51  
Wave length 73, 78

Yu, T.S. 35, 36.

- G 2963 -

